S3A STM Reprocessing - "Spring 2018" (Level 0 to Level 2)

EUMETSAT
Eumetsat-Allee 1, D-64295 Darmstadt, Germany
Tel: +49 6151 807-7

Doc.No. : EUM/OPS-SEN3/REP/18/978053
Issue : v1 e-signed
Date : 28 May 2018
WBS/DBS :

Document Change Record

Issue / Revision	*Date*	*DCN. No*	*Changed Pages / Paragraphs*
V1 Draft	23 February 2018		Initial version
V1	28 May 2018		Release version

Table of Contents

Table of Figures

Table of Tables

1 Introduction

1.1 Purpose

This document reports the technical work done for the preparation and validation of the Sentinel-3 STM (Surface Topography Mission) Reprocessing 'Spring 2018'.

1.2 Scope

This document is applicable to the Sentinel-3 STM Reprocessed dataset 'Spring 2018' and is addressed to the agencies and users making use of the reprocessed dataset.

1.3 Applicable Documents

AD-1	SRAL L1 Product Notice	S3A.PN-STM-L1.04
AD-2	Sentinel-3A Product Notice – STM L2 Marine (NRT, STC and NTC)	EUM/OPS-SEN3/DOC/16/893228 v1F
AD-3	Product Data Format Specification - SRAL-MWR Level 2 Marine	S3IPF.PDS.003.3 i2r11
AD-4	Product Data Format Specification - SRAL and MWR Level 1 products	S3IPF.PDS.003.1 i2r10
AD-5	Product Data Format Specification - Level 0 Products	S3IPF.PDS.001 i1r3

2 Executive Summary

The reprocessing of all Sentinel-3A SRAL data to the latest Baseline collection makes available to the end-users a consistent full mission reprocessing dataset, from 01 March 2016 (SRAL instrument turn-on) until the present date. This reprocessing provides not only updated SRAL/MWR Level 2 data, but also Level 1 products (L1B, L1A and L1B-S).

The data provided is consolidated into pole-to-pole passes and fully calibrated. Special care was taken with the Long Term Monitoring calibration of the instruments, for more details see section 5.

The geophysical verification of the data content was made at Level 2 and the reprocessing dataset is consistent and within the mission requirements for the Open Ocean, for all key marine parameters (Sea-Surface Height, Significant Wave Height and Wind Speed). The geophysical parameters show good agreements with other altimeters and also with models. Further details on the validation can be found in Section 4.

Sea-ice measurements retrievals are not yet tuned, but are expected to improve with the upcoming Processing Baselines.

A characterization of the initial period of the mission is also provided (section 4.3.2) allowing users to have insight on issues that can be found in the dataset before cycle 6, during S3A Cal/Val.

Overall the reprocessing can be considered very useful, it has allowed to better characterize the Sentinel-3A surface topography mission in terms of trends and bias and will allow for a better cross comparison with S3B, during the Cal/Val period of the latest.

3 Reprocessing Context

3.1 Processing evolutions

Since launch of Sentinel-3A, the processing algorithms and auxiliary data have gone through many changes, either as a result of bug fixes or evolutions to those algorithms or auxiliary data. Every change is marked by an increase of the Processing Baseline (PB) version. Major changes are marked by the increase of the Baseline Collection number, which can be seen in the name of the directory (just before the .SEN3 extension) containing the SRAL netCDF data set. The PB used during the previous reprocessing campaign ("Spring 2017") was 2.15, the Baseline Collection 002.

A major evolution was introduced late 2017 with the Processing Baseline (PB) 2.24. This lead to the increase of the Baseline Collection from 002 to 003. The evolutions between the Baseline Collections 002 and 003 (i.e., between the Spring 2017 and the current reprocessing) comprise, among others:

- The updated version of the SAMOSA retracking algorithm (now following DPM 2.5) improves the consistency of SAR and PLRM retrievals for sea surface height and to be even more in line with the ECMWF models for winds and waves.
- Updated Mean Sea Surfaces (DTU 15 [default] and CNES/CLS 15), updated tide model (FES 2014 [default] and GOT 4.10).
- There are also newer additions to the L2 product, these should make it easier to use by the users. There is now a flag (orbit_type_01), at measurement level, describing the type of orbits used in the processing, this is particularly relevant for NRT data.
- New indexing scheme is available to allow easy matching between 1-Hz and 20-Hz data, the same approach used by Envisat. The following variables were added (index_1hz_meas_20_[ku|c], index_first_20hz_meas_01_[ku|c], num_20hz_meas_01_[ku|c]).
- There are improvements on the radiometer wet tropospheric correction, especially near the coast, as a 5-parameter algorithm was improved
- The backscatter coefficient is now corrected for attenuation, bringing Sentinel-3 in line with other altimeter product formats.
- Improvements on sea ice detection are also part of the updates of this Processing Baseline.

The PB version used in this reprocessing campaign is PB 2.27 and has minor updates with respect to PB 2.24. The latest version used operationally is PB 2.33, which contain mainly some fixes for LRM (discovered thanks to this reprocessing campaign).

A consistent dataset of STM (Surface Topography Mission) products for the complete reprocessing period, since the Beginning of the Mission, allows to derive long term trends. This would be valuable for the Cal/Val of S3B, as better cross comparison between the satellites could be achieved.

All of the above led to the need to reprocess the Sentinel-3A dataset. The user products in the reprocessed dataset will be made available to end-users.

3.2 Sensing time

This reprocessing spans the period from 2016-03-01 to 2018-01-20. Data produced operationally by EUMETSAT with sensing times after 2018-01-20 have been already produced with PB 2.27 for the NTC timeliness (see Section 3.4), and thus this reprocessing allows for a consistent data set from 1 March 2016 to present.

3.3 Input data

The input data are the L0 granules of SRAL (SR_0_SRA___, SR_0_CAL___) and MWR (MW_0_MWR___).

The EUM dataset was retrieved from UMARF and provided to the Reprocessing platform. For certain period/files the ESA's Svalbard archive (available to MPC) was used.

3.4 Processing Baseline and logic

PB 2.27 used for the reprocessing consists of the following processors:

- SRAL L1 IPF v6.13 (Calibration and Measurement processors)[1]
- MWR L1 IPF v6.04 (Calibration and Measurement processors)[2]
- SRAL/MWR L2 IPF v6.12 (Measurement processor)[3]
- The associated static Auxiliary Data Files (ADFs).

Further details can be found in the Product Notices corresponding to this Processing Baseline (see Sections 1, 2, 3):

- The reprocessing used the NTC (Non-Time Critical) standard for orbits and ADFs (orbits, platform information, corrections, etc.).
- The calibrations (SRAL and MWR) were reprocessed and consolidated into Long Term Monitoring files and are applied at L1.
- The SRAL L0 granules were processed by the L1 processor generating L1A, L1B, L1B-S data.
- The MWR data were processed from L0 to L1.
- The SRAL L1 and MWR L1 data were input to the SRAL/MWR L2 processor for generating the L2 products.

In the following Sections, further details are given on each processing step and its validation.

[1] For SRAL L1 the latest Product Notice is available here:

http://www.eumetsat.int/website/wcm/idc/idcplg?IdcService=GET_FILE&dDocName=PDF_S3A_ALT_PN_STM_L1_04&RevisionSelectionMethod=LatestReleased&Rendition=Web

[2] MWR L1 is not a user product. Details about MWR can be found in the SRAL/MWR L2 Product Notice (see note[3]).

[3] For SRAL/MWR L2 the latest Product Notice is available here:

http://www.eumetsat.int/website/wcm/idc/idcplg?IdcService=GET_FILE&dDocName=PDF_S3A_PN_STM_L2_NRT_STC_1F&RevisionSelectionMethod=LatestReleased&Rendition=Web

4 SRAL/MWR L2

4.1 Data completion and Processing Baseline

In the processing of SRAL L2 there were some processing errors that generated data gaps, these errors and the overall gaps (due to input data) are provided in Table 1. Besides these run time errors (non-recoverable), the data availability at L2 is very much the same as at L1 (considering that the Land-Sea Mask is applied to L2 and the SR_2_WAT___ product only contains the marine measurements).

The same tools currently used to monitor the Processing Baseline in the S3 PDGS were used to verify the correctness of the static processing baseline used. We verified that all the L2 products were created with the correct L2 PB (IPF version and static ADF).

The only difference with respect to PB 2.27 was the usage of a more up-to-date MWR CHD[4] file, in preparation for the new MWR calibration scheme that started on 2018-03-01. It has no impact on the data quality acquired before. Limitations in the products related to the Reprocessing Campaign

The meteorological correction files (AX___MA1_AX, AX___MA2_AX) for 2016-03-28 were not available, and thus the variables model dry (mod_dry_tropo_cor) and wet tropospheric correction (mod_dry_tropo_cor) are degraded for that day. In turn the measurement of the sea surface height anomaly (SSHA) is also impacted. This is traced in anomaly EUM/Sen3/AR/4183.

The Iono GIM correction was not available for the early mission time period: 2016-03-01 to 2016-03-09.

The MOG2d correction is missing (entirely or partially) in the following early-mission products:

S3A_SR_2_WAT____20160301T112401_20160301T120129_20180212T170814_2248_001_222_____MR1_R_NT_003
S3A_SR_2_WAT____20160321T232955_20160322T001409_20180212T191207_2654_002_130_____MR1_R_NT_003
S3A_SR_2_WAT____20160322T052733_20160322T061351_20180212T191958_2778_002_133_____MR1_R_NT_003
S3A_SR_2_WAT____20160322T111650_20160322T120306_20180212T191725_2776_002_137_____MR1_R_NT_003
S3A_SR_2_WAT____20160322T171626_20160322T180042_20180212T191536_2655_002_140_____MR1_R_NT_003
S3A_SR_2_WAT____20160322T235912_20160323T004443_20180212T191951_2731_002_144_____MR1_R_NT_003
S3A_SR_2_WAT____20160323T054742_20160323T063303_20180212T191911_2721_002_148_____MR1_R_NT_003
S3A_SR_2_WAT____20160323T114333_20160323T123137_20180212T191902_2884_002_151_____MR1_R_NT_003
S3A_SR_2_WAT____20160323T173445_20160323T182255_20180212T192609_2890_002_155_____MR1_R_NT_003
S3A_SR_2_WAT____20160323T233309_20160324T001832_20180212T192209_2723_002_158_____MR1_R_NT_003
S3A_SR_2_WAT____20160324T052131_20160324T060635_20180212T192332_2704_002_162_____MR1_R_NT_003
S3A_SR_2_WAT____20160324T111742_20160324T120527_20180212T192445_2865_002_165_____MR1_R_NT_003
S3A_SR_2_WAT____20160324T180440_20160324T184836_20180212T192516_2636_002_169_____MR1_R_NT_003
S3A_SR_2_WAT____20160324T235222_20160325T003647_20180212T192813_2665_002_173_____MR1_R_NT_003

[4] In SRAL/MWR L2 processing the newer MWR_CHD_AX was used instead of the older file. No scientific differences are expected. This was done due to operational reasons.
S3A_MW___CHDNAX_20160216T000000_20991231T235959_20170908T120000_____MPC_O_AL_004.SEN3
S3A_MW___CHDNAX_20160216T000000_20991231T235959_20161014T120000_____MPC_O_AL_002.SEN3.

4.2 Data Gaps

The Level 2 gaps internal or between files larger than 1250 seconds are reported in Table 1. These gaps result from the SAFE manifest (xdfumanifest.xml) analysis that reports internal data gaps. The external gaps (between products) were analysed checking the L2 product's start/stop times.

The 'allowed' gap window used was larger for L2 to avoid any false positive results due to the application of the Land Sea Mask that creates non-continuous products.

The following gaps at L2 are due to gaps at L1 (see 7.3) or due to IPF failures, shown below.

Table 1 – Data gaps at L2 - summary table

Gap ID	Sensing Start	Sensing Stop	Gap duration
GAP_SM2W_001	20160308T122026	20160308T130643	1508
GAP_SM2W_002	20160308T140126	20160308T144816	1758
GAP_SM2W_003	20160314T230326	20160315T000641	3794
GAP_SM2W_004	20160315T073610	20160315T082129	1442
GAP_SM2W_005	20160406T204859	20160406T213345	1421
GAP_SM2W_006	20160411T073609	20160411T082128	1440
GAP_SM2W_007	20160416T190359	20160416T203429	5430
GAP_SM2W_008	20160418T033656	20160418T061350	9413
GAP_SM2W_009	20160427T044342	20160427T054012	3389
GAP_SM2W_010	20160428T202815	20160428T211847	3032
GAP_SM2W_011	20160430T024040	20160430T033332	3171
GAP_SM2W_012	20160511T050848	20160511T061652	4083
GAP_SM2W_013	20160515T033700	20160515T041307	2167
GAP_SM2W_014	20160515T043255	20160515T051723	1742
GAP_SM2W_015	20160518T123156	20160518T132016	2235
GAP_SM2W_016	20160518T132017	20160518T140627	2235
GAP_SM2W_017	20160519T165925	20160519T175127	3121
GAP_SM2W_018	20160523T074901	20160523T093227	6205
GAP_SM2W_019[5]	20160525T174918	20160525T184255	3218
GAP_SM2W_020	20160525T221015	20160525T225930	2956
GAP_SM2W_021	20160531T041755	20160531T051228	3272
GAP_SM2W_022	20160601T203453	20160601T221558	6064
GAP_SM2W_023	20160603T034422	20160603T043510	3048

[5] IPF Failure: "C2: retrack the waveforms"

GAP_SM2W_024	20160603T044023	20160603T052459	1784
GAP_SM2W_025	20160610T152805	20160610T160139	2014
GAP_SM2W_026	20160611T033700	20160611T041307	2167
GAP_SM2W_027	20160611T043255	20160611T051723	1743
GAP_SM2W_028	20160616T074422	20160616T081932	2110
GAP_SM2W_029[5]	20160617T110817	20160617T120145	3208
GAP_SM2W_030	20160617T185132	20160617T194233	3061
GAP_SM2W_031	20160618T235325	20160619T001755	1470
GAP_SM2W_032[5]	20160619T050936	20160619T060626	3410
GAP_SM2W_033	20160621T021941	20160621T024523	1542
GAP_SM2W_034	20160623T082335	20160623T093238	4143
GAP_SM2W_035	20160623T142737	20160623T174937	12119
GAP_SM2W_036	20160715T063236	20160715T090742	9305
GAP_SM2W_037	20160718T115651	20160718T133639	5987
GAP_SM2W_038	20160728T073549	20160728T091653	6063
GAP_SM2W_039	20160808T124106	20160808T143159	6653
GAP_SM2W_040[5]	20160810T184456	20160810T194232	3456
GAP_SM2W_041[7]	20160810T202640	20160810T212225	3344
GAP_SM2W_042[5]	20160812T083253	20160812T092823	3330
GAP_SM2W_043[5]	20160816T000311	20160816T005942	3390
GAP_SM2W_044	20160823T044021	20160823T053502	3281
GAP_SM2W_045[5]	20160826T114644	20160826T123924	3159
GAP_SM2W_046[6]	20160827T052116	20160827T061736	3379
GAP_SM2W_047[7]	20160830T054358	20160830T064002	3364
GAP_SM2W_048[5]	20160902T175645	20160902T185014	3209
GAP_SM2W_049[5]	20160904T065534	20160904T075107	3332
GAP_SM2W_050[5]	20160904T111305	20160904T120547	3162
GAP_SM2W_051	20161002T113411	20161002T122759	3227
GAP_SM2W_052	20161005T220028	20161005T225621	3353
GAP_SM2W_053	20161009T042144	20161009T051617	3272
GAP_SM2W_054	20161103T142514	20161103T151959	3284
GAP_SM2W_055	20161106T162912	20161106T172326	3254

[6] IPF Failure: "A25: compute parameters depending on surface type"

[7] IPF Failure: "C3: SAR retrakcing: Margin retracking"

GAP_SM2W_056	20161106T195219	20161106T204536	3197
GAP_SM2W_057	20161214T081747	20161214T091323	3336
GAP_SM2W_058	20161230T080256	20161230T085828	3332
GAP_SM2W_059	20170107T052900	20170107T062401	3300
GAP_SM2W_060	20170421T021051	20170421T030358	3187
GAP_SM2W_061	20170430T132406	20170430T142056	3409
GAP_SM2W_062	20170901T143100	20170901T162626	6925
GAP_SM2W_063	20171114T110928	20171114T125028	6059
GAP_SM2W_064	20171124T064737	20171124T074155	3258
GAP_SM2W_065	20171229T013712	20171229T023040	3208
GAP_SM2W_066	20180101T033517	20180101T052019	6302

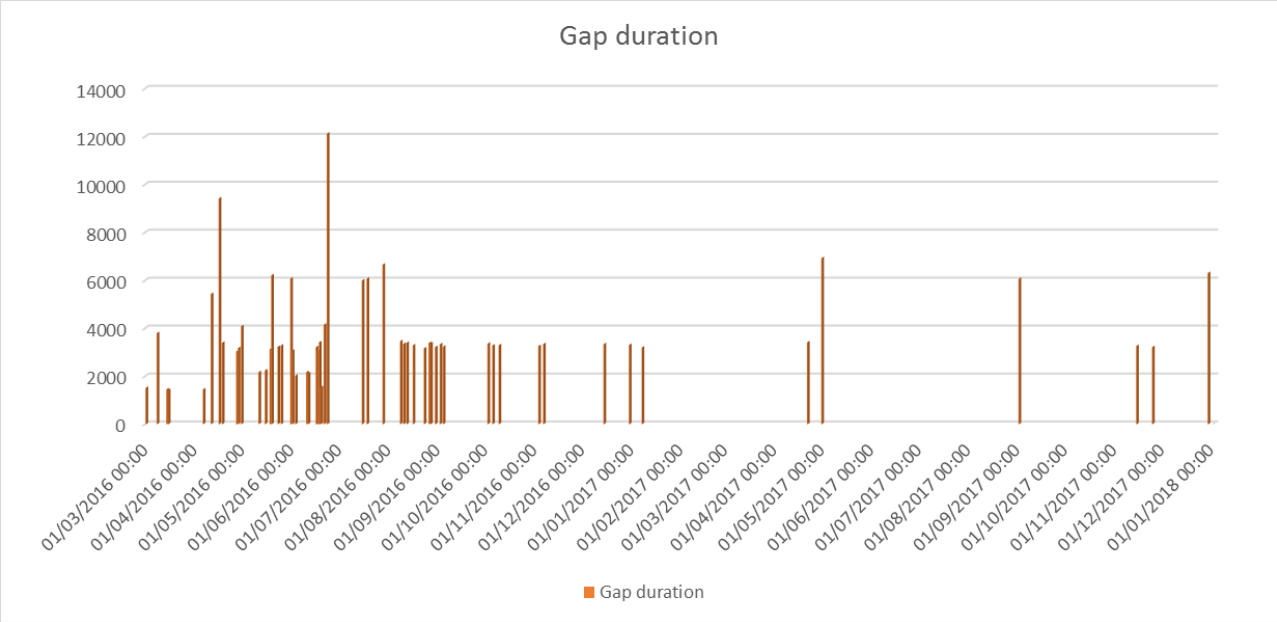

Figure 1 – SRAL L2 Gaps over time

4.3 Scientific Validation over Open Ocean

This Section provides the scientific validation over Open Ocean of the reprocessed data. When applicable, results from SAR mode and PLRM are comprised. Multi-satellite calibrations are also provided (e.g. with respect to the reference mission Jason-3). The differences between the current and previous datasets is also given.

4.3.1 Screening criteria

The results available in this document derived from RADS and STM tools. Different but coherent filtering criteria are used and provided in detail in Section 4.3.1.1 and Section 4.3.1.2. The filtering criteria used is shown next to the figures. If no filtering criteria is used, this is also stated.

4.3.1.1 RADS criteria

In the analysis, we have screened out all the following points:

- in coastal zone
- covered by sea ice
- impacted by rain
- |sea level anomaly| > 3 m
- dry tropo correction < -2.4 m or > -2.1 m
- radiometer wet tropo correction < -0.6 m or > 0.0 m
- dual-frequency iono correction < -0.4 m or > 0.04 m
- |MOG2D DAC| > 0.4 m
- |GOT4.10 ocean tide| > 5 m
- |SSB| > 1 m
- SWH > 8 m
- sigma0 < 6 dB or > 27 dB
- rms of 20-Hz range > 0.4 m
- rms of 20-Hz SWH > 2.1 m
- rms of 20-Hz sigma0 > 1 dB
- number of 20-Hz measurements to construct 1-Hz measurements < 17

4.3.1.2 STM Tools criteria

In the analysis, we have screened out all the following points:

- | Latitude | > 66
- Distance to Coast < 10Km
- | SSHA | > 1m
- SWH > 15m
- Affected by Rain

4.3.2 Sentinel-3A SRAL Initial Phase

In this Section recaps the major anomalies and limitations which have been raised in the Sentinel-3A STM in the early mission phase and their impact the STM data quality is shown.

4.3.2.1 MWR Calibration Timeline

Starting from the switch-on (29-Feb-2016), the MWR radiometer was initially configured to have a special calibration timeline designed to assess the preliminary performance of the instrument. This initial calibration timeline featured a calibration sequence every 27 seconds, and each calibration sequence was 13 seconds long. Such a calibration timeline resulted in consecutive 23 seconds gaps in the wet tropo correction every 5 seconds of valid data, and thus having a major impact in SSHA data availability.
In order to overcome this limitation, users are advised to use the ECMWF model wet tropo correction for all the time during which the initial calibration timeline was in place.

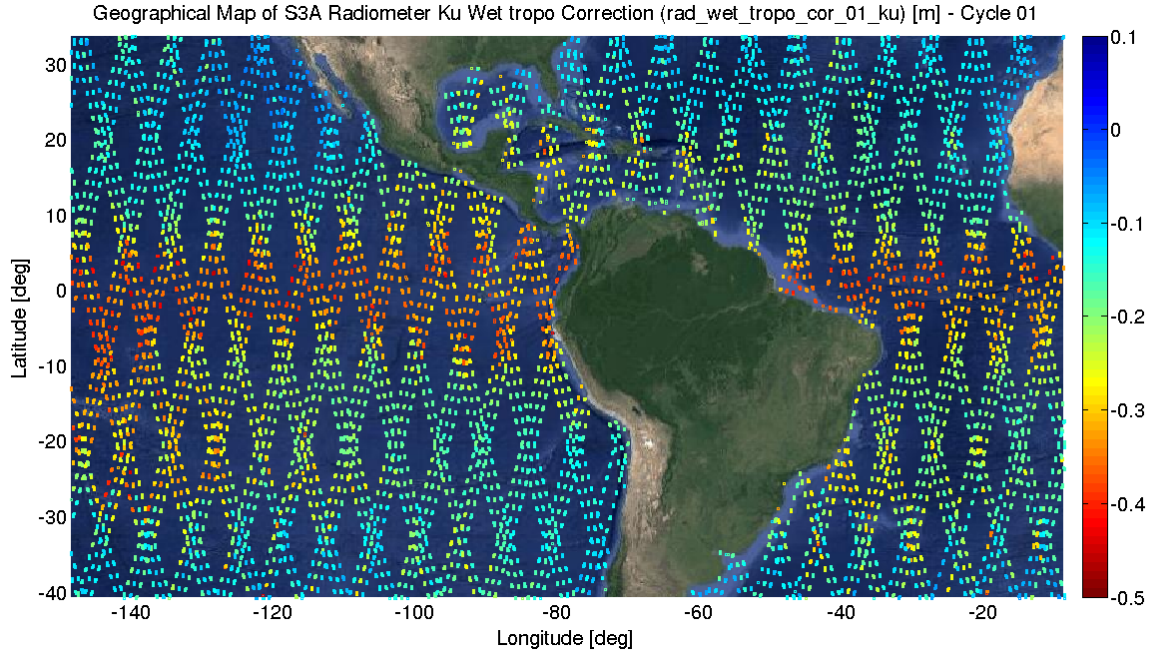

Figure 2 – Data gaps (23 seconds long) in the MWR Wet Tropo Correction as consequence of the initial MWR calibration timeline. The segments of valid data are 5 seconds long.

On 2016-03-17 13:26:24 UTC time, the initial MWR calibration timeline was updated to have 3 calibration sequence per orbit, each of them 9 seconds long. This calibration timeline gives rise to only 3 gaps of 15 seconds per orbit in the MWR wet tropospheric correction.

Finally, on 2018-03-01 08:19 UTC Time, the MWR calibration timeline was updated to have a calibration sequence every 30 seconds, each of them is now 0.6 seconds long. After this last update, the MWR wet tropospheric correction does not exhibit anymore temporal gaps.

Gaps in the MWR's Wet tropospheric correction will generate gaps in the SSHA calculated in the L2 products.

4.3.2.2 Sentinel-3A Attitude Mispointing

Because of a misconfiguration of the Sentinel-3A Star Tracker sensor subsystem (MH-STR), the Sentinel-3A platform initially was mispointed with respect the geodetic reference system. This anomaly has been corrected on 4 April 2016 13:56:00 UTC time.

Nevertheless, the Sentinel-3A POD platform files, during the early mission phase, are still not showing the true mispointed values in pitch, roll and yaw angles because those POD platform files have not been reprocessed yet taking into consideration the anomaly's solution.

Because of such mispointed attitude and inaccurate POD platform files, the SAR L2 measurements exhibit degraded performance up to 4 April 2016. Also the pitch, roll and yaw platform angles in the L2 products are hence inaccurate up to 4 April 2016.

The LRM/PLRM waveform off-nadir angle from ML4 retracker shows an offset of 0.045 degrees with respect the local vertical direction until 4 April 2016.

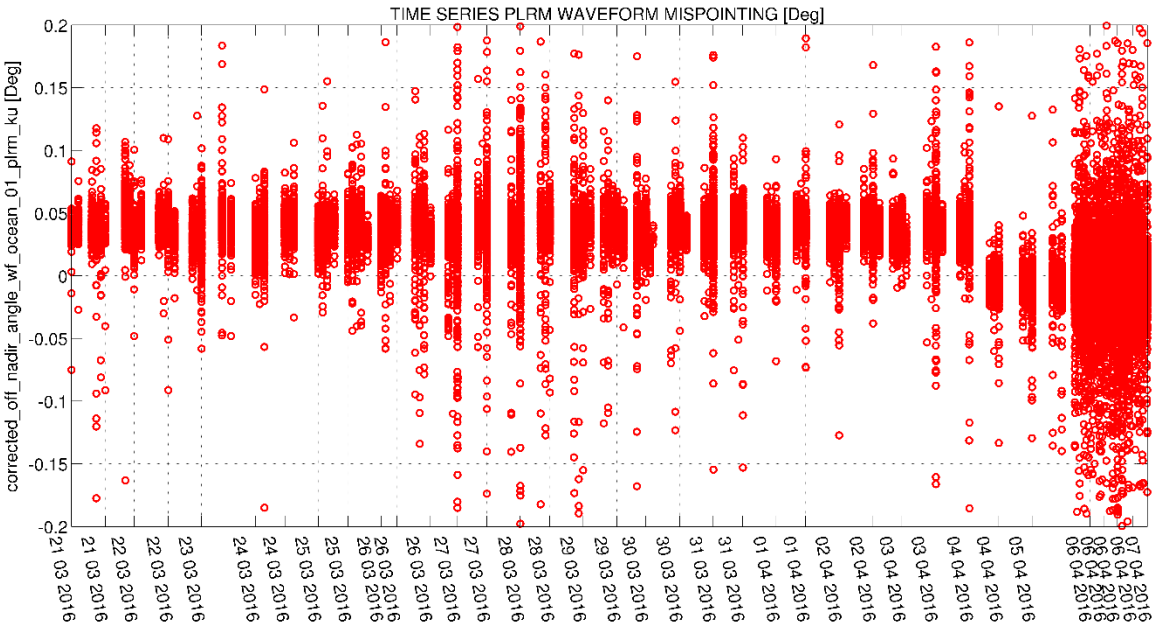

Figure 3 – Time Series of PLRM waveform off nadir angle

Figure 4, Figure 5 and Figure 6 display the effect of the anomaly's correction occurred on 4 April 2016 respectively for SSHA, SWH and sigma nought. From it, we can understand how, until it was corrected, the anomaly has introduced a bias of –2 cm in SAR range, a bias of +10 cm in SAR SWH and a bias of –0.045 dB in SAR sigma nought.

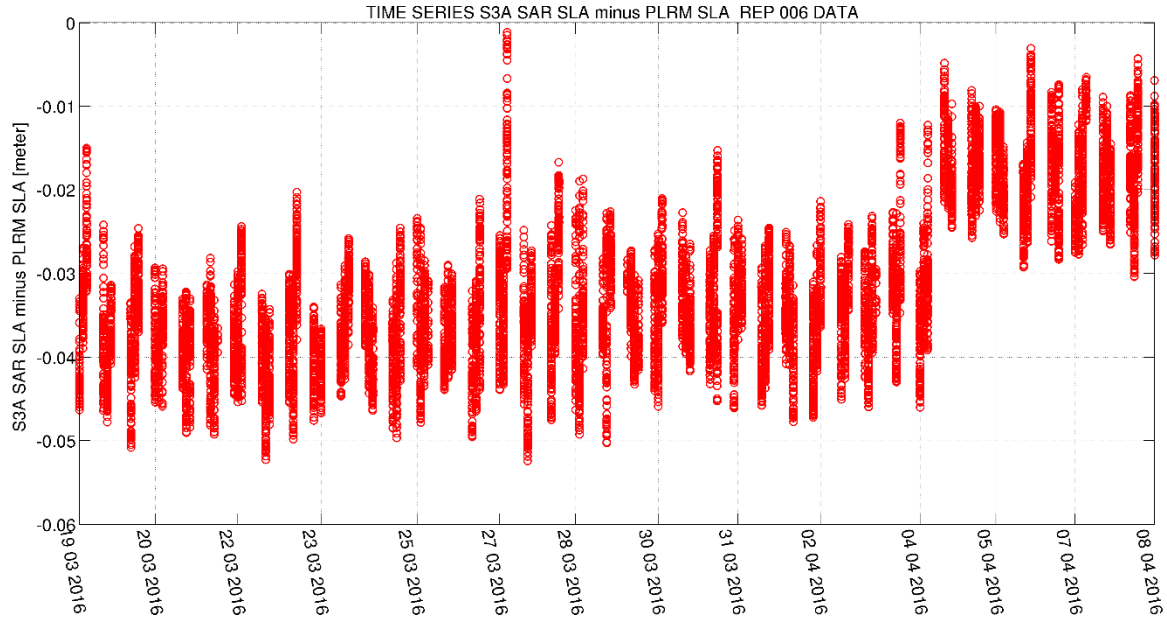

Figure 4 – Time Series of Difference between SAR SSHA and PLRM SSHA

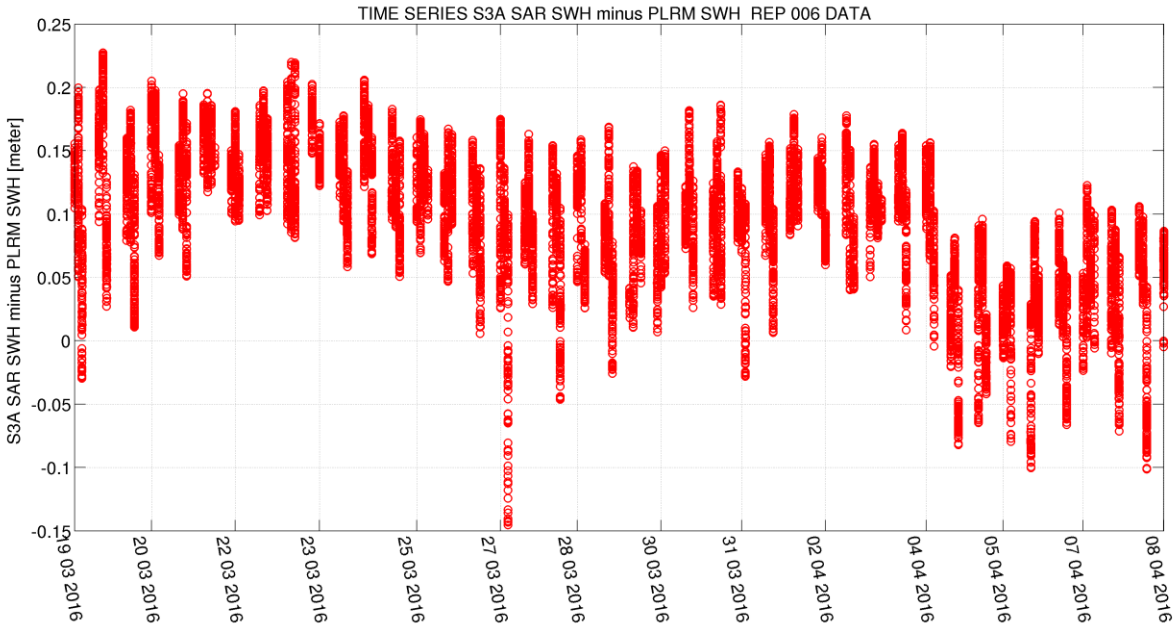

Figure 5 – Time Series of Difference between SAR SWH and PLRM SWH

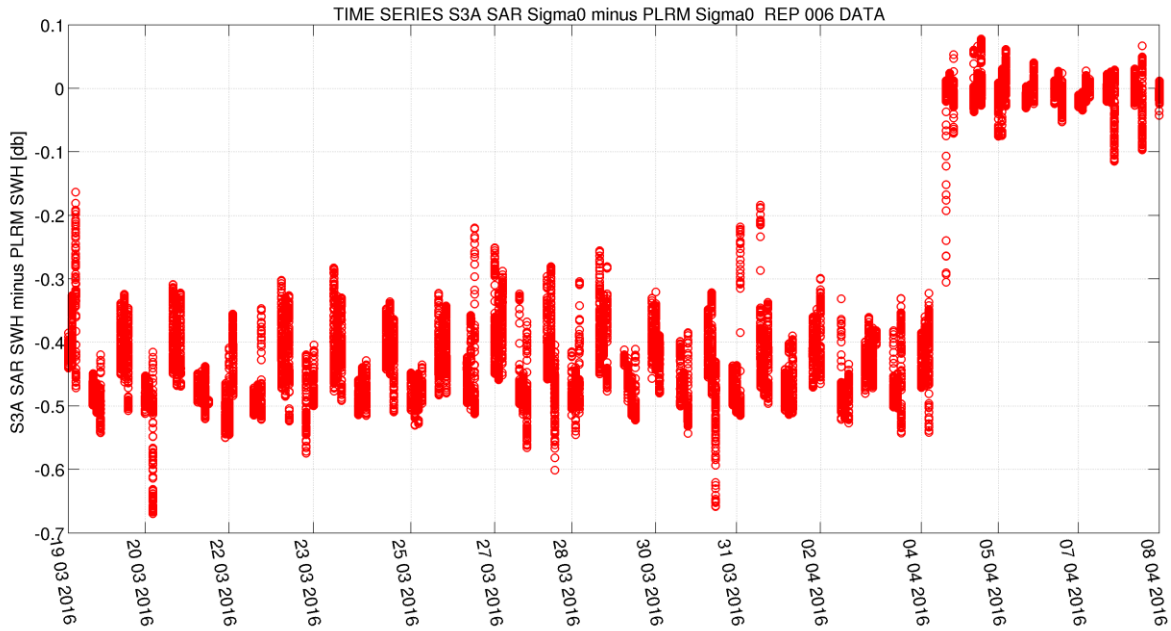

Figure 6 – Time Series of Difference between SAR Sigma nought and PLRM Sigma nought

Work is on-going to try to recover this anomaly for future reprocessing campaigns.

4.3.2.3 LRM processing issues

Inspecting the Ku LRM dataset, the following IPF anomalies have been identified:

- 20 Hz LRM SSHA (ssha_20_ku) is always set to Fill value (EUM/Sen3/NCR/4165)[8]
- 20 Hz LRM altimeter-derived Ionospheric Correction (iono_cor_alt_20_ku) is always set to Fill Value
- The field "elevation_ocog_20_ku" is always set to Fill Value in LRM mode(EUM/Sen3/NCR/4164)[8]
- the field "elevation_ice_sheet_20_ku" is set very often (99.99%) set to Fill Value in LRM mode (EUM/Sen3/NCR/4166) [8]
- Sea Ice Concentration (sea_ice_concentration_20_ku), Snow Depth (snow_depth_20_ku), Snow Density (snow_density_20_ku) are always set to Fill Value in LRM mode (EUM/Sen3/NCR/4144)[8]
- The fields "range_ocog_20_ku" and "sig0_ocog_20_ku" are often (around 7%) set to Fill Value in LRM mode over open ocean (EUM/Sen3/NCR/4167)[9]

[8] Closed as part of PB 2.33 (not available in this reprocessing)

[9] Anomaly not yet closed.

4.3.2.4 Erroneous Centring of the Return Waveform in Open Loop Tracking Mode

In the Sentinel-3A SRAL early mission phase the return waveform, in Open Loop Tracking Mode, was not centered around range sample 44 (as expected) but erroneously around range sample 40. Such a bad-centering has had an impact on the PLRM/LRM estimation of the waveform thermal noise and waveform off nadir angle.

This anomaly was fixed with a patch of SRAL sensor on 22 June 2016.

In Figure 7 and Figure ***8***, the waveforms for the two passes with the same relative orbit number 381 but respectively for Cycle 02 and Cycle 26 are displayed. The waveforms for the plot in Figure 7 in Cycle 02 (8th April 2016) are centred around range sample 40 whereas the waveforms at same geo-position for Cycle 26 (16th Jan 2018) is centred at range sample 44.

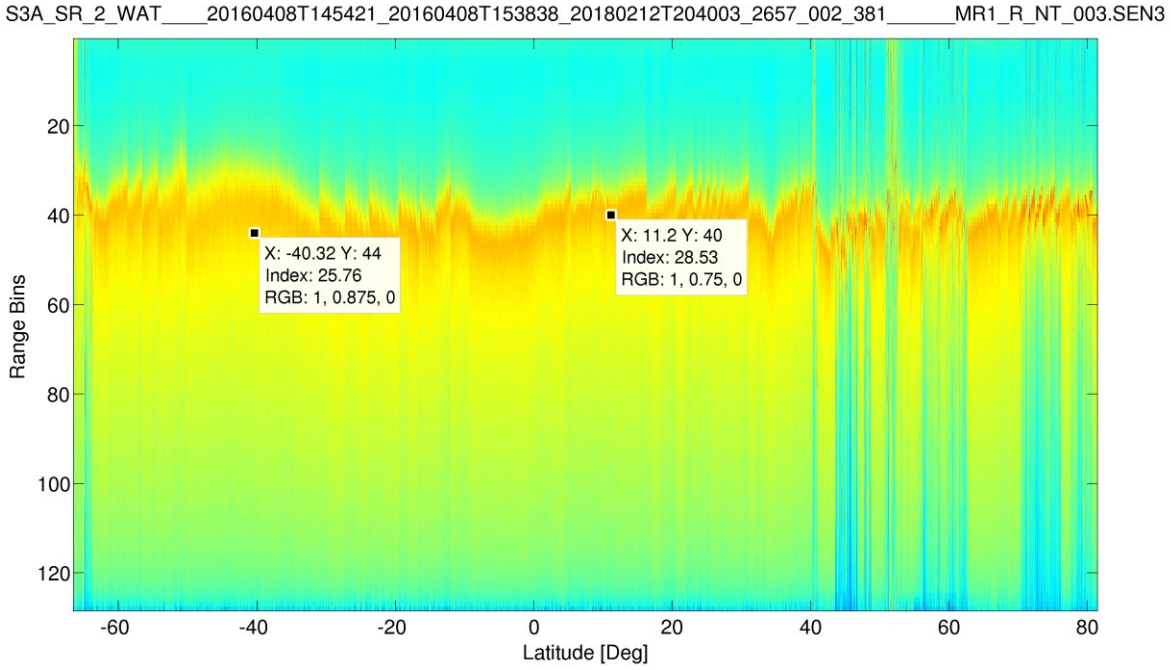

Figure 7 – SAR Waveforms for Product with Relative Orbit Number 381 in Cycle 2 (8th April 2016)

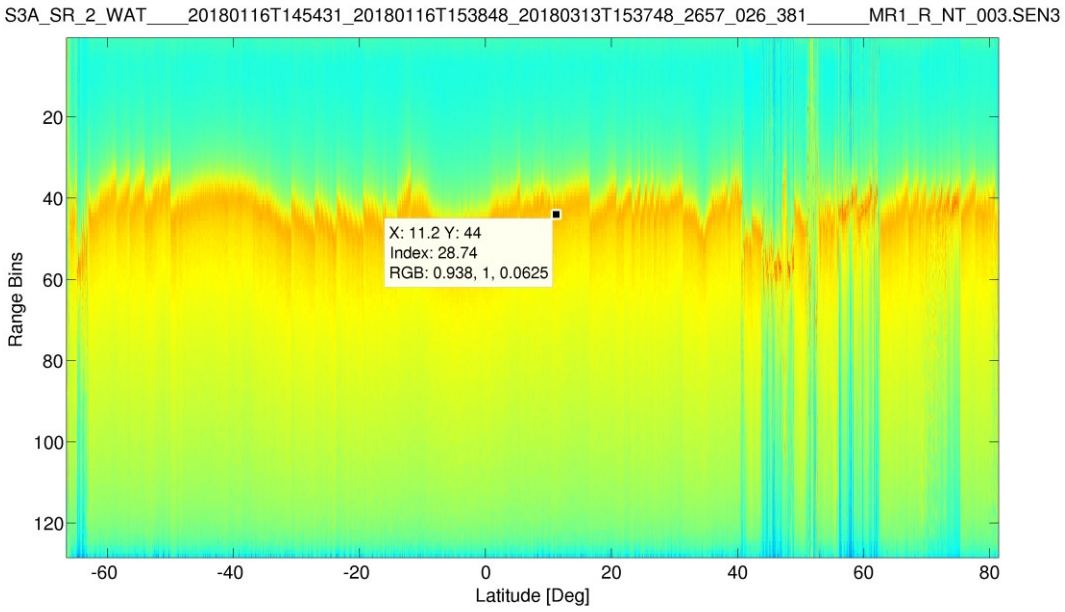

Figure** 8 – **SAR Waveforms for Product with Relative Orbit Number 381 in Cycle 26 (16 Jan 2018)

As consequence of this anomaly, the PLRM/LRM data are slightly degraded prior 22 June 2016 while SAR Data are expected to be not affected.

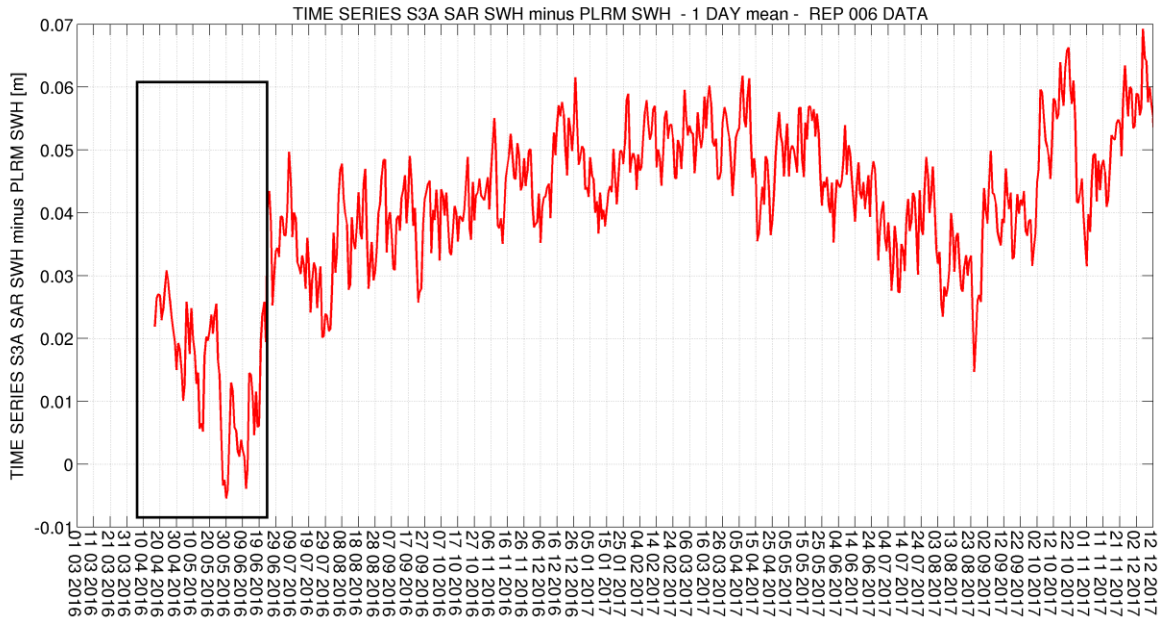

Figure 9 – Discontinuity (square-boxed) in the Time Series of the Difference SAR SWH and PLRM SWH occurred on 22 June 2016

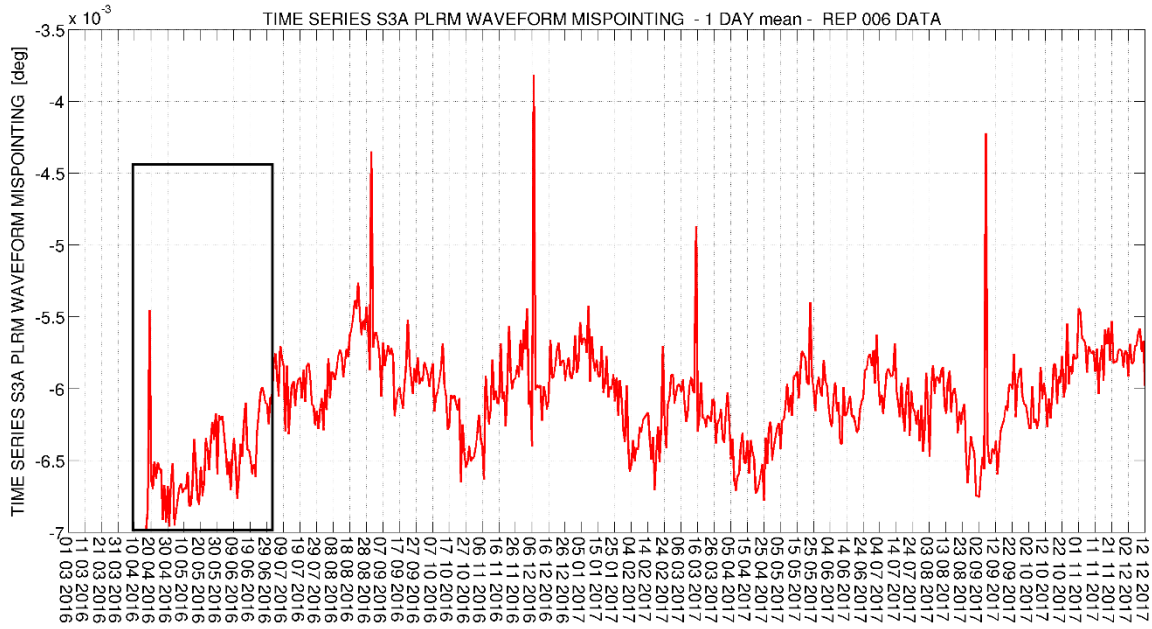

Figure 10 – Discontinuity (square-boxed) in the Time Series of the PLRM waveform off-nadir angle occurred on 22 June 2016

4.3.2.5 Space Wire ASIC Anomaly

Starting from 16 April 2016, there was an anomaly on the transmission of data from SRAL Digital Processing Unit (DPU) to Satellite Payload Data Handling Unit (PDHU) through the Space Wire link, resulting in sporadic losses of science packet data and occasionally in the breaking of the continuity of 4 consecutive bursts in a radar Cycle. This anomaly was fixed on 23 June 2016 09:30:20 UTC Time.

In case of occurrence of this anomaly, the L1b product, in which the anomaly is occurring, cannot be processed in the processing baseline 2.27. The anomaly in the IPF will be mitigated in the next reprocessing baseline.

4.3.2.6 OLTC Table Anomalies

The OLTC version 4.0 had an anomaly in the OOP (On Orbit Position) time coordinate. This has resulted in:

- Up to 15 km geo-location errors for ascending orbits in the tracking commands

- Up to 25 km geo-location errors for descending orbits in the tracking commands

The OLTC v.4.1 on board upload has started on 23 May 2016 10:06 and it was completed on 24 May 2016 12:20 UTC time.

The OLTC v4.1 did not allow a correct return waveform tracking over the Salar Uyuni lake. In order to be able to measure the Sala Uyuni Lake level, OLTC v4.2 was prepared and the upload on board was carried out on 22 June 2017 08:54 UTC time.

We remind that OLTC v4.2 still features some errors in the tracking commands when crossing the Greenwich Meridian.

4.3.2.7 Measurement Mode Timeline in the Sentinel 3-A SRAL Early Phase

From the time of the switch-on (1 March 2016) to 5 April 2016 23:59:59, SRAL Sensor was commanded nominally in LRM measurement mode globally, except for the two geographical patches:

- [160 W 85 W, 3 S 25 S] (South Pacific Ocean Patch)
- [12 W 2 W, S 13 19 S] (South Atlantic Ocean Patch)

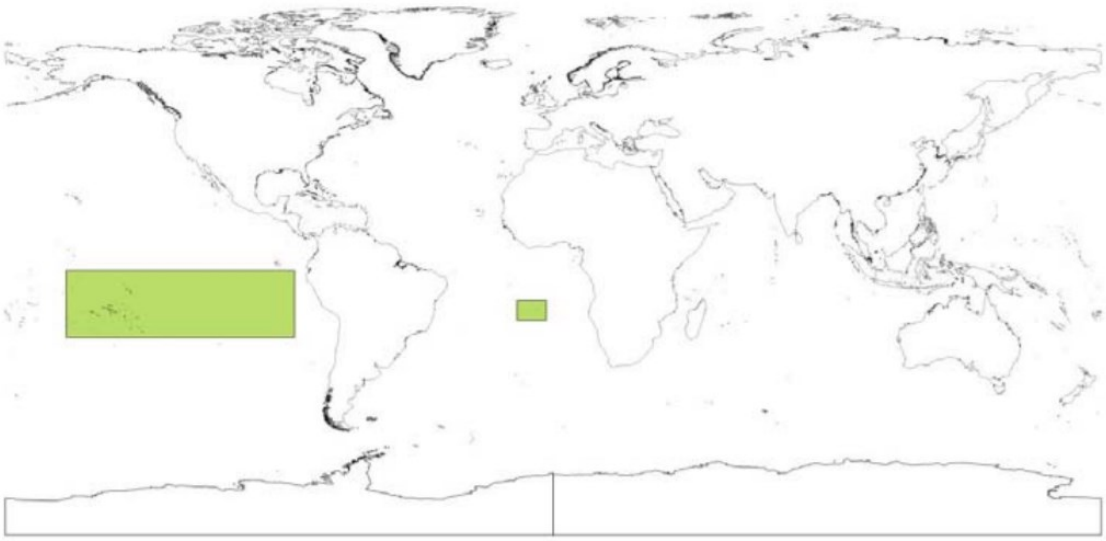

Figure 11 – Geographical Location of the two patches where SRAL Sensor was commanded in SAR mode

Within these areas (green in Figure 11) SRAL was operating in SAR measurement mode.

On 6 April 2016 00:00:00, the SRAL Sensor was commanded in global SAR mode until 08 April 2016 23:59:59. During these 3 days of SAR mode, the SRAL calibrations have been suppressed.

After this time, the SRAL sensor was commanded again in global LRM + SAR mode in the two geographical patches as in Figure 11.

On 12 April 2016 09:30:00 UTC time, the SRAL sensor has been commanded to global SAR measurement mode.

4.3.2.8 Tracking Mode Timeline in the Sentinel 3-A SRAL Early Phase

From the time of the switch-on (1 March 2016) to 6 April 2016 23:59:59, SRAL Sensor was commanded nominally in closed loop tracking mode.

On 7 April 2016 00:00:00 a full day of SAR open-loop/closed-loop transitions with a simplified ZDB (Zone Database) was commanded.

On 8 April 2016 00:00:00, SRAL sensor was commanded in open-loop mode globally.

On 9 April 2016 00:00:00, SRAL sensor was commanded in closed-loop mode globally.

On 15 April 2016 11:03:03 UTC time, SRAL sensor was commanded in open-loop/closed-loop transition mode according the ZDB in Figure 12.

Between 23 May 2016 10:06 UTC Time and 24 May 2016 12:20 UTC time, SRAL was commanded in closed-loop globally for the ongoing update of the OLTC v4.1 Table.

On 6 December 2016 14:00 UTC Time, the Zone Data Base was updated in order to avoid the data loss (non-recoverable) at the Ice Margins in Antarctic and Greenland.

On 27 November 2017 18:00 UTC Time, the the Zone Data Base was updated in order to avoid data loss (non-recoverable) when Crossing the Greenwich Meridian.

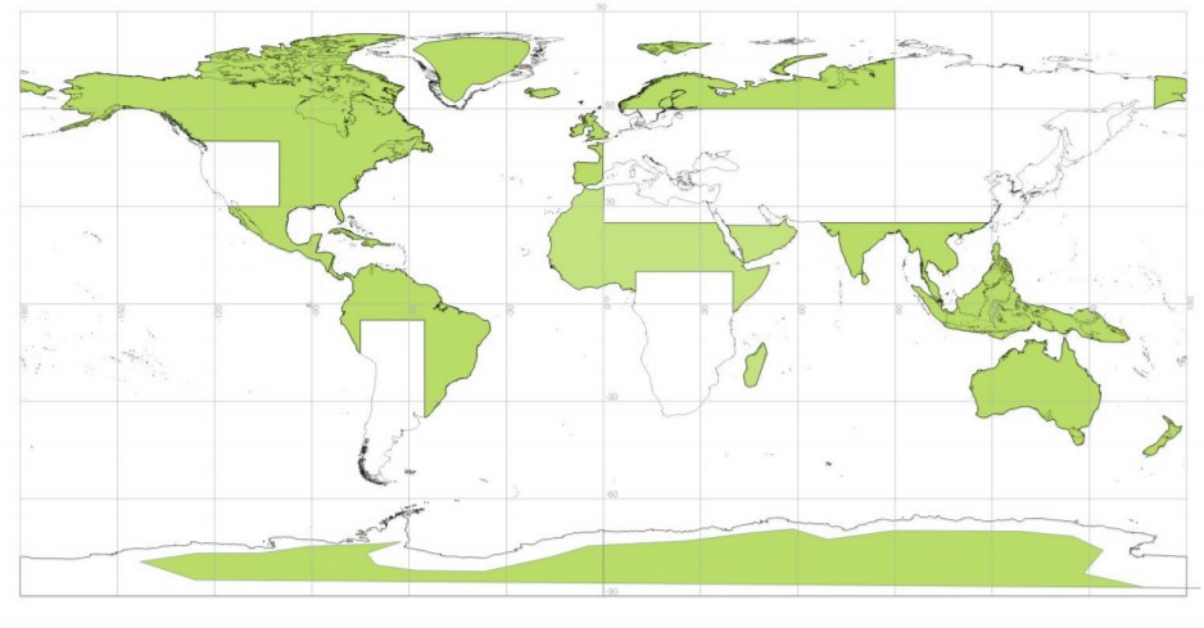

Figure 12 – Zone Database (ZDB) in place between 12 April 2016 09:30:00 UTC and 06 December 2016 14:00 UTC. Green is closed-loop and white is open-loop

4.3.2.9 Platform Guidance Mode Timeline in the Sentinel 3-A SRAL Early Phase

The nominal platform guidance mode (GDC_YED, Geodetic with yaw steering) was swapped to another (non-nominal) guidance mode at the following times:

- GDC_YEO (Geocentric with yaw steering): since 21/3 13:20 until 21/3 21:40
- GDC_GEO (Geocentric without yaw steering): since 21/3 21:40 until 22/3 06:00
- GDC_GED (Geodetic without yaw steering): since 22/3 06:00 until 22/3 14:20

4.3.2.10 Processing LRM data with PLRM configuration

The LRM data have been processed using the LUTs and the retracking configuration parameters (as sigma nought bias) which have been tuned for the PLRM measurement mode. Hence slightly sub-optimal performance in LRM mode is expected.

4.3.2.11 Overall recommendation for the early phase

From all the above issues present in the early stage of the S3A mission, the usage of the data, prior to Cycle 6 (started 2016-06-28) is discouraged, except for expert users. Further studies on how to bring these less than 4 months on par, in terms of quality, with the rest of the mission are on-going.

4.3.3 Sea Surface Height Anomaly

In the case of Sentinel-3, the Sea Surface Anomaly (SLA) is named Sea Surface Height Anomaly (SSHA), but it is equivalent to the SLA definition of other altimetry missions.

4.3.3.1 SSHA wavenumber spectrum and precision plot

The estimated 1-Hz range noise in Cycle 15 is 1.07 cm for SAR and 1.76 cm for PLRM (as expected, SAR being more precise than PLRM) at a value of SWH of 2 m.

It is noted how the SAR range noise level is slightly higher than the one in the previous reprocessing campaign (i.e. 1.05 cm) for the same Cycle.

This slight increase is attributed to the still-present imperfect range-alignment of the most outer Doppler Beams in the stack. Because in the new processing baseline the number of accumulated Doppler beams is 180 in place of 174, the most outer Doppler beams get accumulated in building the SAR return waveform. The imperfect range-alignment of the most outer Doppler Beams in the stack is due to the missing application of the SAR intra-burst correction in the L1b IPF processing. The range noise level of PLRM mode is unchanged.

This observation is also confirmed at wavenumber spectrum level. Figure ***13*** shows that the new reprocessing campaign improves the range data quality at long and medium scale, as well as allows to observe again the slight increase of random noise at short scale (less than 10 km).

SAR ranging shows to be more precise than PLRM ranging as depicted in Figure 14, where 20 Hz SSHA for Cycles 14 and 15 is computed and compared. The same figure also allows for demonstrating that SAR mode is able to observe the sea surface more accurately than PLRM at scales shorter than 100 km. As expected, the “spectral bump” between roughly 5 and 50 km wavelengths is visible in the PLRM spectrum, but not in SAR.

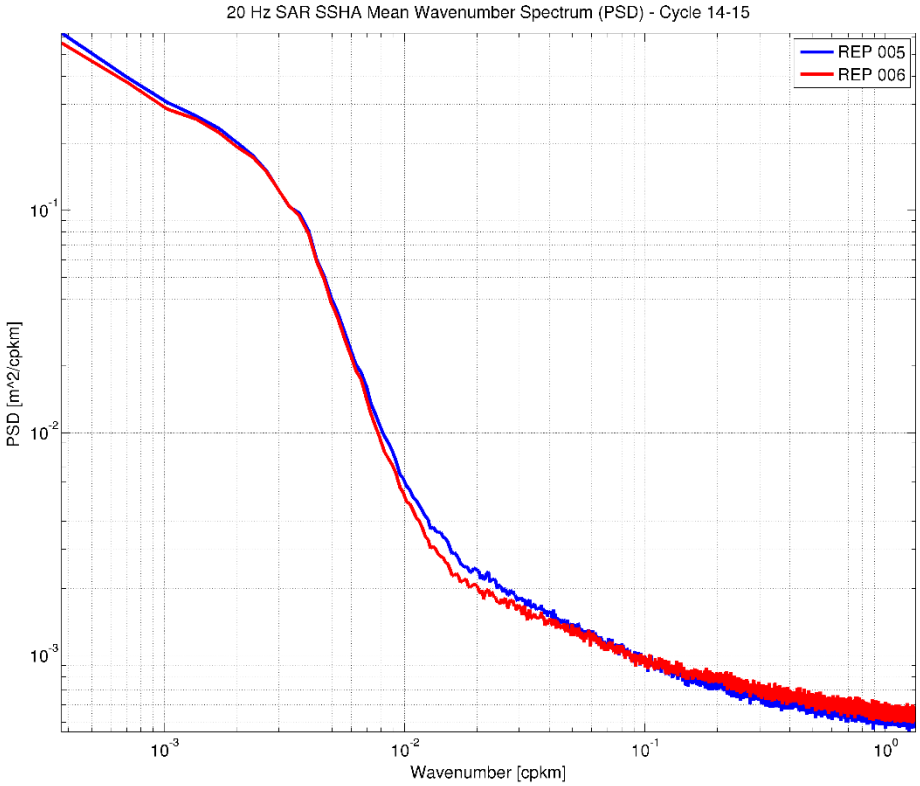

***Figure** 13 – 20-Hz SSHA averaged wavenumber spectrum for Cycles 14, and 15, comparing the new reprocessing (006) and the previous one (005).*

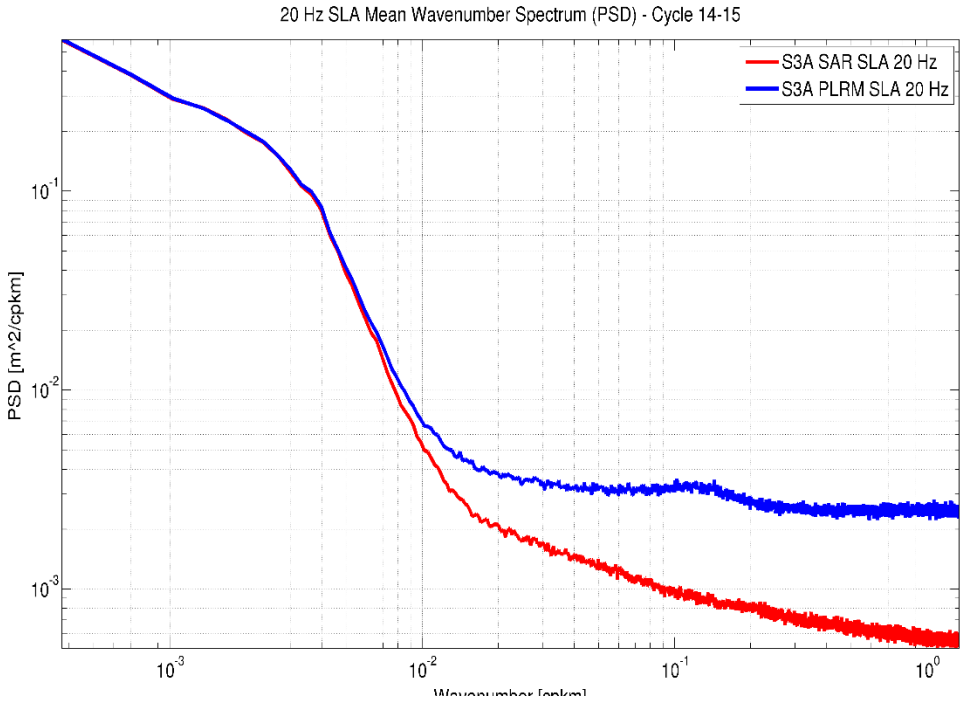

Figure 14 – 20-Hz SSHA averaged wavenumber spectrum for Cycles 14 and 15.

4.3.3.2 Comparison S3 SAR versus S3 PLRM

Here, we have analysed the 1-Hz SSHA measurements during Cycle 15. The scatterplot between SAR sea level anomaly (uncorrected) and PLRM sea level anomaly (uncorrected) shows a very good level of consistency between the two datasets (standard deviation of the differences about 3.5 cm, regression slope of 1.004, bias around –1.1 cm). We have decided to analyse the uncorrected sea level anomalies in order to not be impacted by different geophysical corrections between the two datasets (as sea state bias).

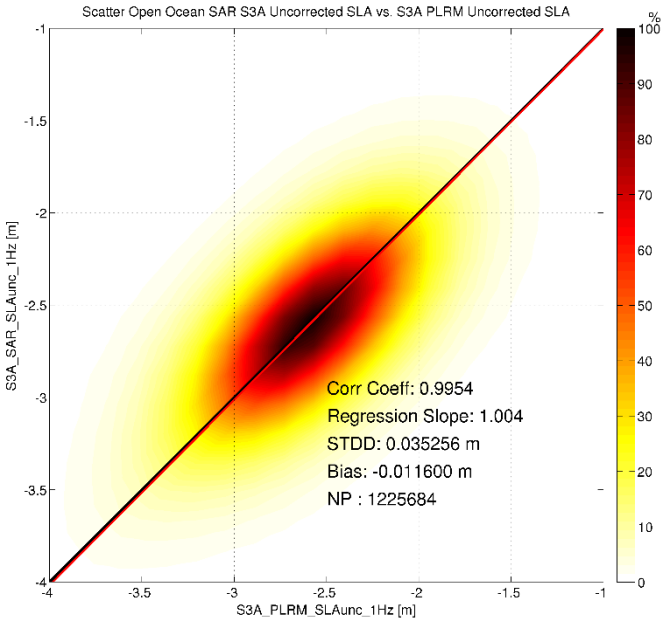

Figure 15 – Scatterplot of uncorrected SSHA, SAR versus PLRM (during Cycle 15). The colours indicate point density.

We highlight that the STDD (standard deviation of the difference) between SAR and PLRM uncorrected SSHA in Cycle 15 has improved in the new reprocessing campaign (it went from 3.7 cm to 3.5 cm).

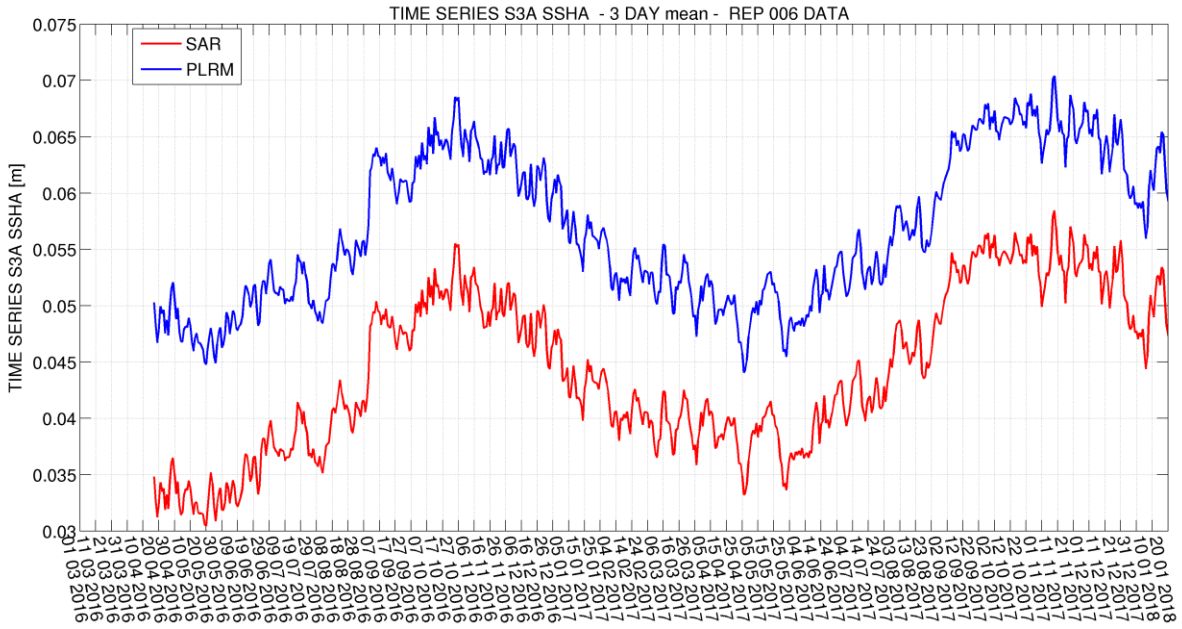

Figure** 16 – **Time Series of SSHA mean, as retrieved by S3 SAR (red) and S3 PLRM (blue).

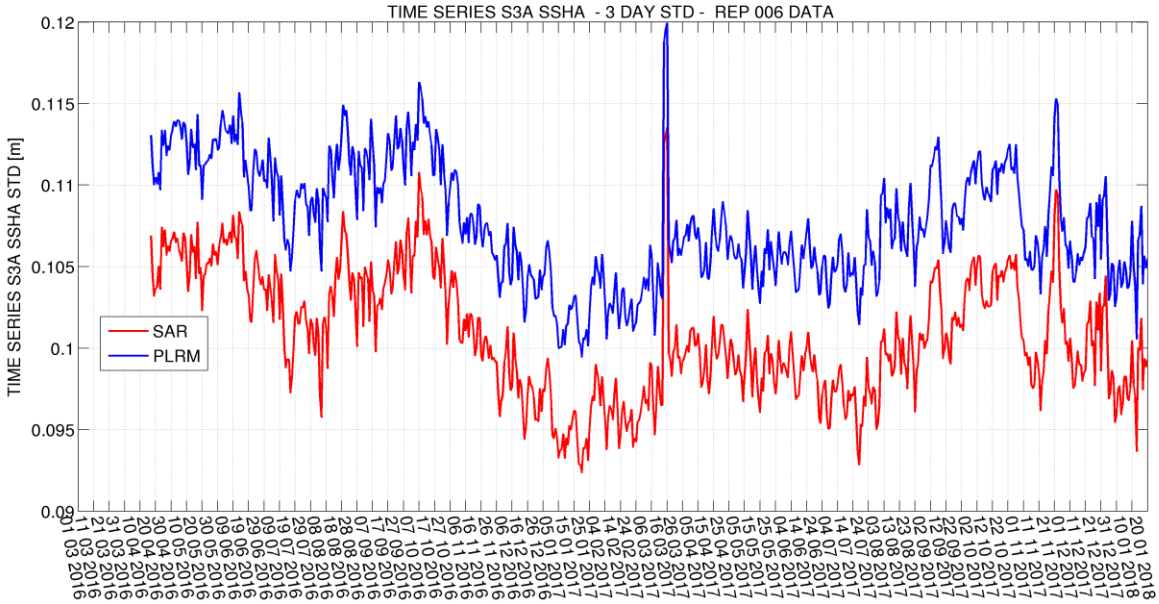

Figure 17 – Time Series of SSHA std in SAR mode (red curve) and PLRM mode (blue curve).

Figure 16 depicts the time series for the mean SSHA as derived by SAR and PLRM. The mean is computed every 3 days. The RADS filtering criteria is applied.

Figure 17 illustrates the time series for the standard deviation (std) as derived by SAR and PLRM. Results are computed over 3-day periods. The SAR SSHA std is significantly lower than PLRM SSHA std: the average value for SAR SSHA std is 9.90 cm whereas the average value of PLRM SSHA std is 10.6 cm.

Figure 18 shows the geographical comparison between SAR and PLRM for Cycle 14. The figures demonstrate that there is no specific pattern for ascending or descending passes. The

differences between SAR and PLRM are small. PLRM sees slight higher Sea Level than SAR (average difference of 2.99 cm without any data filtering).

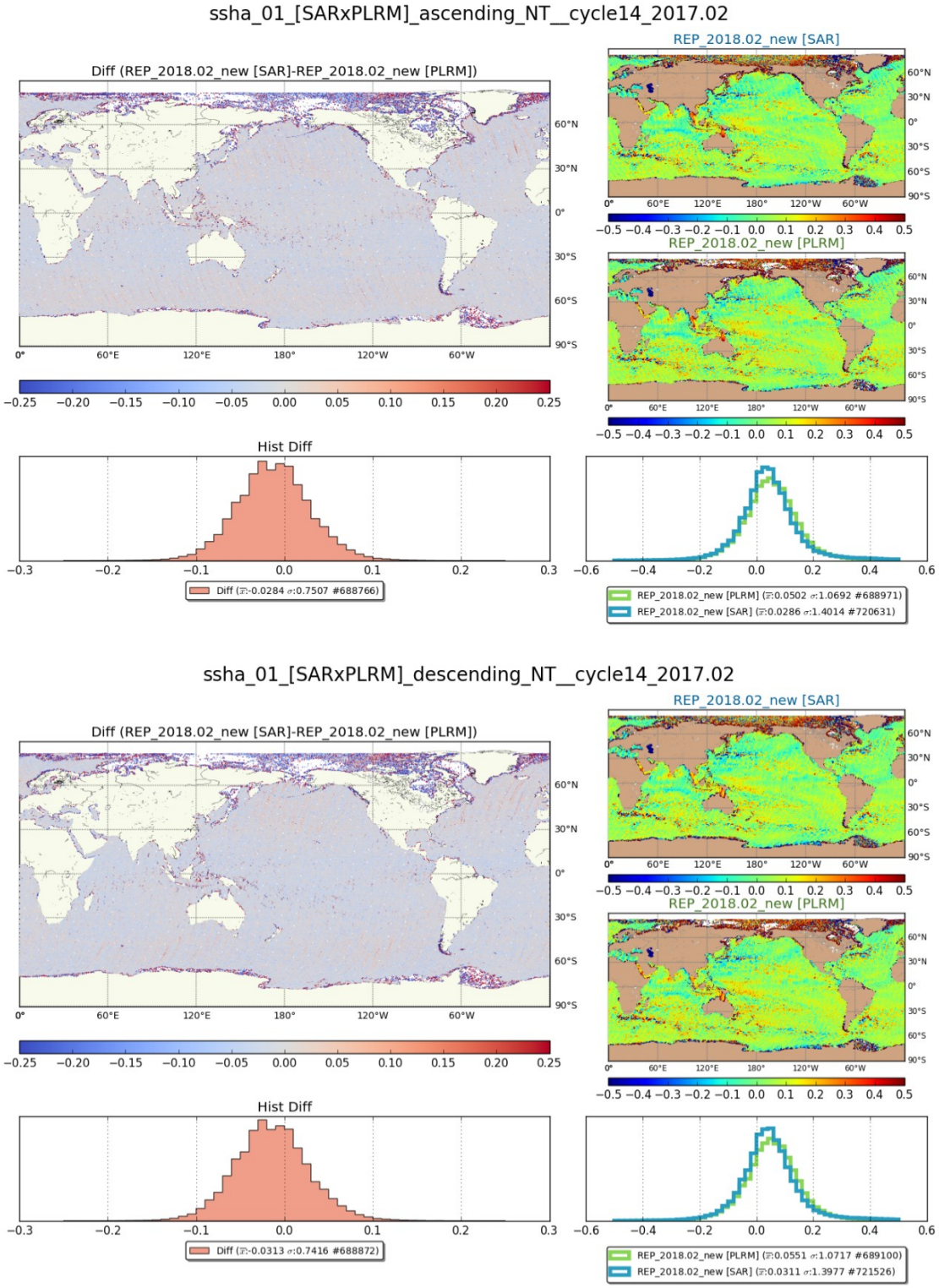

Figure 18 – SSHA: Geographical comparison between S3 SAR and PLRM. Ascending (top image), descending (bottom image).

4.3.3.3 SSHA SAR minus PLRM dependency on SWH

The consistency between SAR and PLRM SSHA has improved in the new processing baseline: the density plot of the difference between SAR and PLRM as a function of SWH highlights how in average the difference between the two modes are negligible up to 4 m. After 4 m SWH, differences show as ascending trend function of SWH. The slope of the median curve of the cloud is reduced to 0.23% from 0.5% when passing from the previous processing campaign to the new processing campaign.

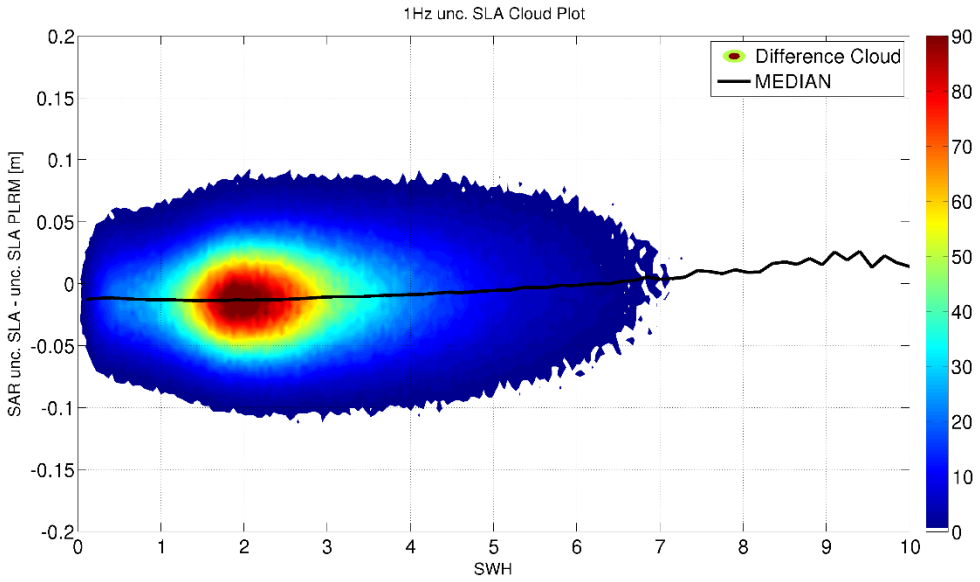

Figure 19 – Point density of the difference in uncorrected SSHA between SAR and PLRM as a function of SWH, Cycle 15. Uncorrected SSHA is Altitude – Range – Mean Sea Surface.

4.3.3.4 Range Drift

The difference of SAR and PLRM SSHA drifts in time. The drift slope is **+1.72 mm/year** from 23 June 2016 to 20 Jan 2018. The screening criteria used to reach this result is the RADS criteria listed in 4.3.1.1. The data start time is set to 23 June 2016 in order to avoid the known anomalies in the early mission phase (see Section 4.3.2). The source of this drift is presently unknown. Nevertheless, the uncorrected SSHA (i.e. orbit altitude – range – mean sea surface) already shows a drift between both operational modes for the same time period of **1.46 mm/year** (see Figure 21). Further investigations are ongoing to identify the source of the drift.

The following images within this Section refer to a time window from 23 Jun 2016 to 20 Jan 2018. The regression line is traced for the complete S3A period, but the values used to calculate the linear regression slope are only the ones belonging to the stated window.

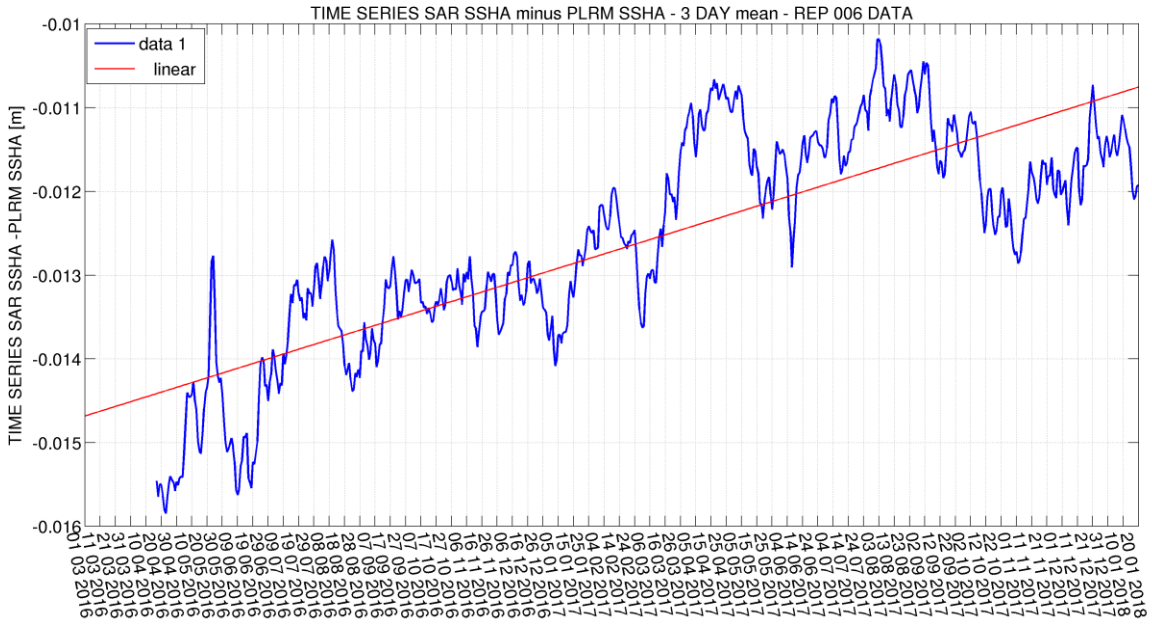

Figure 20 – Time Series of SSHA difference between SAR and PLRM. The regression line is traced for the complete S3A period, but the linear regression slope is only computed over 23 Jun 2016 to 20 Jan 2018.

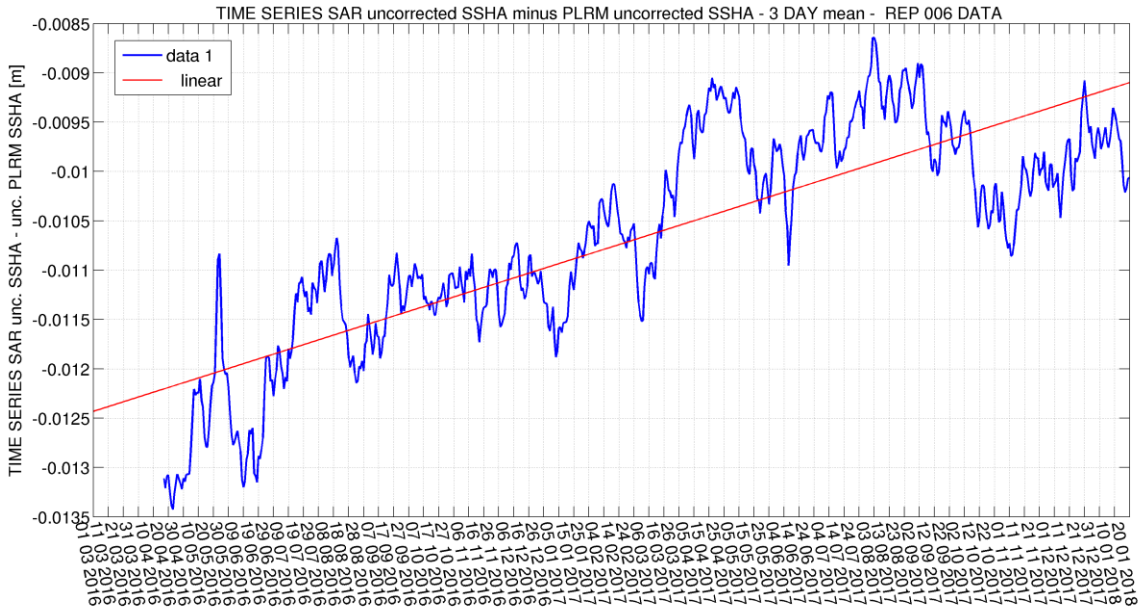

Figure 21 – Time series of uncorrected SSHA difference between SAR and PLRM. Uncorrected SSHA is Altitude – Range – Mean Sea Surface. The regression line is traced for the complete S3A period, but the linear regression slope is only computed over 23 Jun 2016 to 20 Jan 2018.

It is noted that the SSB (sea state bias) correction between SAR and PLRM mode is also drifting with a drift slope of -0.25 mm/year.

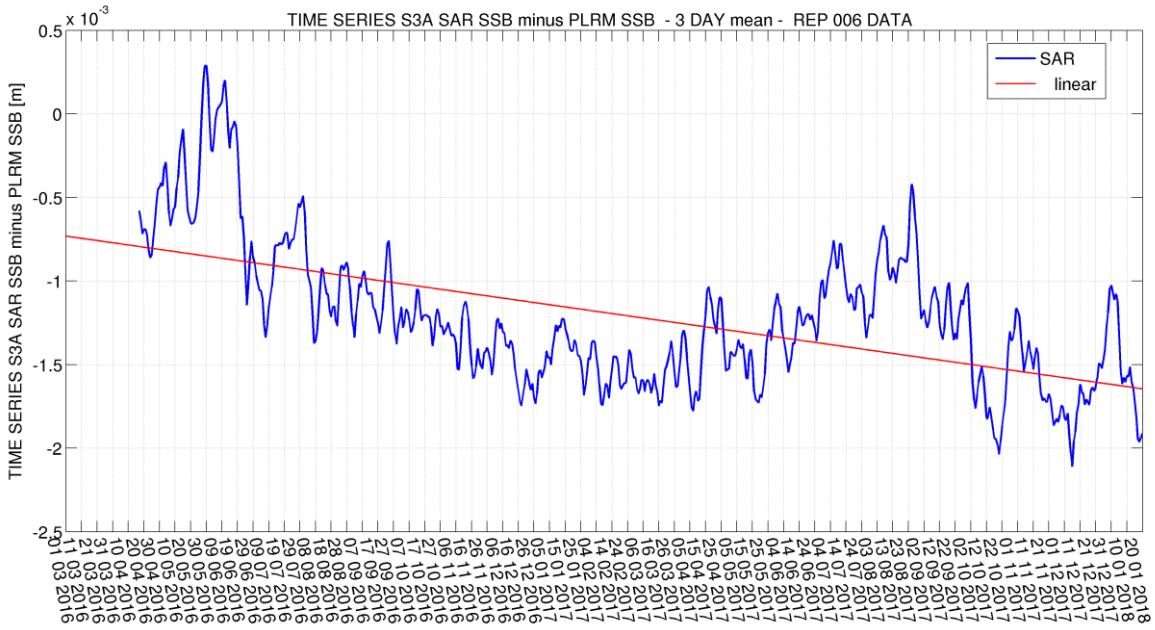

Figure 22 – SSB difference between SAR and PLRM. The regression line is traced for the complete S3A period, but the linear regression slope is only computed over 23 Jun 2016 to 20 Jan 2018.

Figure 22 shows how SAR and PLRM SSB results are slightly inconsistent prior to 22 June 2016. This issue will be discussed in Section 0.

4.3.3.5 Comparison with Jason-3

This Section is dedicated to the comparison of Sentinel-3A and Jason-3 SSHA. It shall be noted that Sentinel-3A and Jason-3 MSS models differ. The first, is using DTU15. The second, CNES/CLS11.

Moreover, to ensure that the statistical comparison is equivalent between Sentinel-3A and Jason-3 statistics are computed every 10 days (to emulate a Jason Cycle) and data coverage has been limited to ±66º latitude.

The 1-Hz SAR SSHA measurements show a bias in average of ~2 cm compared to J3 (see Figure 23 and Figure 24), as well as an ascending trend of 1.42 mm/year.

SSHA PLRM time series compared to J3 show a bias in mean of 3.5 cm and a negligible trend (see Figure 23).

PLRM vs SAR also depict a bias and a drift. The bias is in mean close to 1.5 cm and the drift between the operational modes is 1.82 mm/year. This is in agreement with the drift computed in Section 4.3.3.4 using 20-Hz SAR SSHA measurement (20-Hz SSHA drift being 1.72 mm), and thus results are consistent between the different validation techniques.

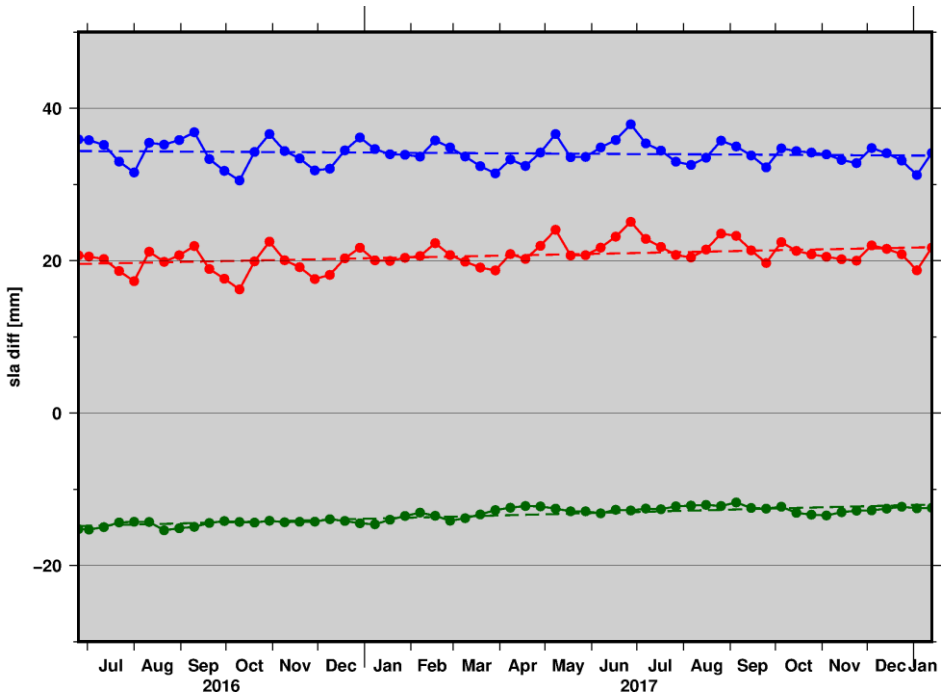

Figure 23 – SSHA differences between J3 and S3 SAR (red), J3 and S3 PLRM (blue) and S3 SAR and PLRM (green)

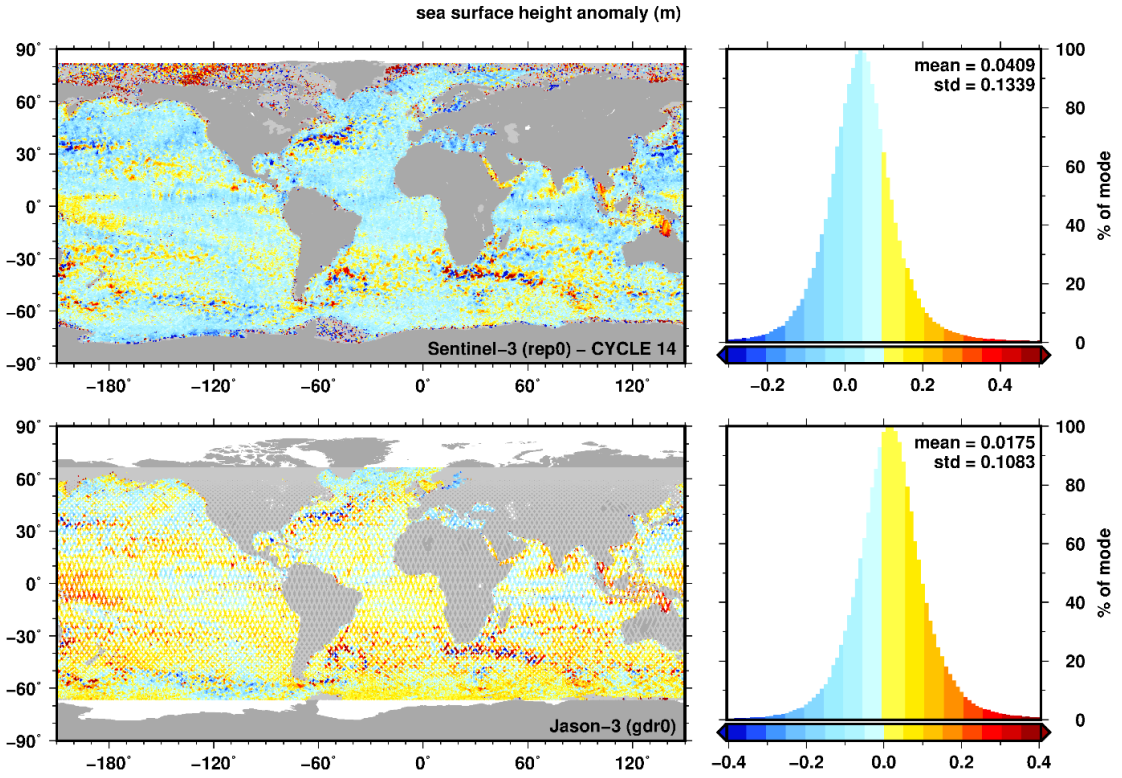

Figure 24 – SSHA cross-comparison between S3A (top), J3 (bottom) for S3 Cycle 14.

4.3.3.6 Comparison with previous datasets

Figure 25 summarises the different datasets delivered by EUMETSAT to the end-users (colour code). Moreover, it clear shows how the SSHA changes over time. The blue colour refers to the reprocessing 2018 dataset (PB 2.27); the red colour corresponds to the dataset from the previous reprocessing (PB 2.15); and the orange colour shows the operational data being generated in NTC with the different PBs over time. The top panel depicts the mean SSHA, while the bottom illustrates the standard deviation. The data is filtered using the STM Tools criteria mentioned in Section 4.3.1.2 and averaged over 10 days. It shall be noted that there is a large jump in the orange line around December 2017. This was due to relevant changes in the PB that led to the change from Baseline collection '002' to '003' (more details in Section 3.1). Once more this figure also allows for demonstrating that the new PB allows for reducing the SSHA std.

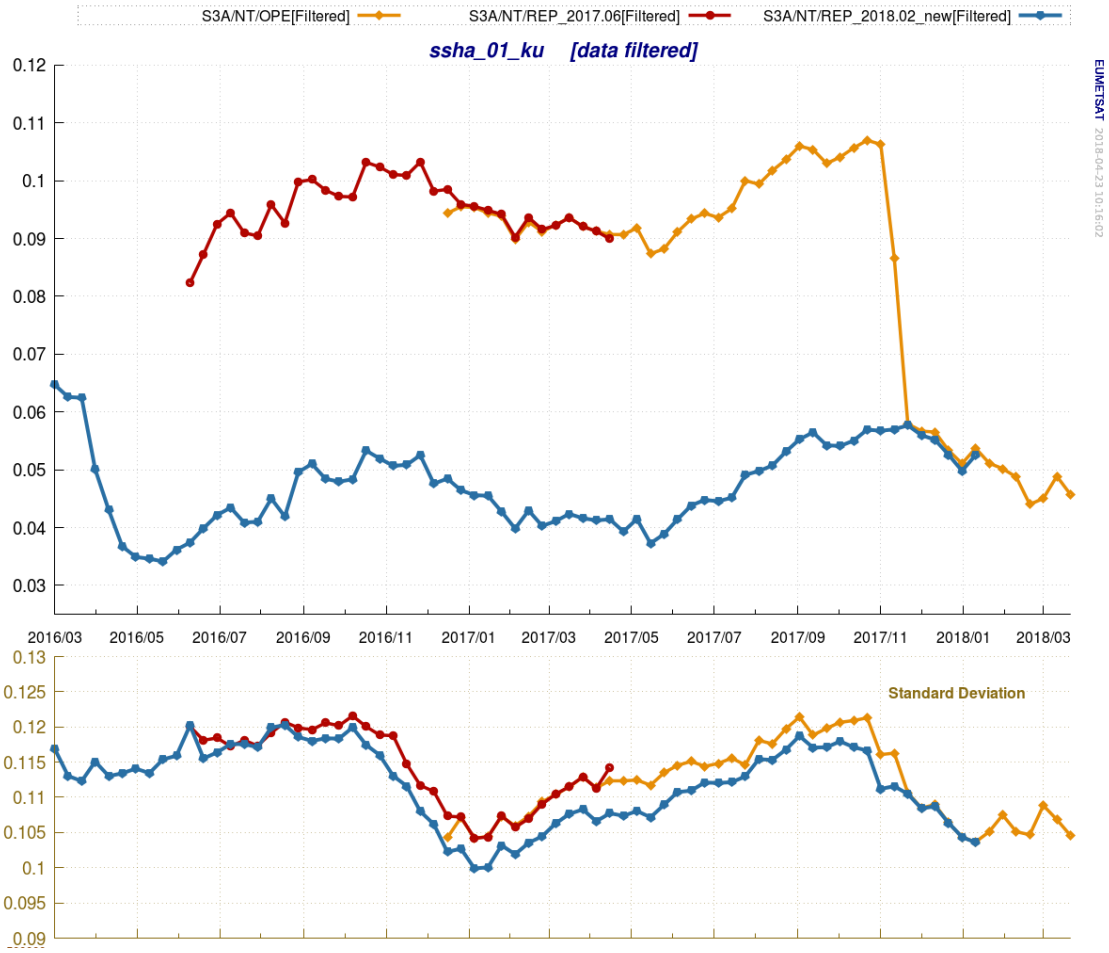

Figure 25 – SSHA: Comparison with previous datasets delivered by EUMETSAT.

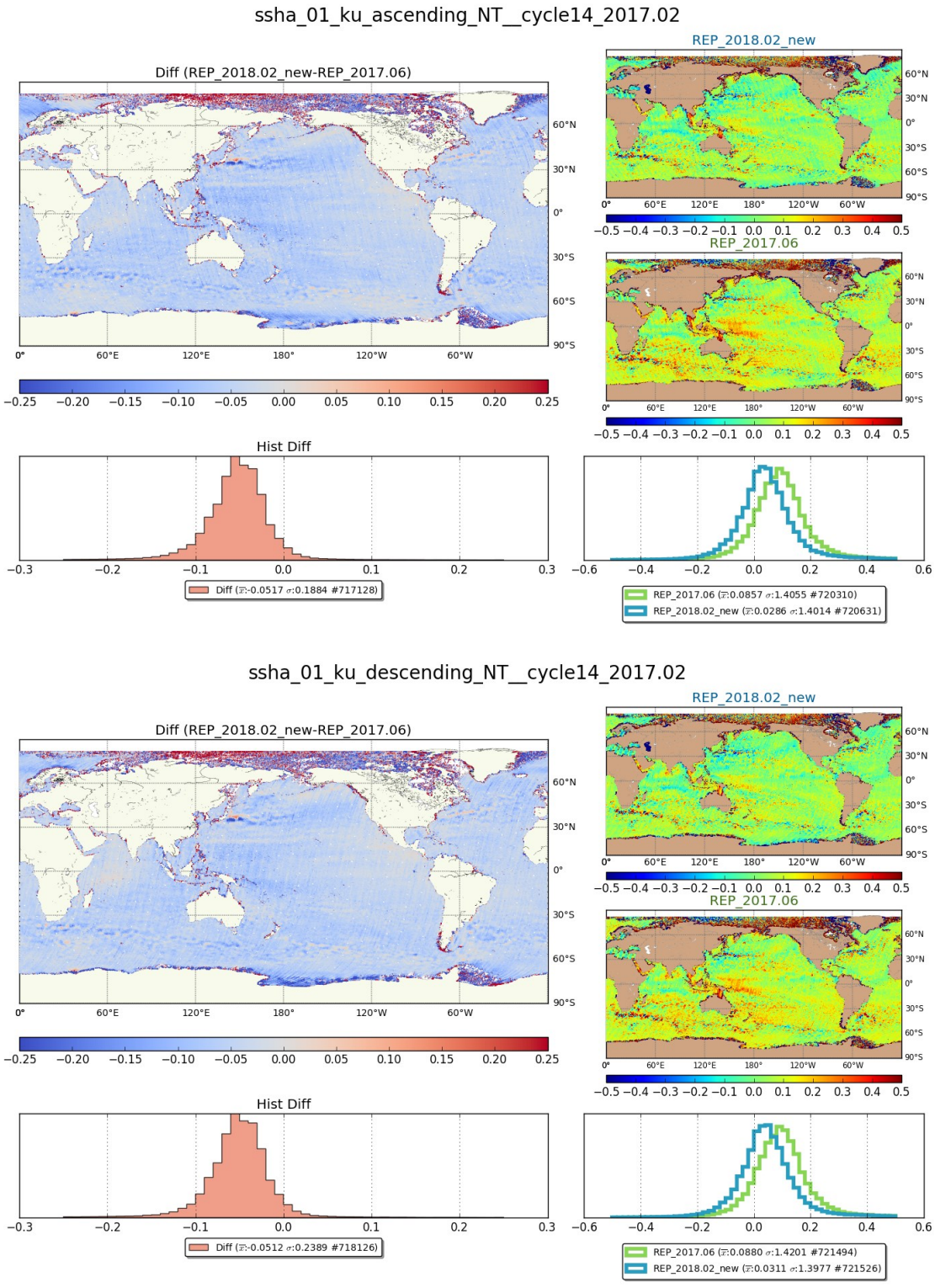

Figure 26 – SSHA: Geographical comparison between the current and previous reprocessing

The above images show the geographical comparison between the previous reprocessing "REP_2017.06" (middle right) and the new one "REP_2018.02_new" (top right). The histograms of both datasets are on the bottom left overlapped.

In the top left, there is the map of differences between both datasets and the histogram of the differences below. No filtering was applied to the datasets on this case. The differences are calculated at 1Hz, in a one-to-one difference.

The top plot shows the Ascending the bottom one Descending. The Cycle shown here is 14 from 2017/02.

4.3.4 Significant Wave Height

4.3.4.1 SWH wavenumber spectrum and precision plot

The estimated 1-Hz SWH precision is 8.25 cm for SAR and 12.03 cm for PLRM (as expected, SAR being more precise than PLRM) at mean SWH (2 meter) for Cycle 15. Both the SWH precision in SAR and PLRM mode have slightly improved with respect the values taken in previous reprocessing campaign in Cycle 15 (they were 8.4 cm in SAR and 12.15 for PLRM). It is very likely that one of the reasons for this improvement is the new CAL2 scheme.

This result (SAR being more precise than PLRM) is confirmed once the wave height averaged wavenumber spectrum for Cycles 14 and 15 is computed from the 20-Hz SWH measurements (Figure 27). From the wavenumber spectrum, it is also manifest how SAR mode is able to observe the wave height more accurately than PLRM at scales shorter than 100 km. Further, from Figure 28, we once again retrieve that SWH range noise in the new processing campaign is lower than the one in the previous campaign.

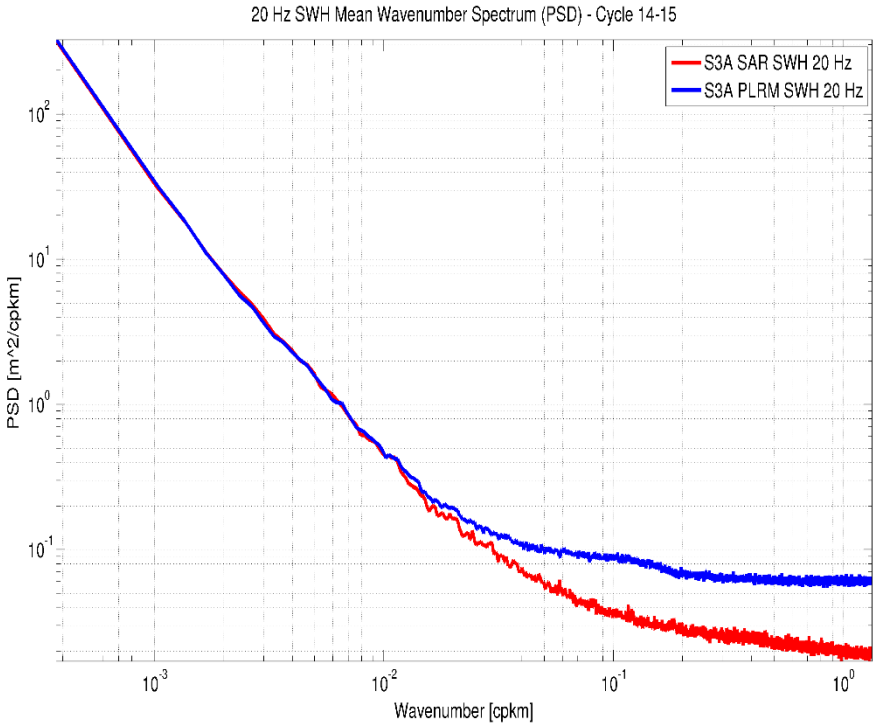

Figure 27 – 20-Hz SWH averaged wavenumber spectrum for Cycles 14 and 15.

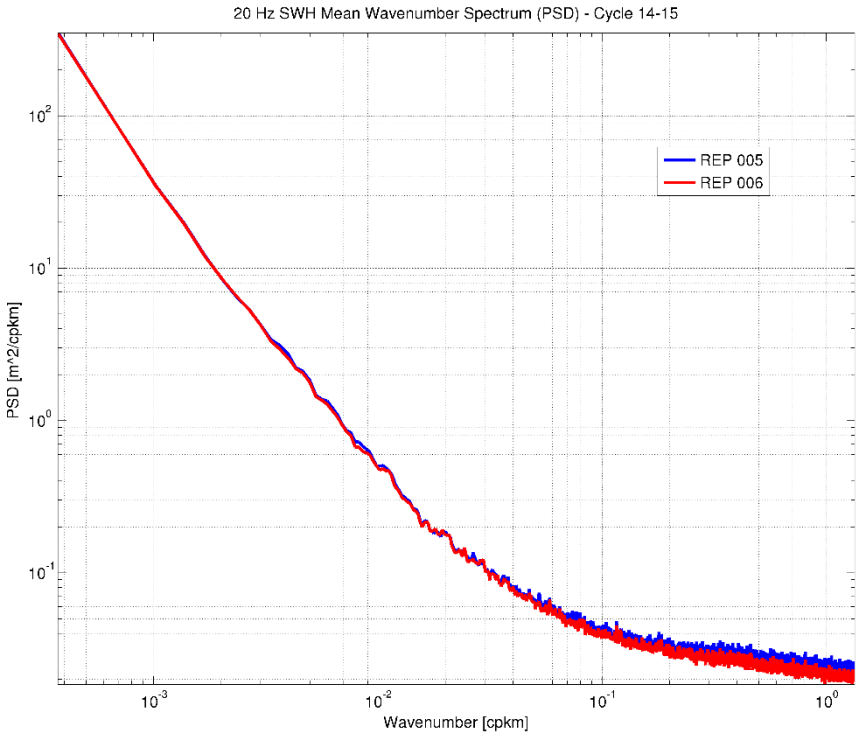

Figure** 28 – **20-Hz SWH averaged wavenumber spectrum for Cycles 14 and 15, comparing the new reprocessing (006) and the previous one (005).

4.3.4.2 SWH SAR and PLRM Time Series and Geographical Maps

Figure 29 compares the SWH time series (3-day averages) as derived by S3A (SAR and PLRM) with those estimated by ECMWF model. The RADS filtering criteria is applied. There is a good consistency between SRAL SAR data and ECMWF model. So is the case for PLRM, but the latter shows approx. 6 cm negative bias with respect the previous two.

Figure 30 shows that the SWH std from the SAR mode is the highest among the three. It is considered that a current open anomaly (see Section 4.3.4.9) is negatively affecting the SAR SWH data quality. Work on improving this is on-going.

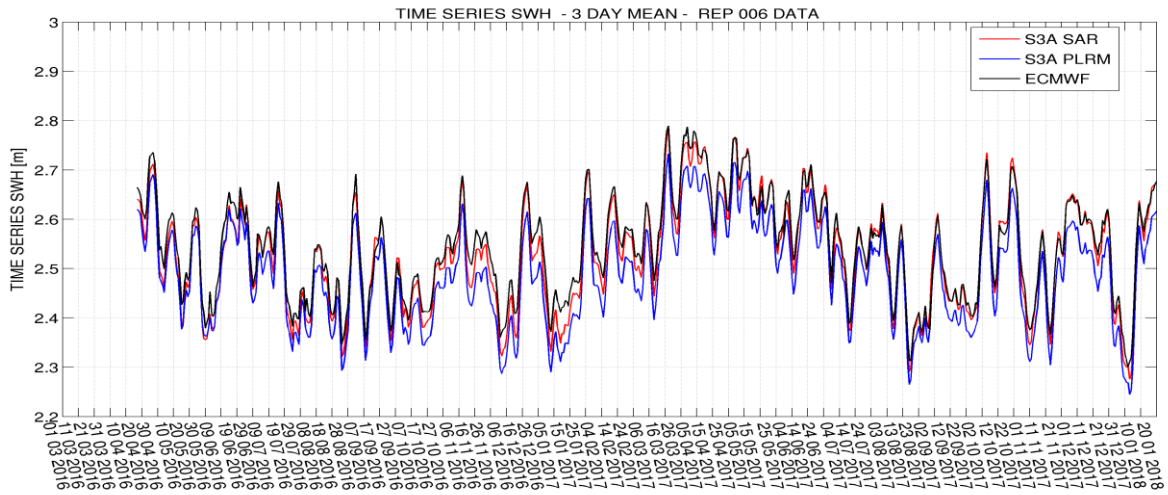

Figure 29 – Time Series of SWH mean, as returned by S3 SAR (red), S3 PLRM (blue) and ECMWF (black)

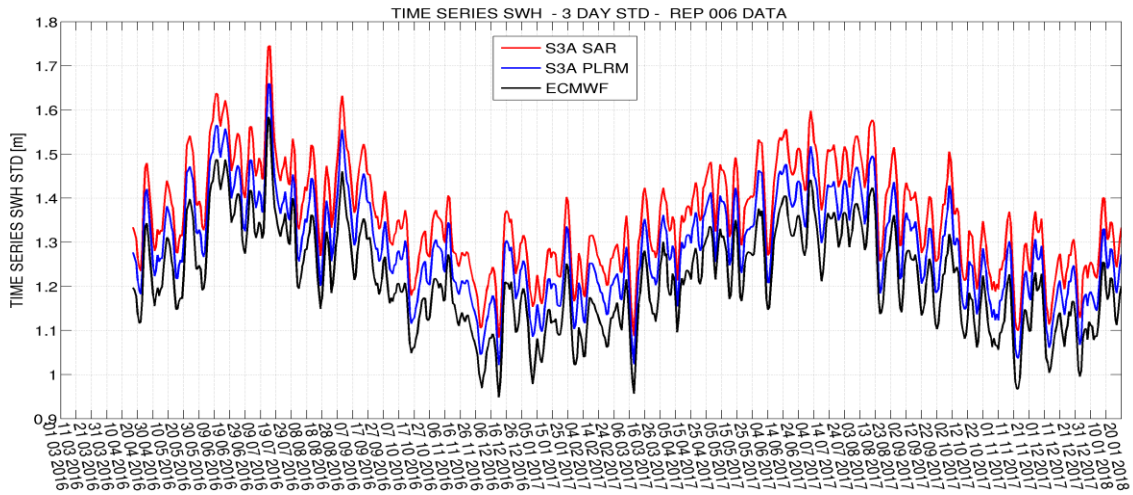

Figure 30 – Time Series of SWH std, as returned by S3 SAR (red), S3 PLRM (blue) and ECMWF (black)

More details on the differences with ECMWF can be found in Section 4.3.4.5.

The following images show a geographical comparison between SAR and PLRM for Cycle 14. There appears to be no pattern specific to ascending or descending. The differences between SAR and PLRM are small, being the main difference bellow 0.5 meters of SWH. PLRM sees slight lower SWH than SAR (average difference of 0.1 m without any data filtering).

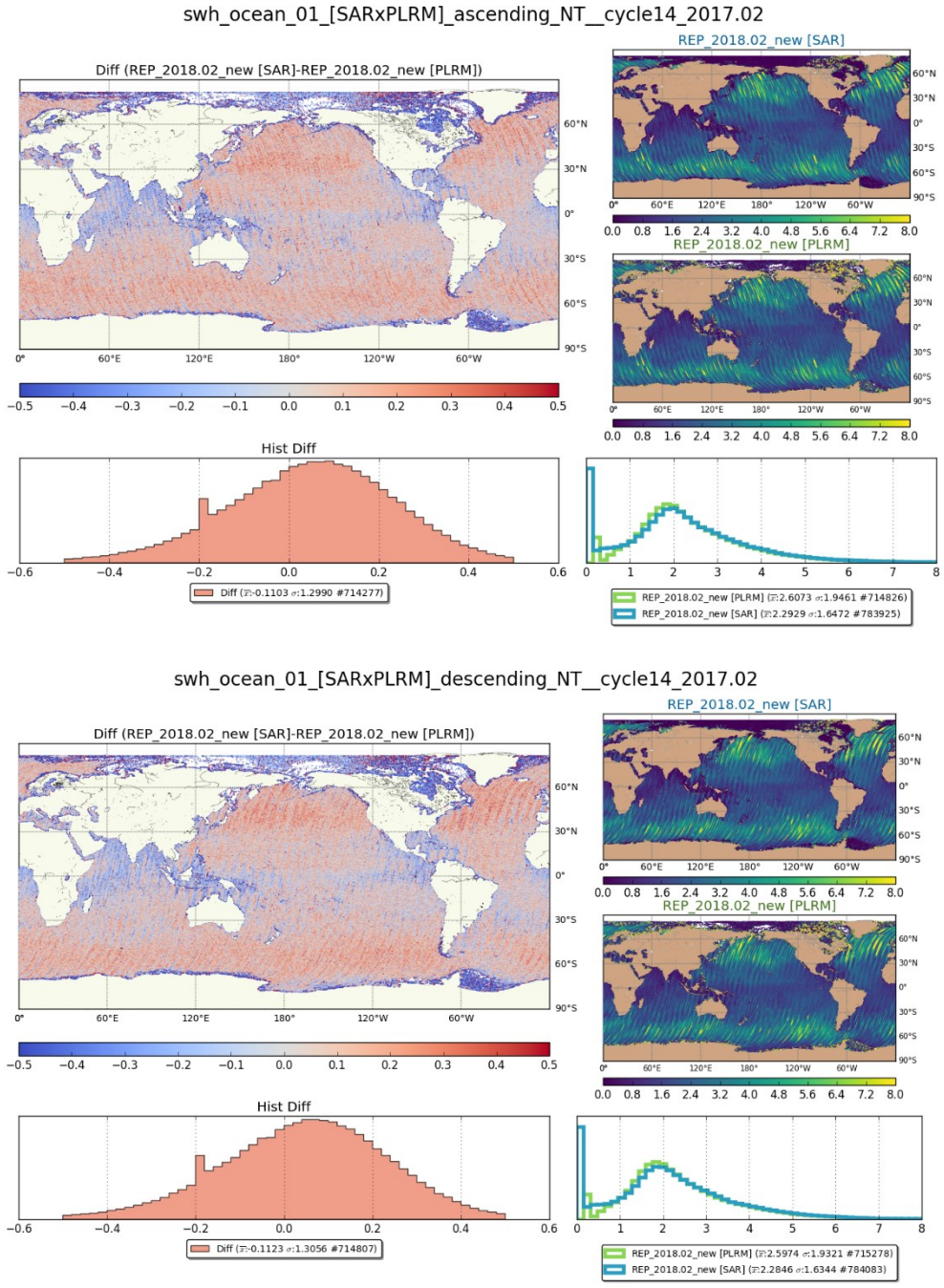

Figure 31 – SWH: Geographical comparison between S3 SAR and PLRM. Ascending (top image), descending (bottom image).

4.3.4.3 SAR SWH and PLRM SWH Scatterplot

Figure 32 illustrates the scatter plot for the 1-Hz SWH measurements SAR vs PLRM during Cycle 15. The results show good agreement between the two datasets (std of the differences about 20 cm and regression slope of 1.04). The new processing baseline allows for a bias reduction in SWH between the two modes to ~6 cm (SAR SWH being higher than PLRM).

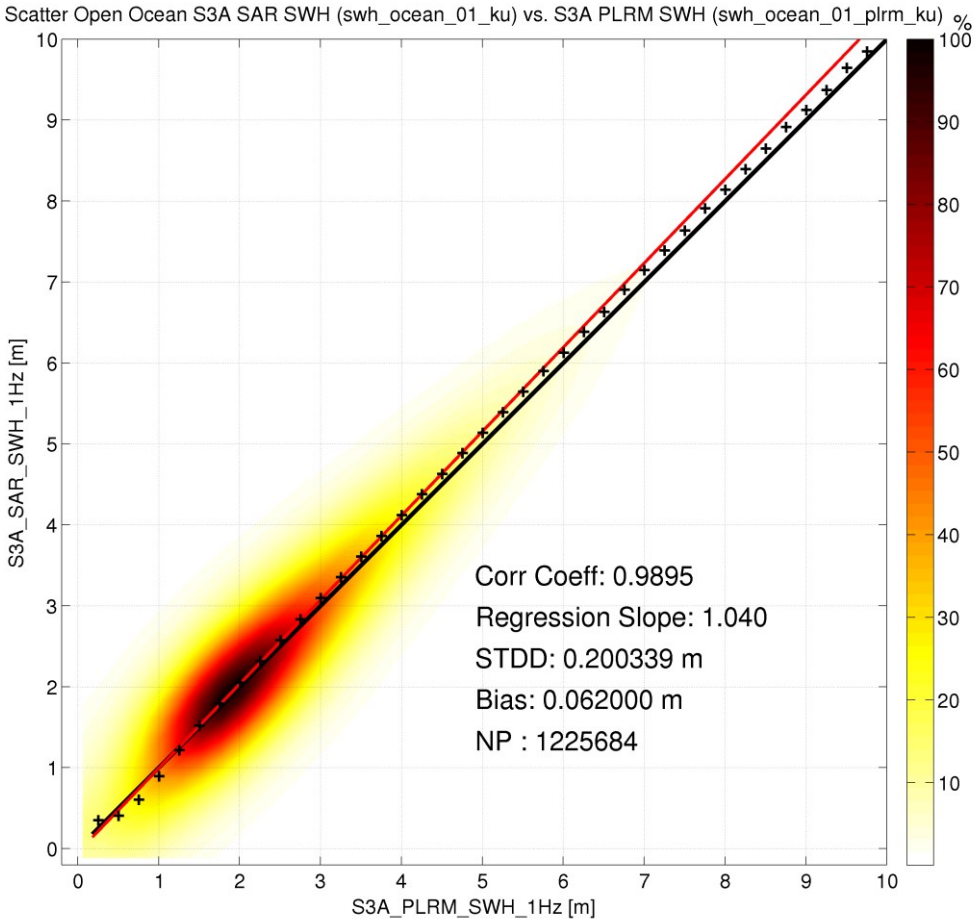

Figure 32 – Scatterplot of SWH (SAR versus PLRM), Cycle 15. The colours indicate point density.

4.3.4.4 SWH SAR minus PLRM dependency on SWH and height rate

The density plot of the difference in SWH between SAR and PLRM shows a non-linear dependency as a function of SWH (see Figure 33). The differences (on average) range from -20 to 20 cm (depending on SWH) in global. Nevertheless, for SWH values from 1.5m to this range is reduced from 10 to 20 centimetres. The latter is an improvement from the new processing baseline.

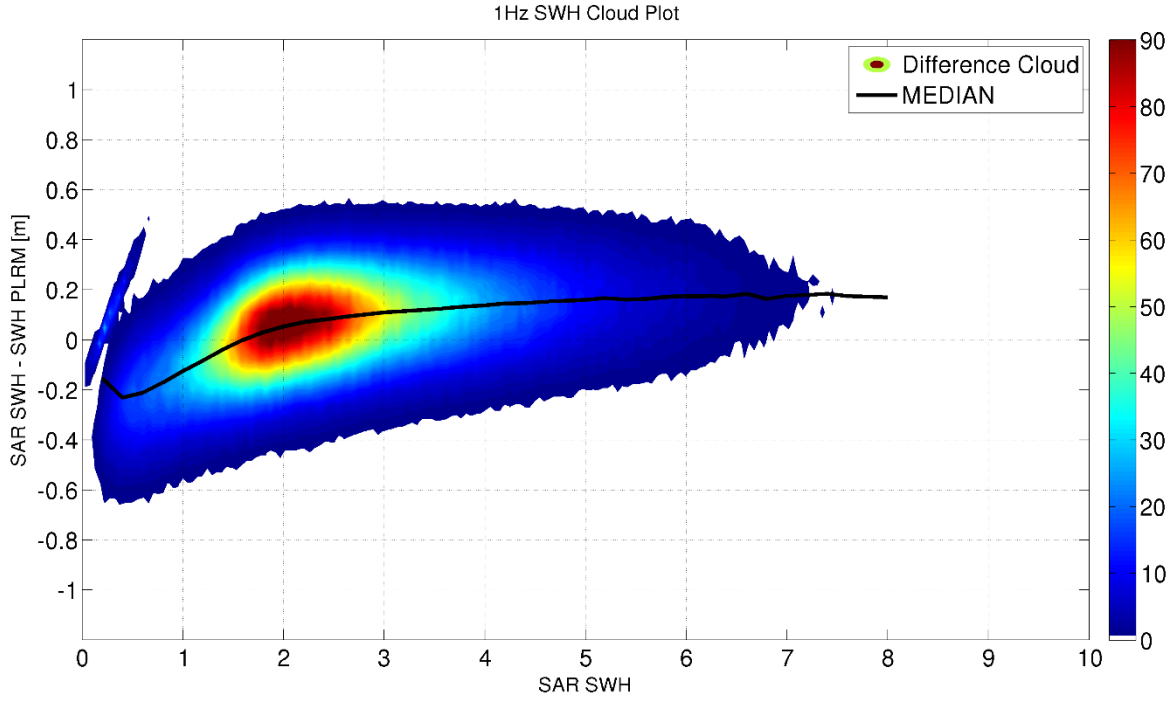

Figure 33 – Point density of the SWH difference between SAR and PLRM as a function of SAR SWH, Cycle 15.

When analysing such a difference as a function of range rate a ~8cm dependency is observed (see Figure ***34***). This error, attributed to the not yet perfect range alignment, was already quantified in the previous reprocessing campaign. The not yet perfect range alignment of the peripheral Doppler Beams in the stack (mainly due to the missing intra-burst orbit range correction in L1b IPF) is still to be implemented in future versions of the PB).

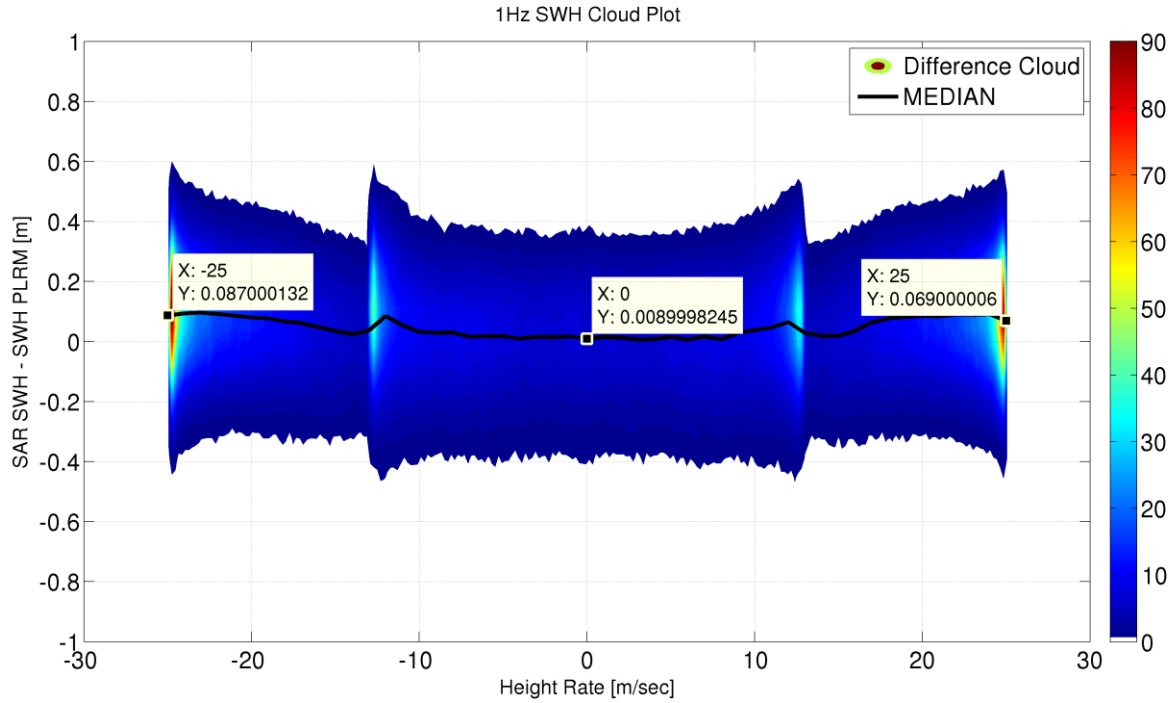

Figure 34 *– Point density of the SWH difference between SAR and PLRM as a function of height rate, Cycle 15.*

4.3.4.5 SWH Drift

The drift slope between SAR SWH and PLRM SWH is estimated to be **+0.7 cm/year** when the period 23 June 2016 to 20 Jan 2018 is considered. The drift is shown in Figure 35. The screening criteria are the RADS criteria listed in 4.3.1.1 and the average period is 3 days. Likewise for SSHA, the period of analysis starts in 23 June 2016.

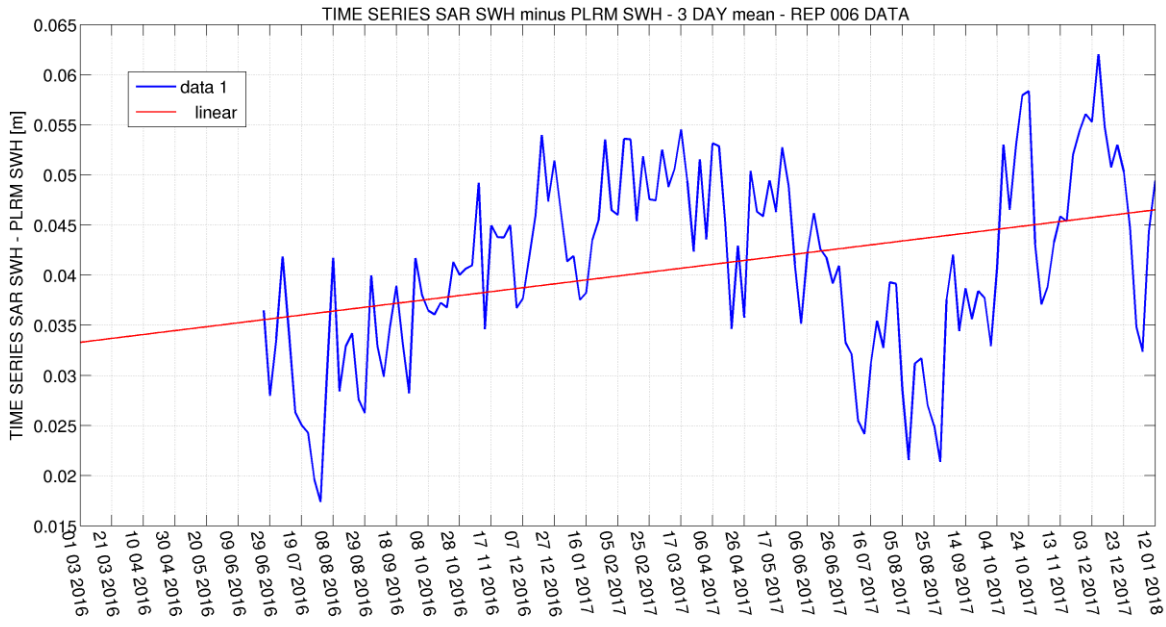

Figure 35 – Time Series of S3A SAR SWH minus PLRM SWH

A drift of 0.7 cm/year translates in around –0.3 mm/year of drift in the SSB correction. This result is consistent with the plot in Figure 22, and with the observed drift of SSB of –0.25 mm/year.

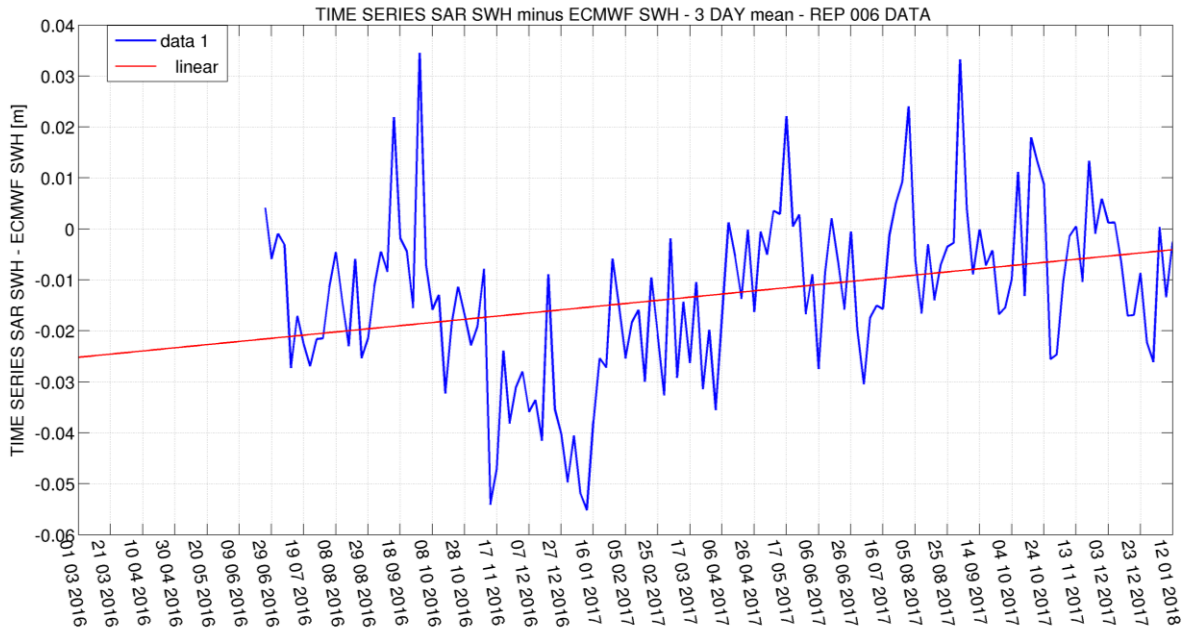

Figure 36 – Time Series of S3A SAR SWH minus ECMWF

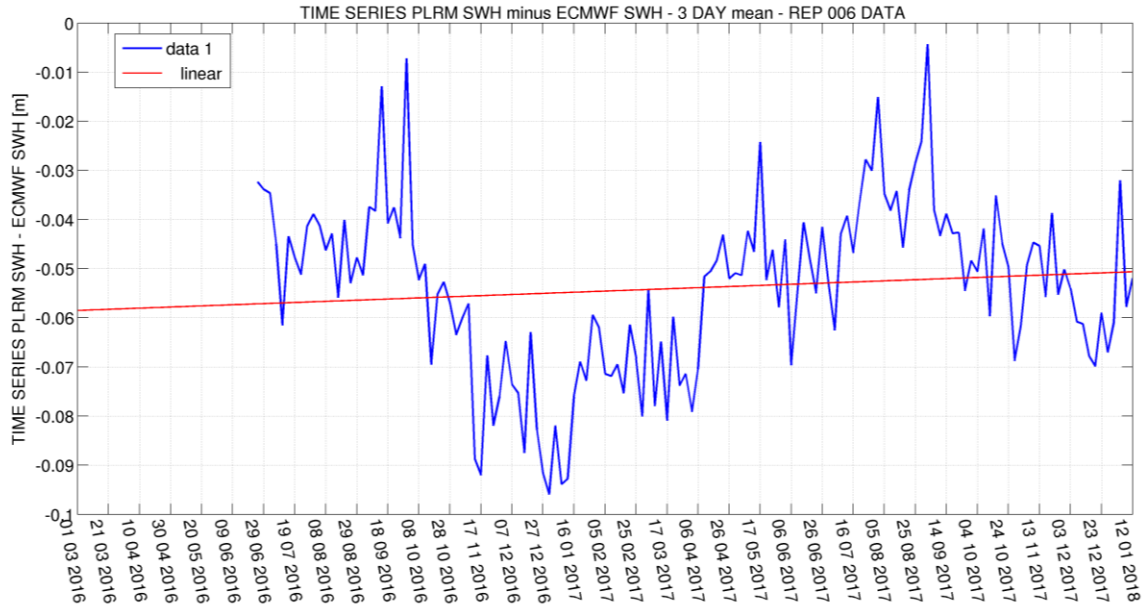

Figure 37 – Time Series of S3A PLRM SWH minus ECMWF

Figure 36 shows the time series of SAR minus ECMWF SWH. Figure 37 illustrates the time series of PLRM and ECMWF SWH. Both figures observe that the difference between S3 and ECMWF drifts in time regardless of the operational mode. Always doing the comparison within the time period 23rd June 2016 to 20th Jan 2018, SAR SWH drifts about **+1.12 cm/year** with respect ECMWF model while the PLRM SWH is only drifting **+0.42 cm/year** with respect the ECMWF model.

The root source of both drifts in SAR and PLRM with respect the ECMWF model is attributed to the Ku PTR width Drift (see Figure 95) which is 0.5 mm/year.

4.3.4.6 Comparison with Jason-3

Likewise as in Section 4.3.3.5, SWH values are compared between Sentinel-3A and Jason-3 also doing a 10 day average, limiting S3A data to +/- 66 degrees and applying the RADS filtering criteria.

S3A SWH SAR data shows a bias and a drift with respect to Jason-3. The bias is ~ -1.5 cm and the drift is +1.03 cm/year.

S3A PLRM SAR data show a bias, and a negligible drift. The bias is in mean ~ -5cm.

SWH derived from S3A SAR and PLRM show a nice agreement with an almost constant bias of 3 cm between the modes and a drift of 3.8 mm/year (see Figure 38).

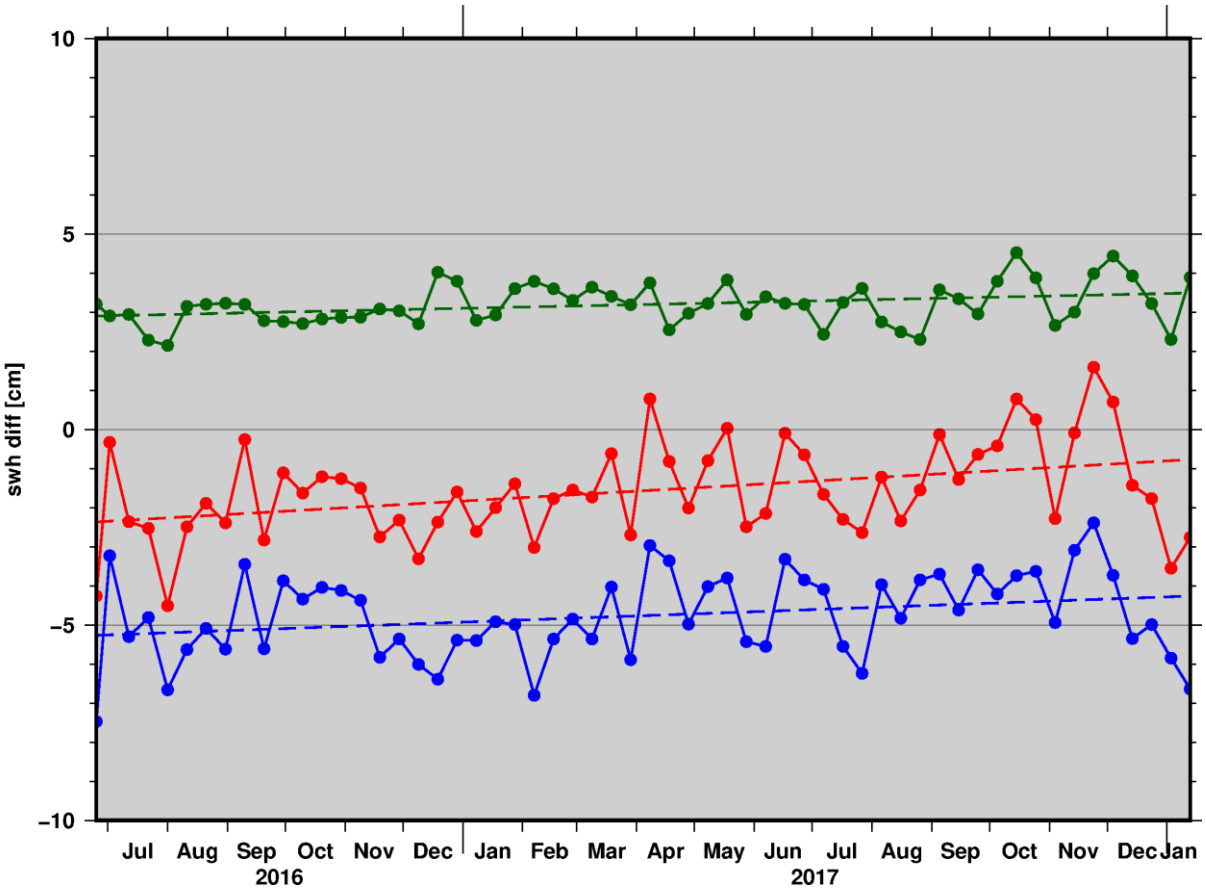

Figure 38 – SWH differences between J3 and S3 SAR (red), J3 and S3 PLRM (blue) and S3 SAR and PLRM (green)

At large scale, there is a good match between the satellites' measured SWH.

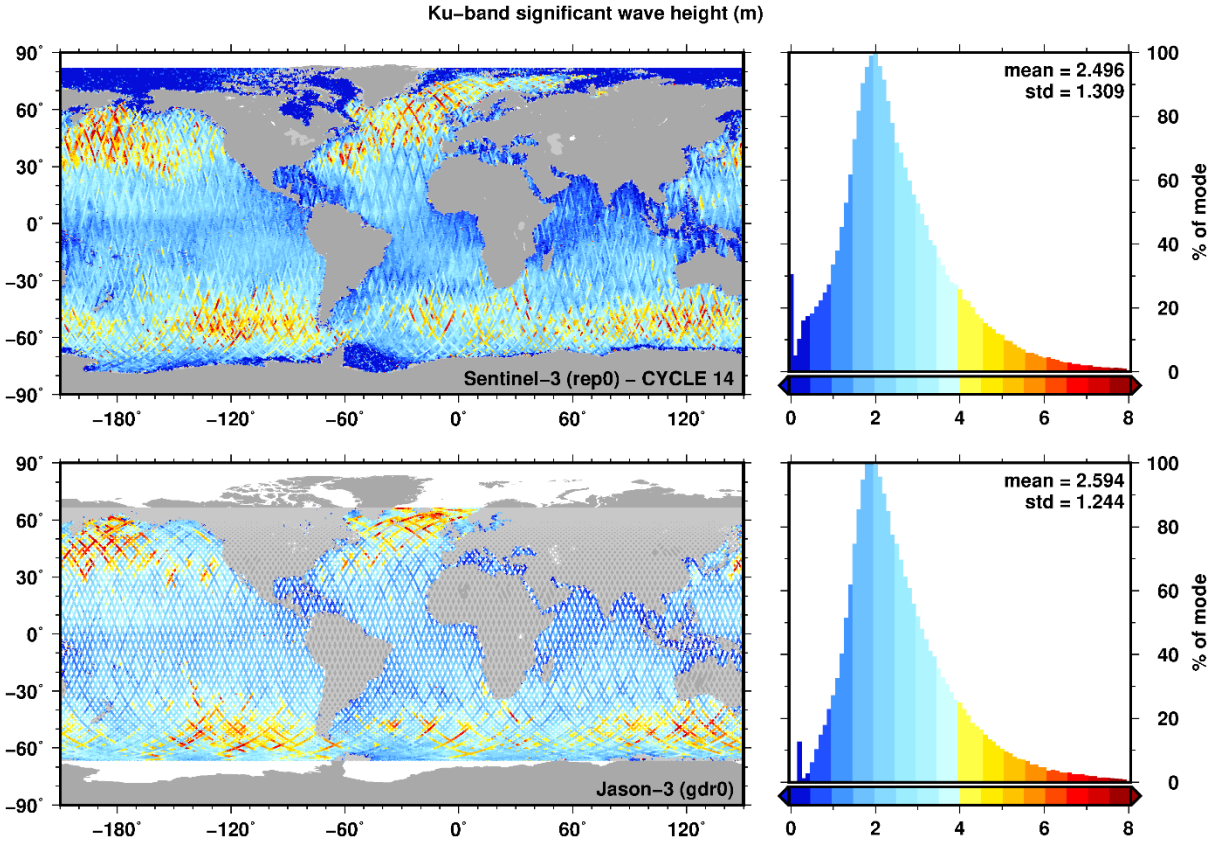

Figure 39 – SWH cross-comparison between S3A (top) and J3 (bottom) for Cycle 14.

4.3.4.7 SAR SWH and ECMWF SWH Scatterplot

We underline that in our comparison between 1-Hz SWH measurements and the SWH modelled by ECMWF, we did not apply to the altimeter SWH any along-track averaging to form super-observations with scales compatible with the model scales of around 75 km.

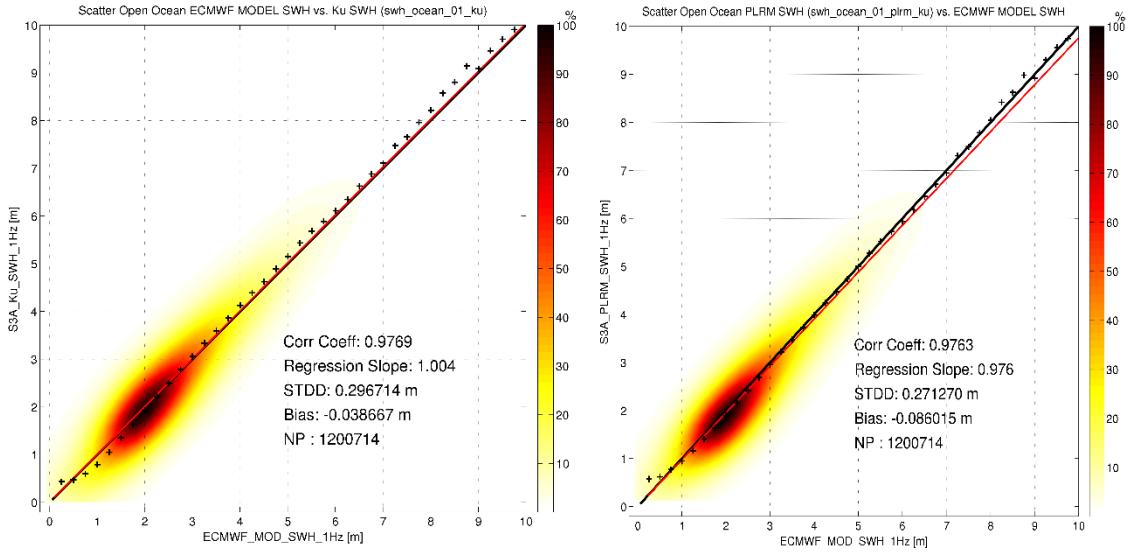

Figure 40 – Scatterplot SAR SWH versus ECMWF SWH (left) and PLRM SWH versus ECMWF SWH (right), Cycle 15. Colours indicated point density.

The scatterplot between SAR SWH (or PLRM SWH) versus ECMWF SWH shows a good level of consistency between the two dataset (Cycle 15). The standard deviation of the differences is about 29 cm and regression slope of 1.004 in SAR mode and it is 27 cm and 0.976 in PLRM mode. It can be pointed out that the previously existing bias of 20 cm in SWH between SAR and ECMWF has disappeared, while there is still have a residual bias of –8 cm in PLRM mode. (PLRM SWH being lower than ECMWF model). It can be identified in the SAR SWH vs ECMWF SWH scatterplot an underestimation of the SAR SWH for SWH less than 1.5 meter as consequence of the open anomaly in 4.3.4.9. This error also makes the SAR SWH to have a std slightly higher than in PLRM mode.

4.3.4.8 Comparison with previous datasets

Figure 41 illustrates the different datasets delivered by EUMETSAT to end users, while providing a historical record of SWH from beginning of mission to end of re-processing 2018. The blue colour refers to the results achieved with the new re-proceed dataset from 2018 (PB 2.27); in red the figure shows the dataset from the previous reprocessing (PB 2.15); and the orange colour depicts the operational data being generated in NTC with the different PBs over time. Moreover, the top panel provides mean SWH, while the second standard deviation.

The data is filtered using the STM Tools criteria, and it is aggregated into 10 days (each point corresponds to 10 days of filtered data).

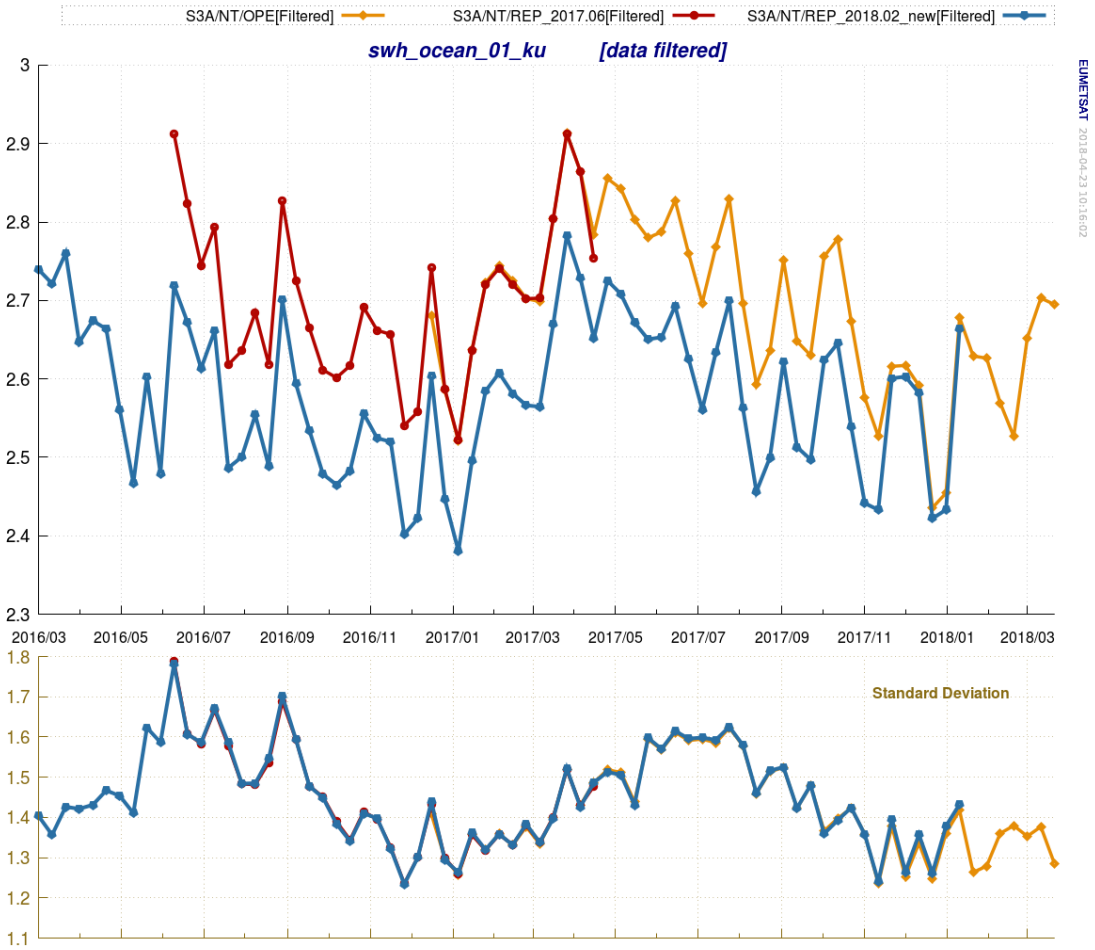

Figure 41 – SWH: Comparison with previous datasets delivered by EUMETSAT

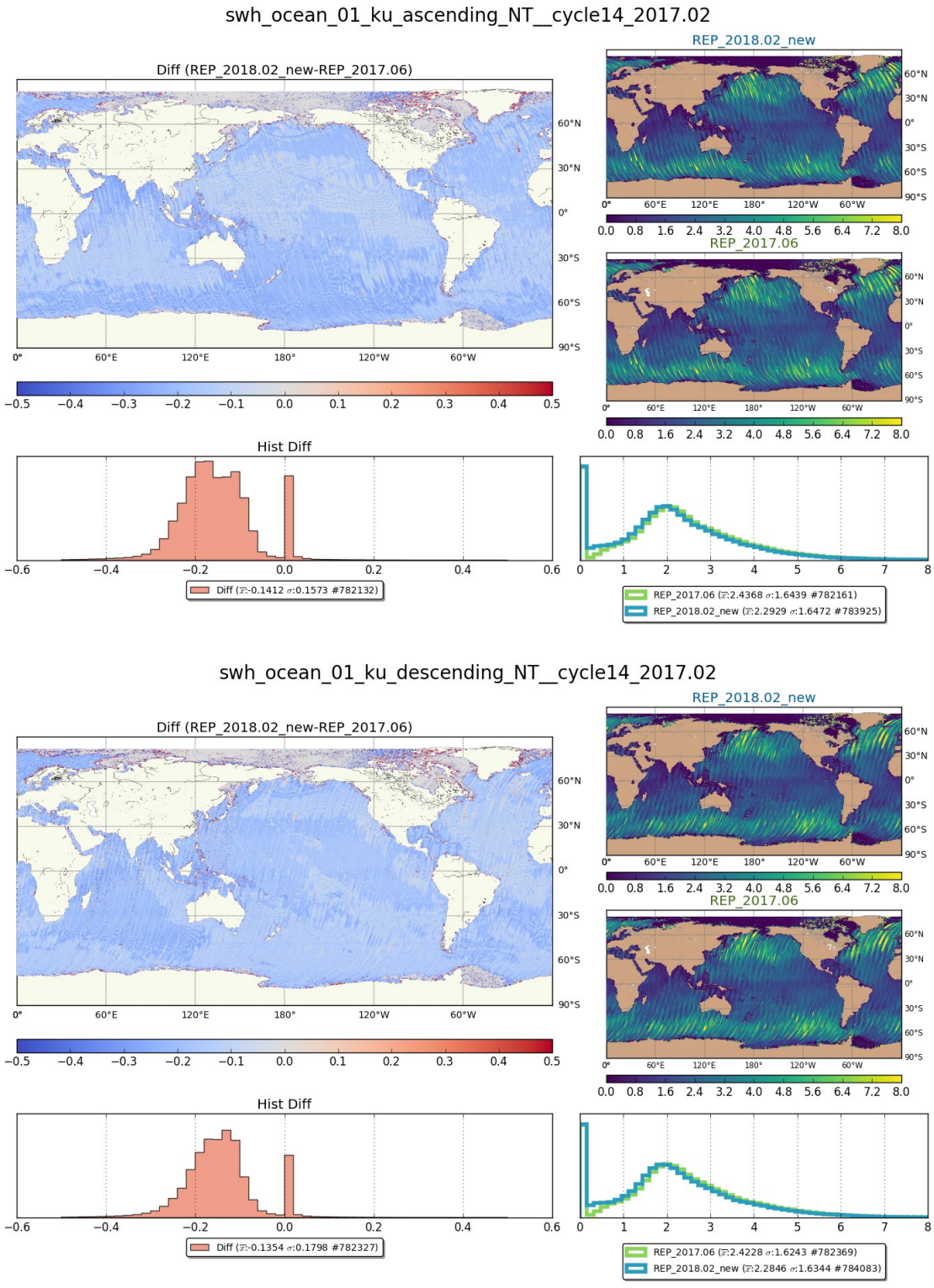

Figure 42 – SWH: Geographical comparison between the current and previous reprocessing

Figure 42 gives the geographical comparison between the previous reprocessing "REP_2017.06" (middle right) and the new one "REP_2018.02_new" (top right). The histograms of both datasets are on the bottom left overlapped.

In the top left, there is the map of differences between both datasets and the histogram of the differences below. No filtering was applied to the datasets on this case. The differences are calculated at 1Hz, in a one-to-one difference.

The top plot shows the Ascending, the bottom one Descending. The Cycle shown here is 14 from 2017/02.

Overall the SWH is lower than on the previous datasets, due to evolution in the SAR retracking algorithm. From the plots it can be seen that ascending and descending have become more consistent with the new reprocessing.

4.3.4.9 Open issue: SWH of 0 meters over open ocean

Four percent of 20 Hz SWH PLRM measurements are set to 0 over open ocean (see Figure 43). The issue was already present in previous baselines. Previously, the SAR SWH at 20 Hz was converted to 20 Hz *sigma*_c, averaged to 1 Hz, and then again converted back from *sigma*_c to SWH at 1 Hz. Since PB 2.27 the 1 Hz SWH is computed directly from an averaging of 20 Hz SWH, without passing through the *sigma_c* conversion step and this makes the anomaly more visible, as the *sigma_c* conversion step would mask some of these 0 values.

Investigation is on-going and it is expected that the root cause is related to Least-Square fitting mechanism or its parametrization.

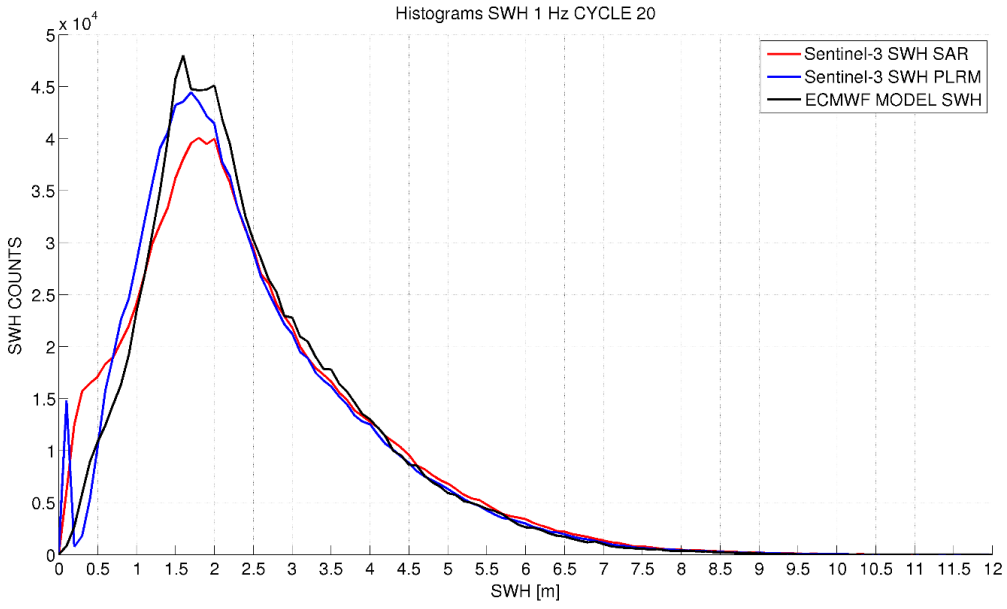

Figure 43 – Comparison of Histograms of SWH 1Hz (S3 SAR, S3 PLRM, ECMWF)

Figure 43 shows the histograms from SAR, PLRM and ECMWF 1 Hz SWH. For the SAR case, it is highlighted the over-population of low 1 Hz SAR SWH (below 1 meter) as direct consequence of the numerous 20 Hz SWH set to 0.

One possible workaround, for users interested in correcting the anomaly for low SWH, is to remove spurious values from the SWH 20Hz, (i.e. when the values are set to 0) and then

compress/average the residual 20 Hz SWH to generate a new 1 Hz measurement. An example of such a user-made compression is shown in Figure 44: SAR 1 Hz SWH histogram gains back the consistency with respect PLRM and ECMWF histogram below 0.75 meters of SWH.

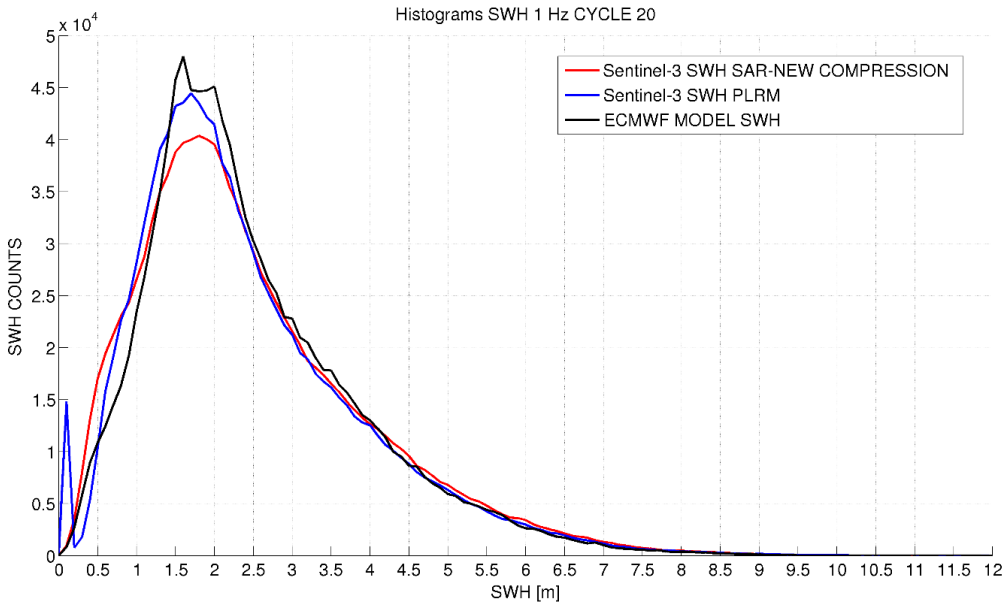

Figure 44 – Comparison of Histograms of SWH 1Hz (S3 SAR user-made compression, S3 PLRM, ECMWF)

Work is on-going to correct this issue and improve even more the SWH data quality.

4.3.5 Sigma0

4.3.5.1 Sigma0 Precision and Wavenumber Spectrum

The estimated 1-Hz sigma nought precision is 0.019 dB cm for SAR and 0.034 dB for PLRM (as expected, SAR being more precise than PLRM) for mean SWH (2 m) along Cycle 15. These values have not changed from the previous reprocessing campaign.

From the wavenumber spectrum (Figure 45), it is clear how the new reprocessing campaign has improved the measurement of the sigma nought at scales lower than 10 km. This is considered an effect of the new CAL1 and CAL2 calibration schemes. This improvement is not visible from the 1 Hz sigma 0 precision, since it is considered that it holds in it a residual non-linear ocean signal variability.

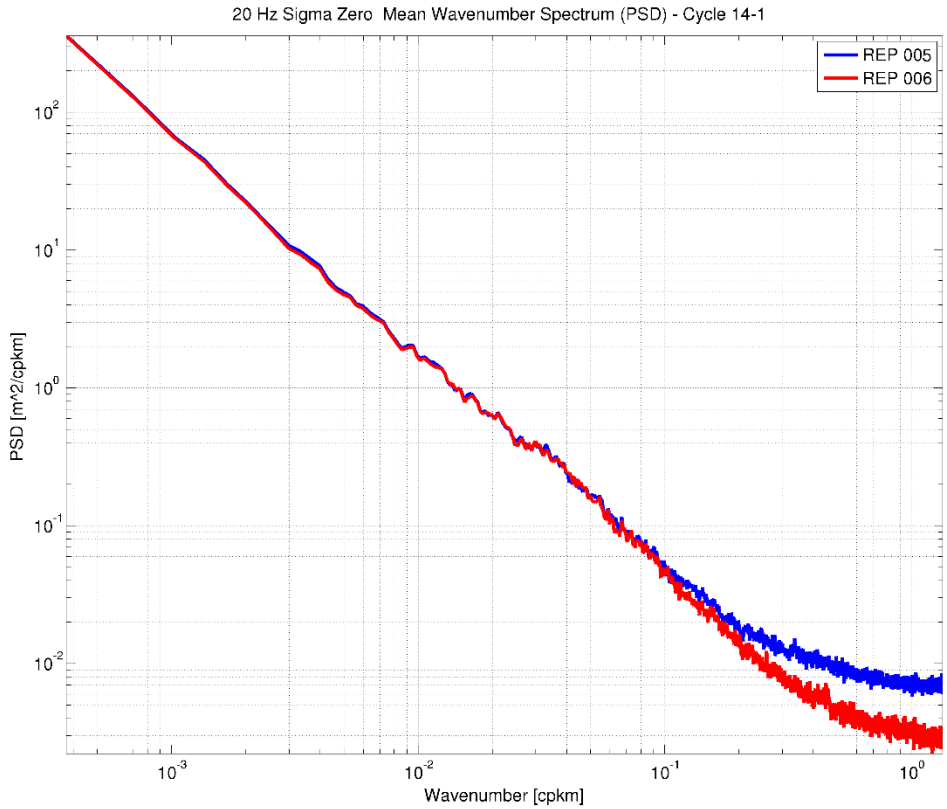

Figure 45 – 20-Hz Sigma 0 averaged wavenumber spectrum for Cycles 14, and 15, comparing the new reprocessing (006) and the previous one (005).

4.3.5.2 Sigma0 SAR vs PLRM Time Series and Geographical Maps

The Sigma0 time series as retrieved by S3A, processed in SAR or in PLRM mode, can be seen in Figure 46. The mean of each 3 days is plotted as one data point. The RADS filtering criteria is applied.

The conclusion from the Figure 46 and Figure 47 is that SAR and PLRM share the same level of sigma nought and the SAR sigma nought std is slightly lower than PLRM sigma nought std.

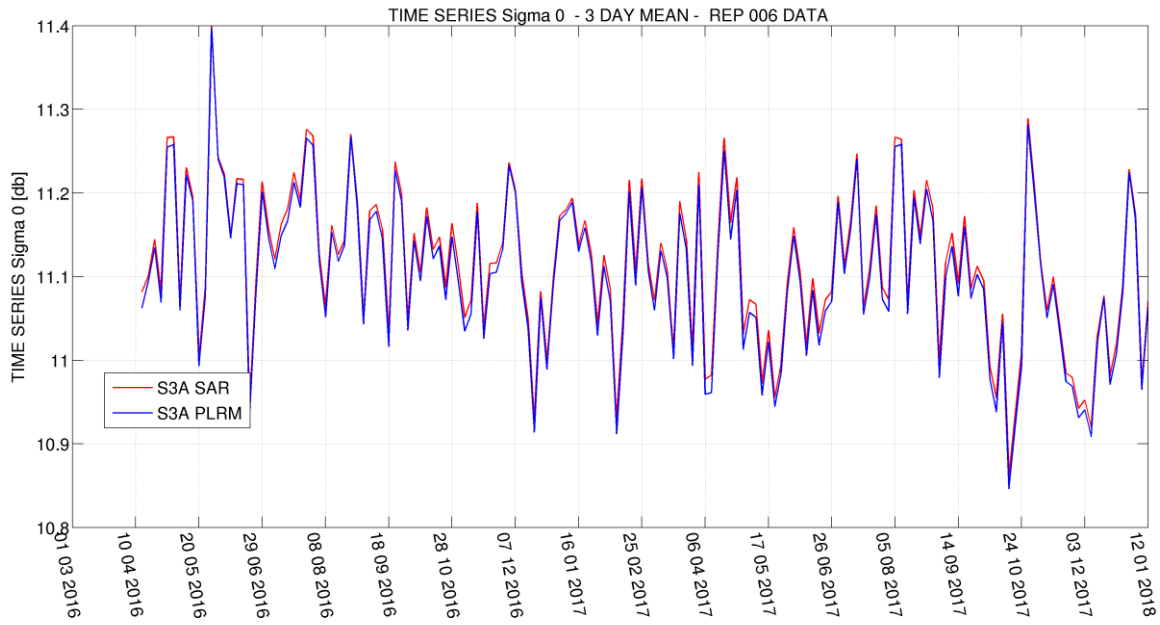

Figure 46 – Time Series of Sigma 0 mean, as retrieved by S3 SAR (red) and S3 PLRM (blue)

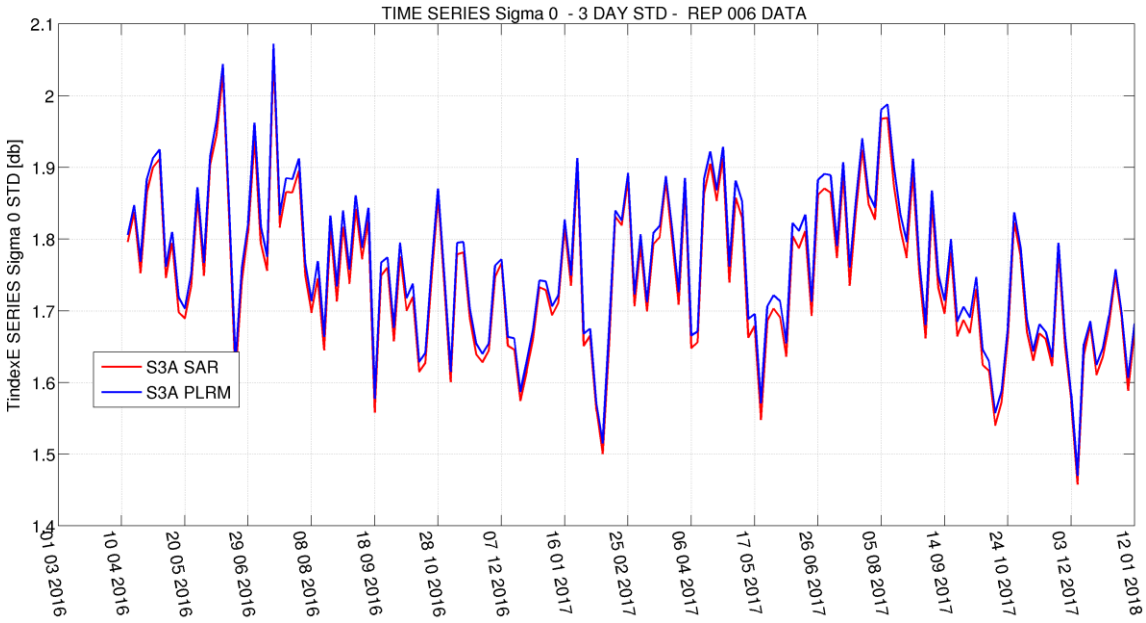

Figure 47 – Time Series of Sigma 0 std, as retrieved by S3 SAR (red) and S3 PLRM (blue)

Figure 48 shows the geographical distribution of Sigma0 differences between S3A SAR and PLRM modes. Results show a clear geographical pattern and there is no clear difference between ascending/descending tracks. It shall be noted that while on the map there is no filtering, for the histograms (right side) the standard RADS filtering criteria is applied, plus only points with latitude less than 66º are considered.

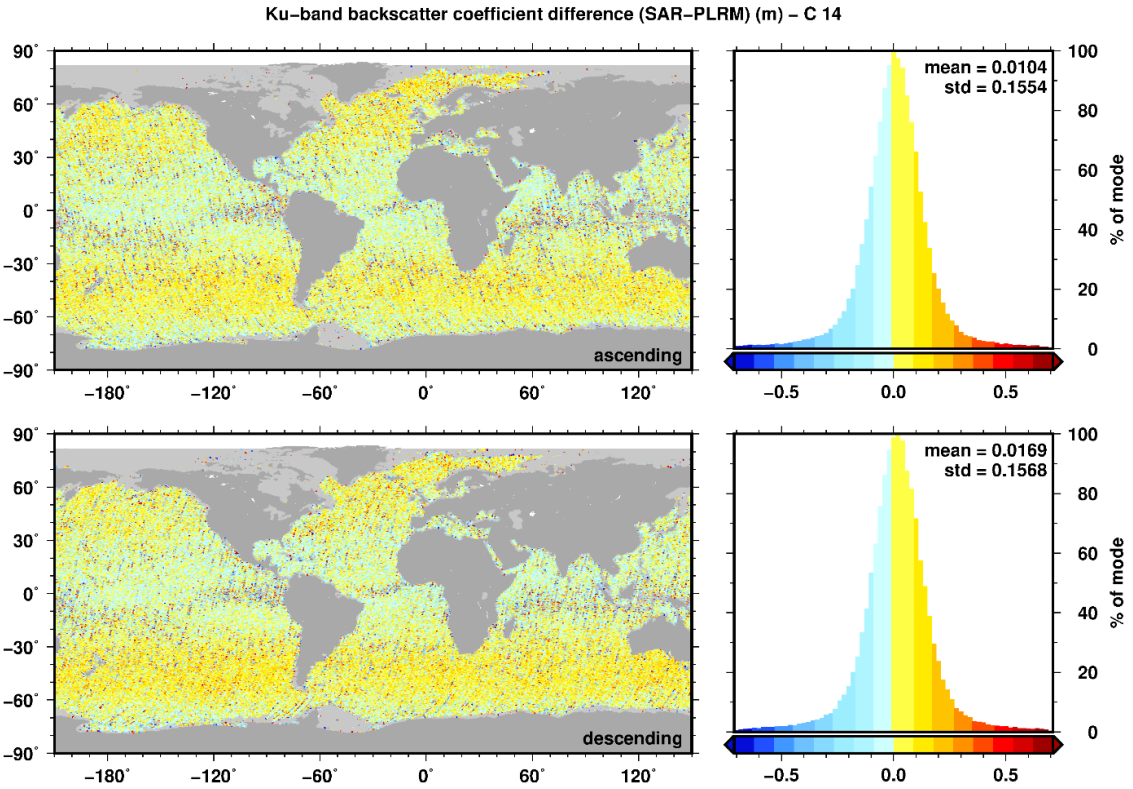

Figure 48 – S3 SAR sigma 0 compared with PLRM sigma 0

4.3.5.3 Sigma0 SAR minus PLRM dependency on Orbit Height and orbit Height Rate

The dependency of the SAR sigma nought with respect orbit altitude is significantly reduced in the last reprocessing dataset (see Figure 49 and Figure 50)

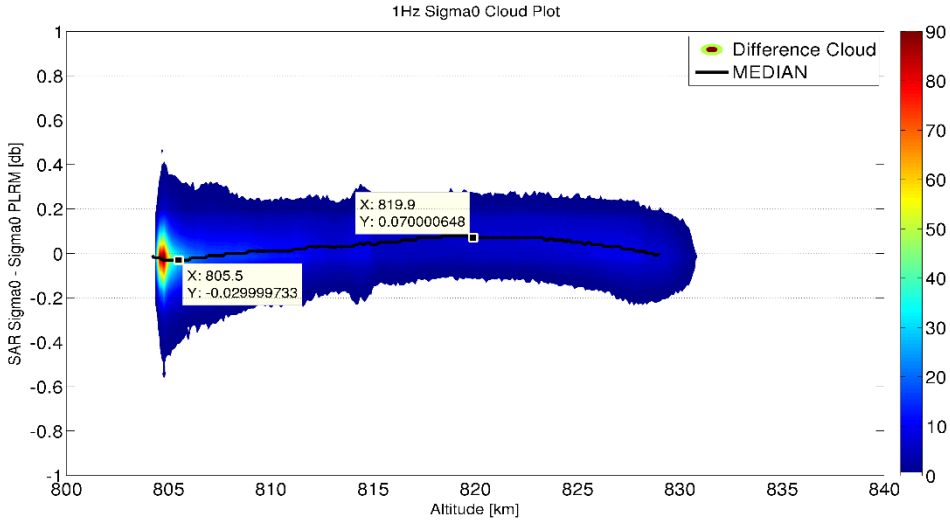

Figure 49 – Density Plot of the Difference between SAR Sigma0 and PLRM sigma0 with respect Orbit Altitude

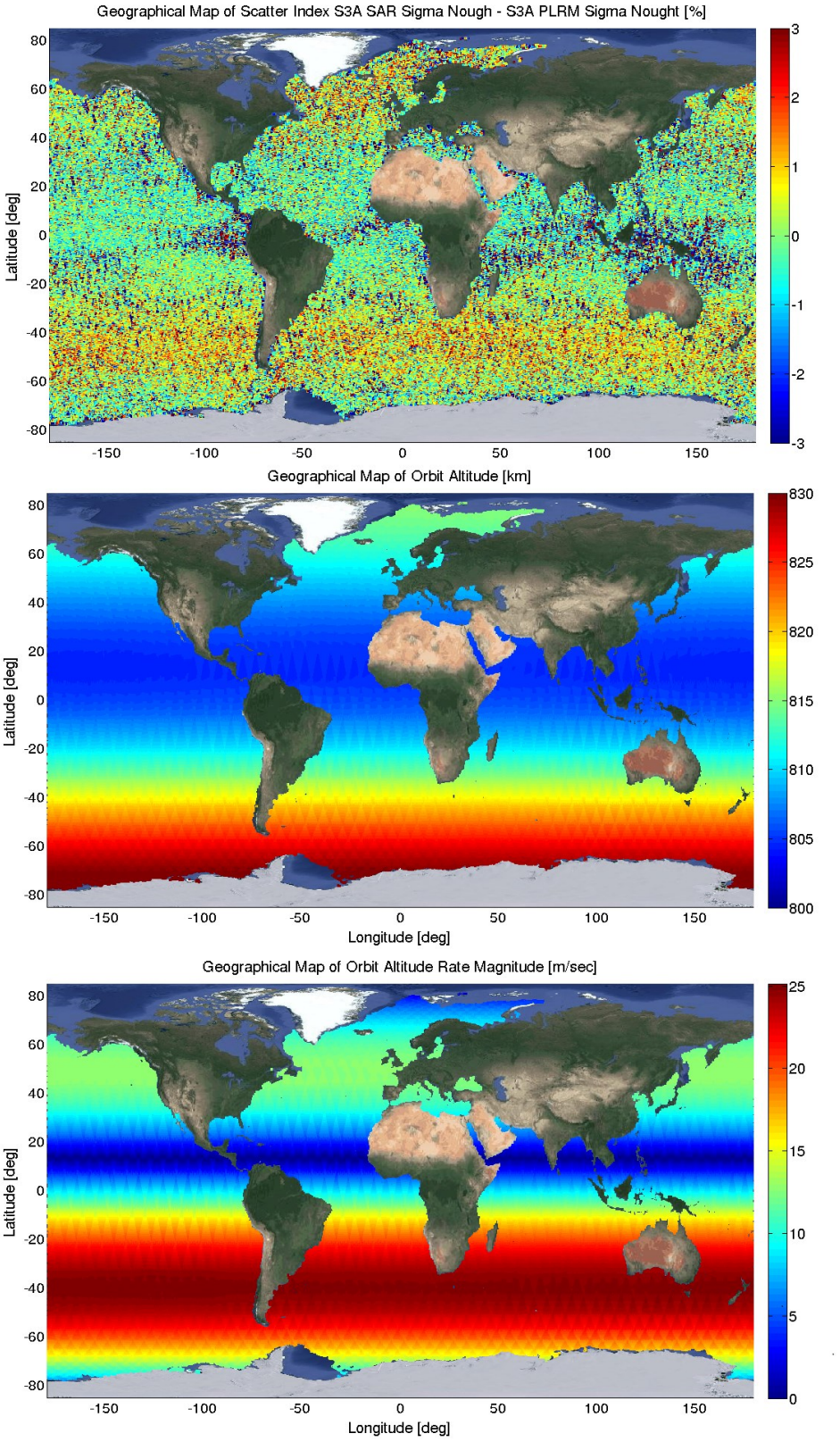

Figure 50 – Top Panel-Geographical Map of Scatter Index (%) between SAR Sigma0 and PLRM Sigma0; Middle Panel-Geographical Map of the Orbit Altitude (km); Bottom Panel-Geographical Map of the Orbit Altitude Rate Magnitude (m/sec).

Also the dependency of SAR sigma nought with respect the orbit altitude rate has decreased passing from an average error of 0.15 dB to 0.1 dB (see Figure 51).

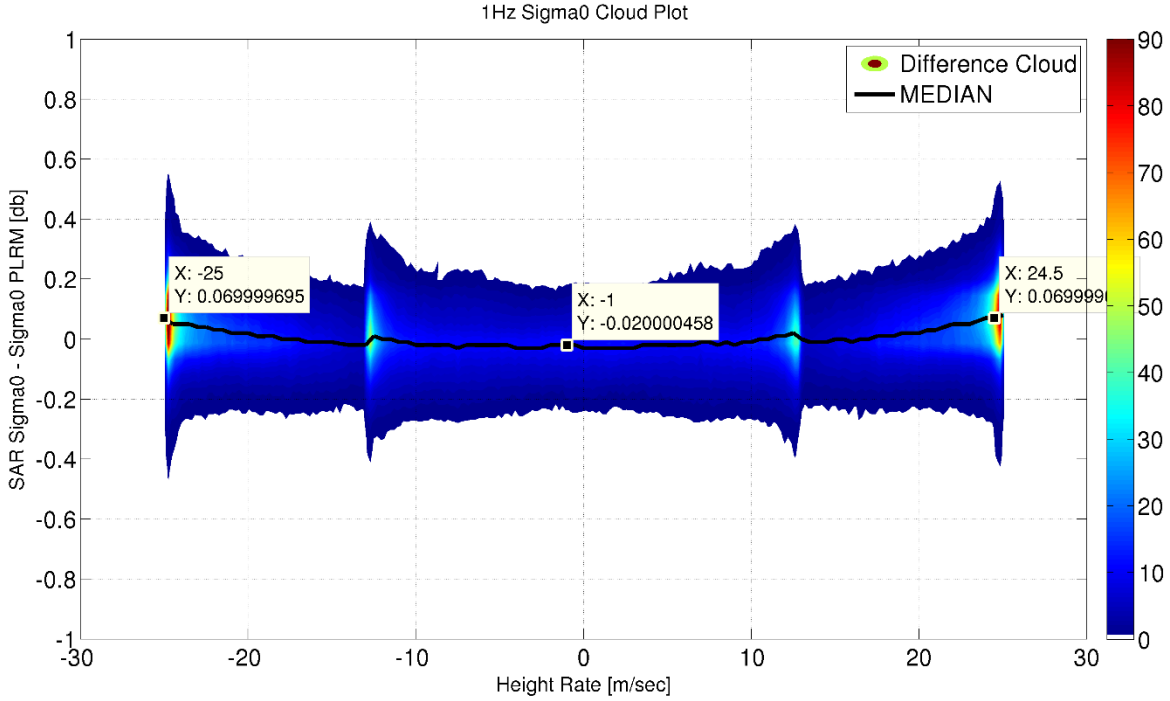

Figure 51 – Density Plot of the Difference between SAR Sigma0 and PLRM Sigma0 with respect Orbital Altitude Rate

4.3.5.4 Sigma 0 Drift

- The difference between SAR and PLRM sigma0 has a negligible drift over time for the time period 23 June 2016 to 20 Jan 2018 (see Figure 52). This is the same result as from the previous reprocessing campaign.

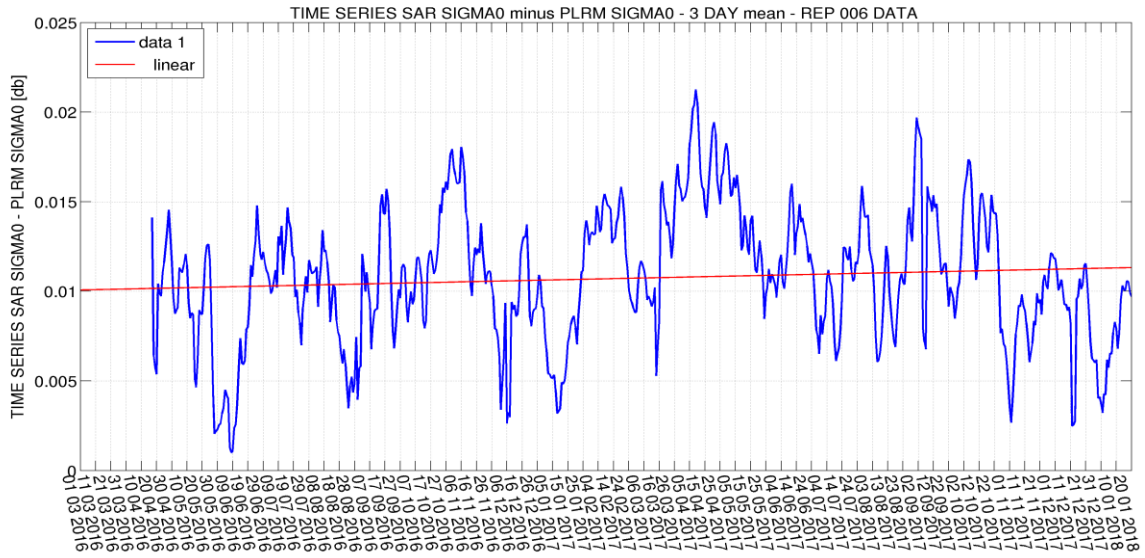

Figure 52 – Time Series of the Difference between SAR and PLRM Sigma nought. Each point is a 3-day mean

4.3.5.5 Comparison with Jason-3

S3A SAR and PLRM Sigma0 estimates show good agreement with J3 GDR data, and between them, with negligible drift. To produce Figure 53 a 2.9 dB bias has been applied to the difference between J3 and S3A SAR, as well as to the difference between J3 and S3A PLRM. The same criteria as in previous equivalent SSHA and SWH Sections of filtering data from ±66º and a 10-day average is applied.

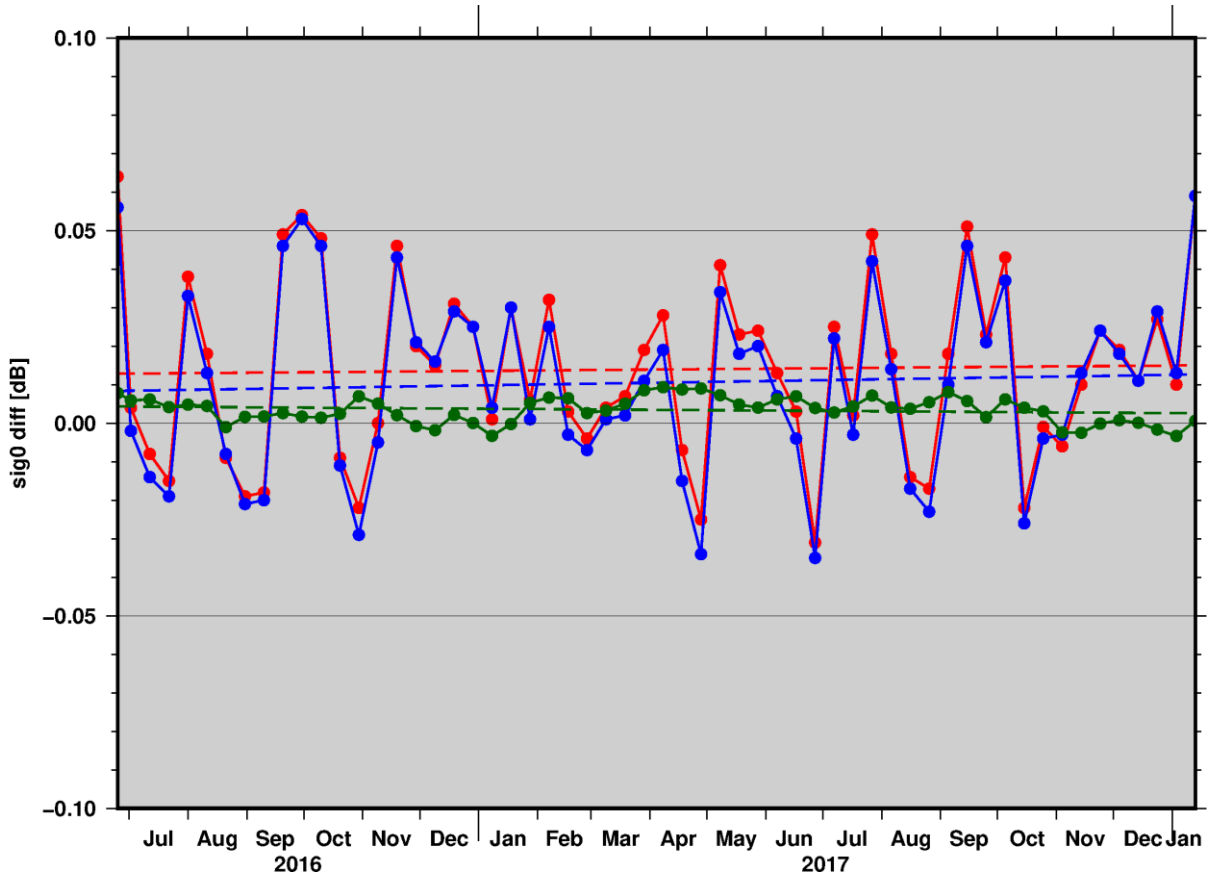

Figure 53 – Sigma0 differences between J3 and S3 SAR (red), J3 and S3 PLRM (blue) and S3 SAR and PLRM (green)

4.3.6 Wind speed

4.3.6.1 Wind speed SAR vs PLRM Comparison

The wind speed scatterplot comparing S3A SAR and PLRM shows a good level of consistency between the two datasets in Cycle 15 (standard deviation of the differences about 43 cm, regression slope of 0.99, and basically zero bias). These values of regression slope and stdd have slightly improved with respect the previous reprocessing campaign.

To be underline that the consistency between the two datasets will be further improved once the issues pointed out in 4.3.5.3 will be mitigated.

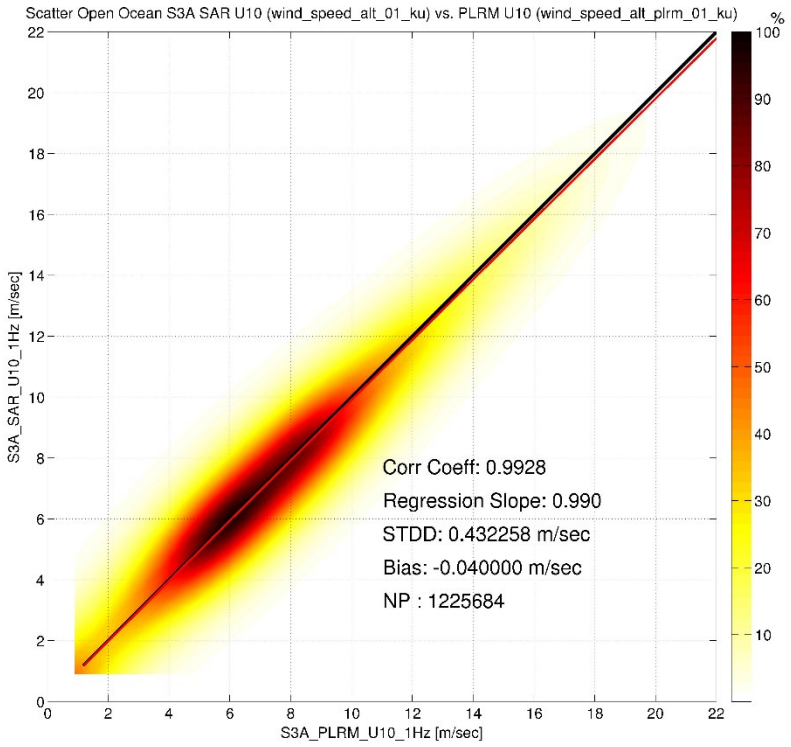

Figure 54 – Scatterplot SAR wind speed versus PLRM wind speed, Cycle 15. Colours indicate point density.

Figure 55 depicts the geographical comparison between SAR and PLRM for Cycle 14. There appears to be no pattern specific to ascending or descending. The differences between SAR and PLRM are small for the ice free regions (average difference of 0.5 m/s without any data filtering).

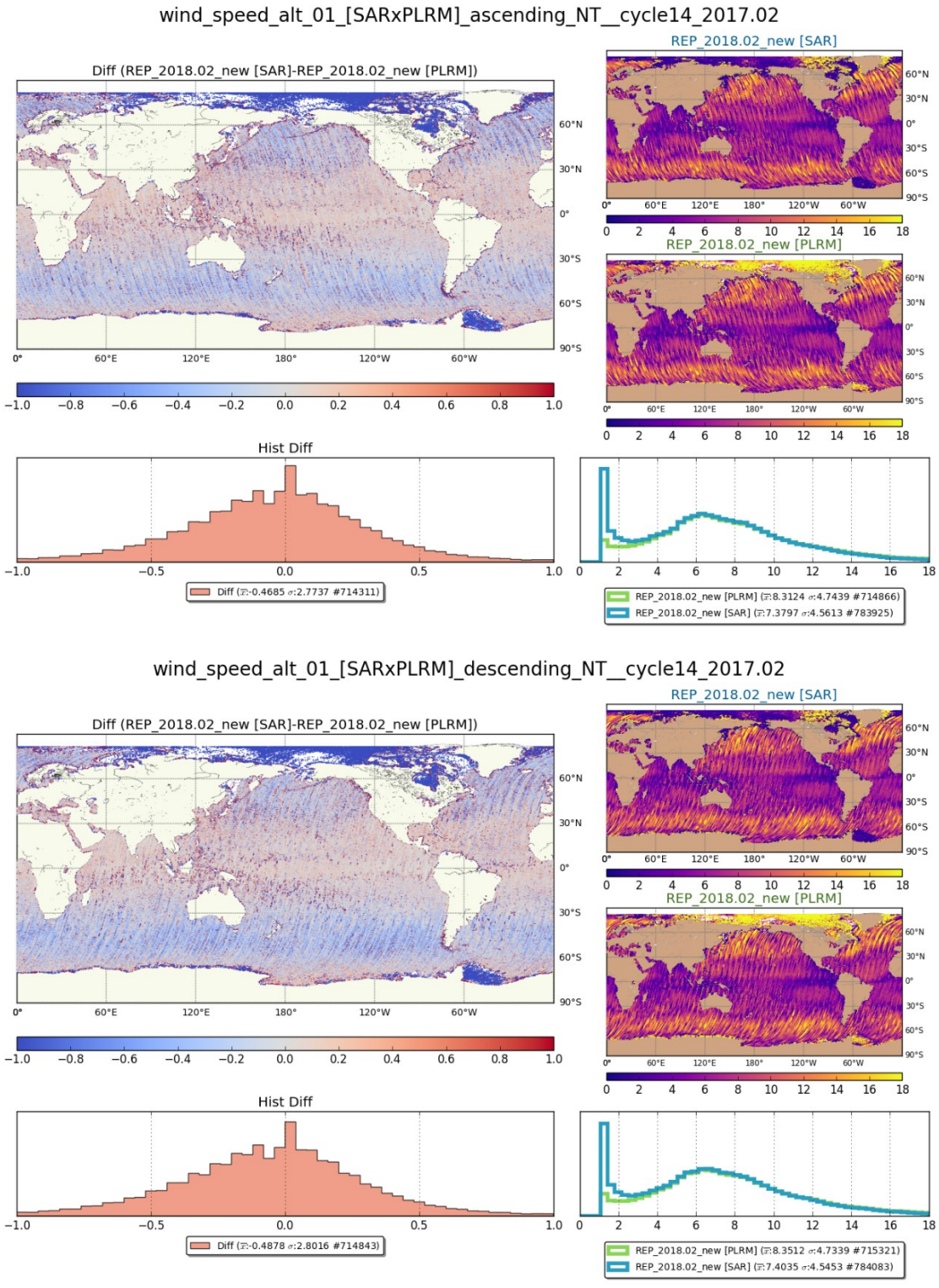

Figure 55 – Wind Speed: Geographical comparison between S3 SAR and PLRM. Ascending (top image), descending (bottom image).

4.3.6.2 Comparison with Jason-3

Figure 56 illustrates the geographical comparison between Wind Speed derived from Sentinel-3 SAR mode (top panel) and Jason-3 GDR (bottom panel).

Note that while on the map there is no filtering, for the histograms (right side) the standard RADS filtering criteria is applied, plus only values with a latitude less than 66º are considered.

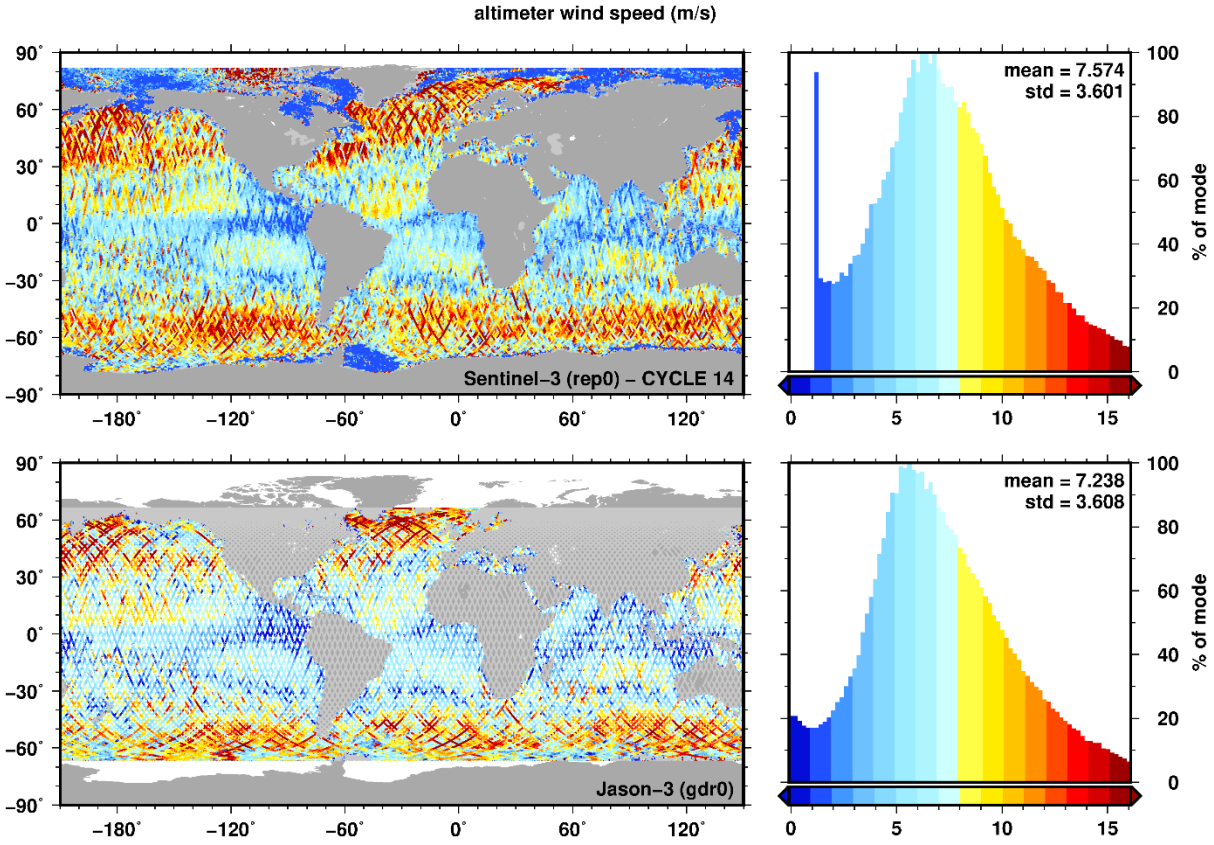

Figure 56 – Wind Speed cross-comparison between S3A (top) and J3 (bottom) for Cycle 14.

At large scale S3 and J3 are observing very similar wind speeds. The mean value are different in about 0.3 m/s (higher wind speed in S3) with slightly lower standard deviation on S3.

4.3.6.3 Comparison with ECMWF model

S3A wind speed retrievals are in good agreement with those derived by the ECMWF model. For SAR the standard deviation of differences is in mean ~1.13m/s for Cycle 14. This is lower than for the previous reprocessing. No major difference in behaviour between ascending and descending passes. For PLRM results are slightly worst, but difference with respect to SAR are negligible. It shall be noted that the results presented in Figure 57 and Figure 58 are computed over Cycle 14. Nevertheless, all Cycles from the reprocessing show the same performance.

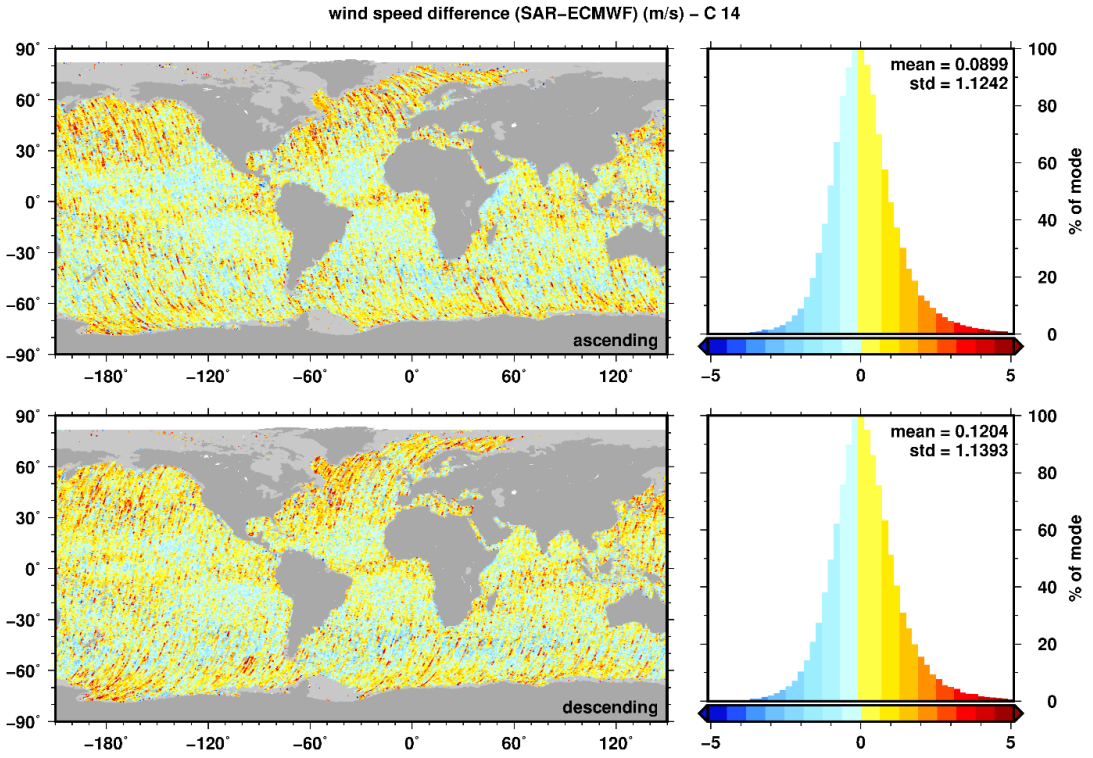

Figure 57 – Wind speed difference (SAR-ECMWF) for S3A reprocessed data during Cycle 14.

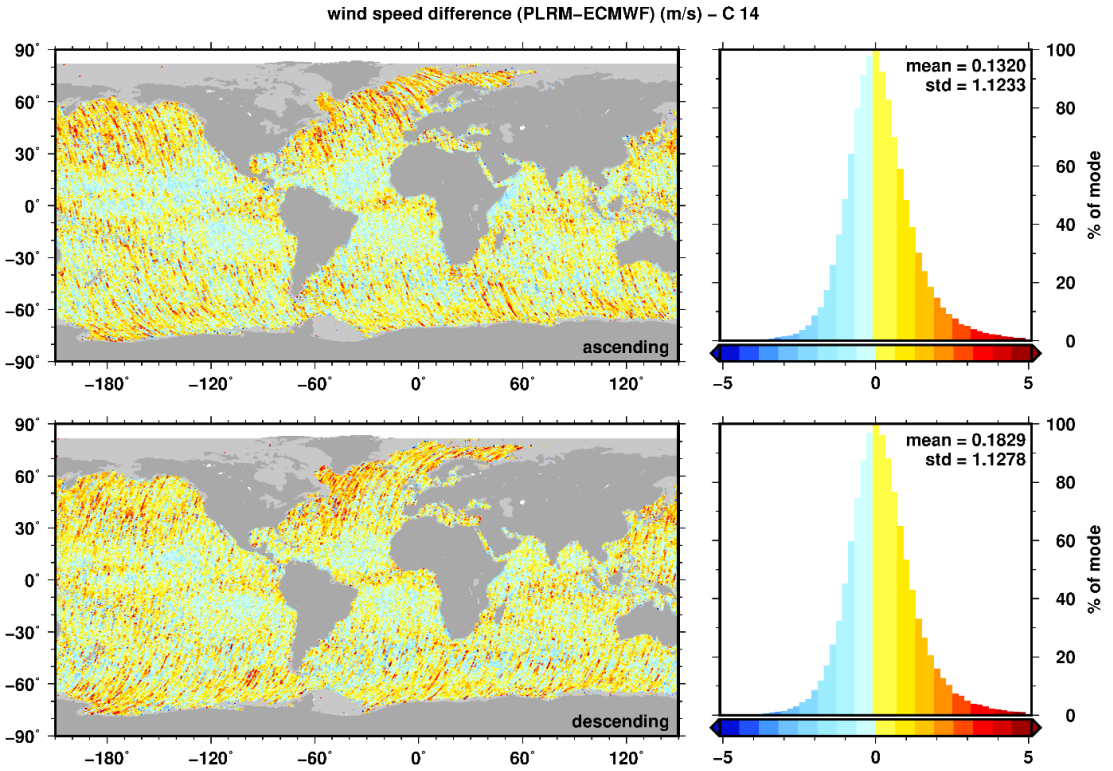

Figure 58 – Wind speed difference (SAR-ECMWF) for S3A reprocessed data during Cycle 14.

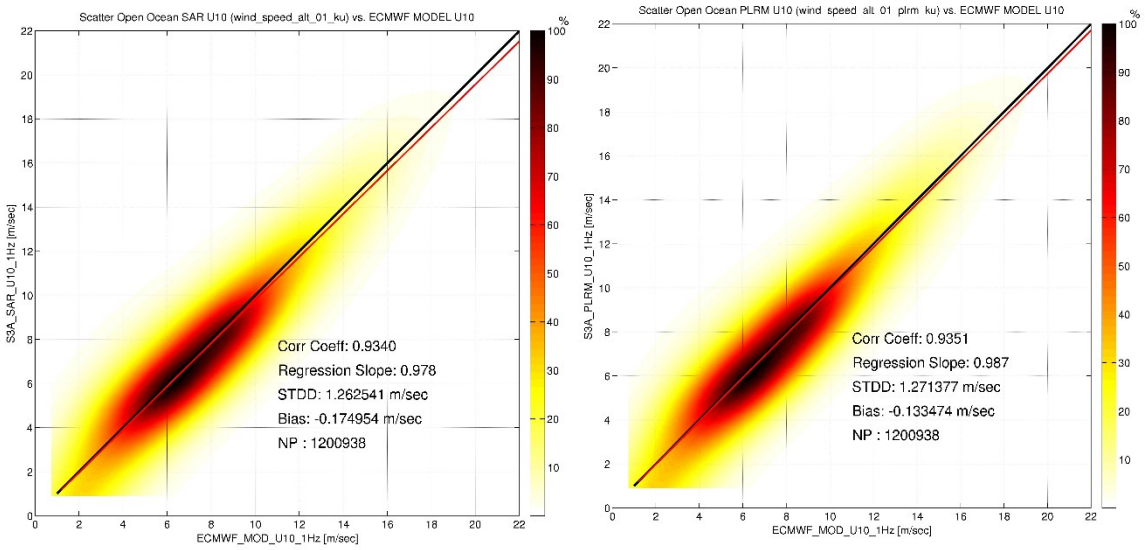

Figure** 59 – **Scatterplot of SAR wind speed versus ECMWF wind speed (left) and scatterplot of PLRM wind speed versus ECMWF wind speed (right), Cycle 15.

The wind speed scatterplots comparing SAR and PLRM to ECMWF wind speed show a high correlation coefficient for Cycle 15 (standard deviation of the differences about 1.26 m/s, regression slope of 0.98, correlation coefficient of 0.03 and very limited bias around –0.15 m/s, SAR/PLRM wind speed being lower than ECMWF model). These results remain similar to the previous reprocessing campaign.

Note that in the comparison between 1-Hz wind speed measurements and the ECMWF modelled wind speed, no along-track averaging was applied to the altimeter wind speed to match the model scales of around 75 km.

Figure ***60*** provides the wind speed time series from the mission start to present. The results confirm that the three data sources SAR, PLRM and ECMWF are unbiased. The std of SAR wind speed is generally lower than PLRM wind speed and closer to the ECMWF wind speed std (see

Figure 61). The time series are generated doing a 3-day average using the RADS' screening criteria.

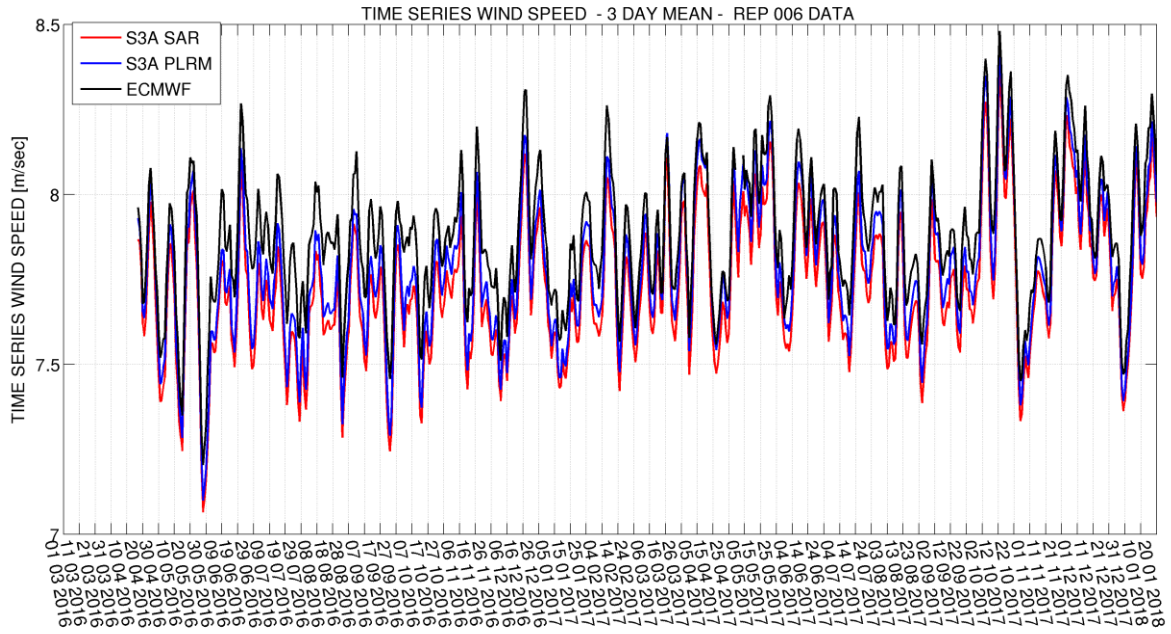

Figure** 60 – **Time Series of the SAR, PLRM and ECMWF Wind Speed Mean (3-day mean)

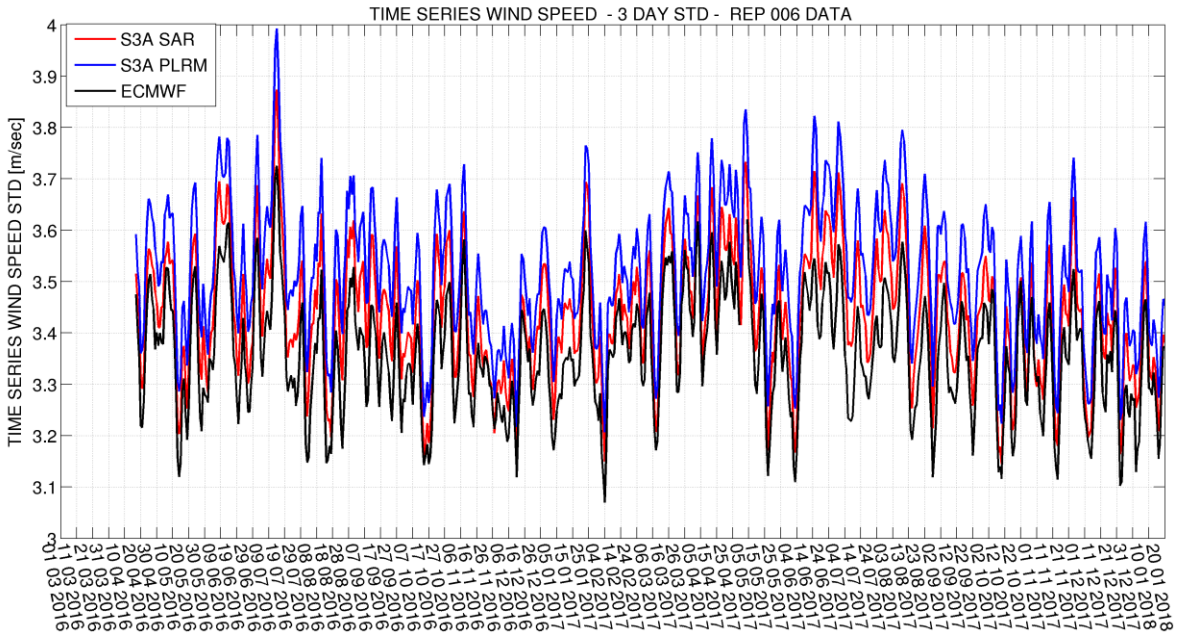

Figure** 61 – **Time Series of the SAR, PLRM and ECMWF Wind Speed Std (3-day std)

4.3.6.4 Comparison with previous datasets

Figure 62 illustrates the different datasets delivered by EUMETSAT to end users, while providing a historical record of wind speed from beginning of mission to end of re-processing 2018. The blue colour refers to the results achieved with the new re-proceed dataset from 2018 (PB 2.27); in red the figure shows the dataset from the previous reprocessing (PB 2.15); and the orange colour depicts the operational data being generated in NTC with the different PBs

over time. Moreover, the top panel provides mean wind speed, while the second standard deviation.

The data is filtered using the STM Tools criteria, and it is aggregated into 10 days (each point corresponds to 10 days of filtered data).

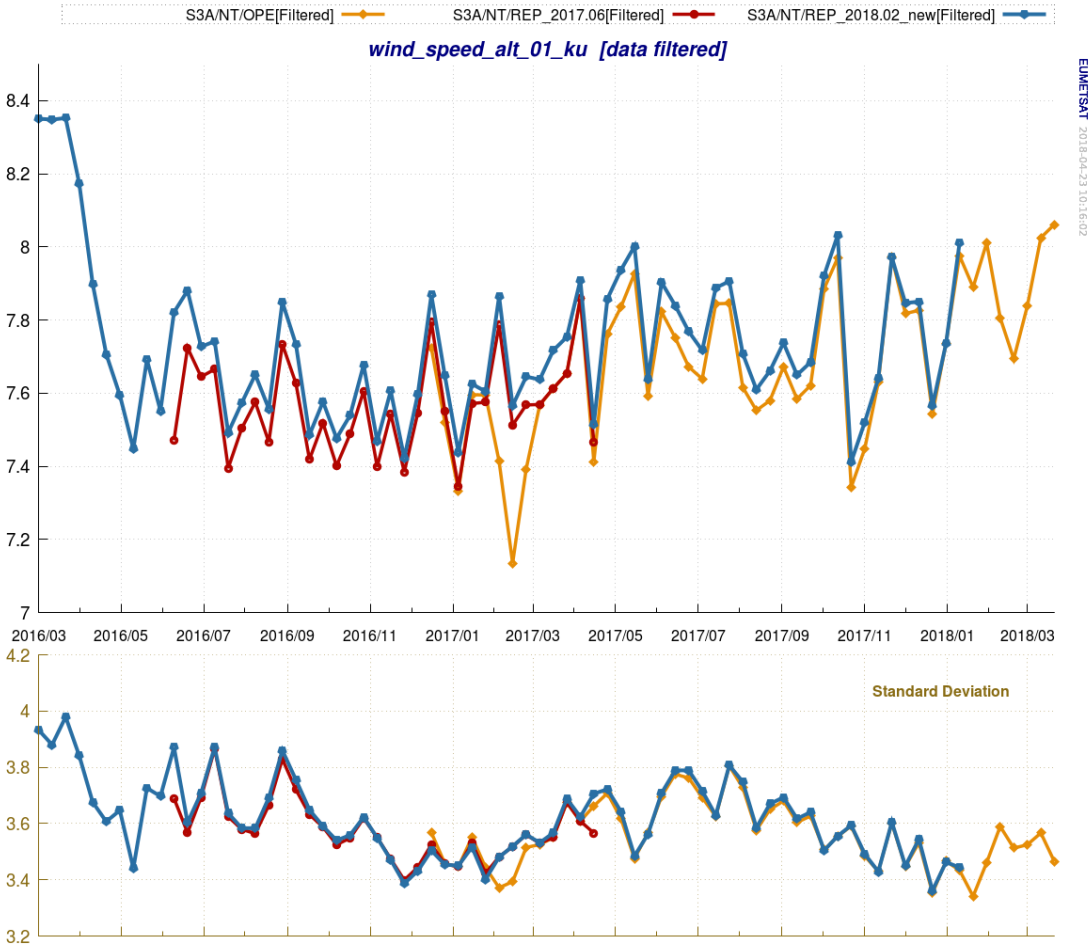

Figure 62 – Wind Speed: Comparison with previous datasets delivered by EUMETSAT

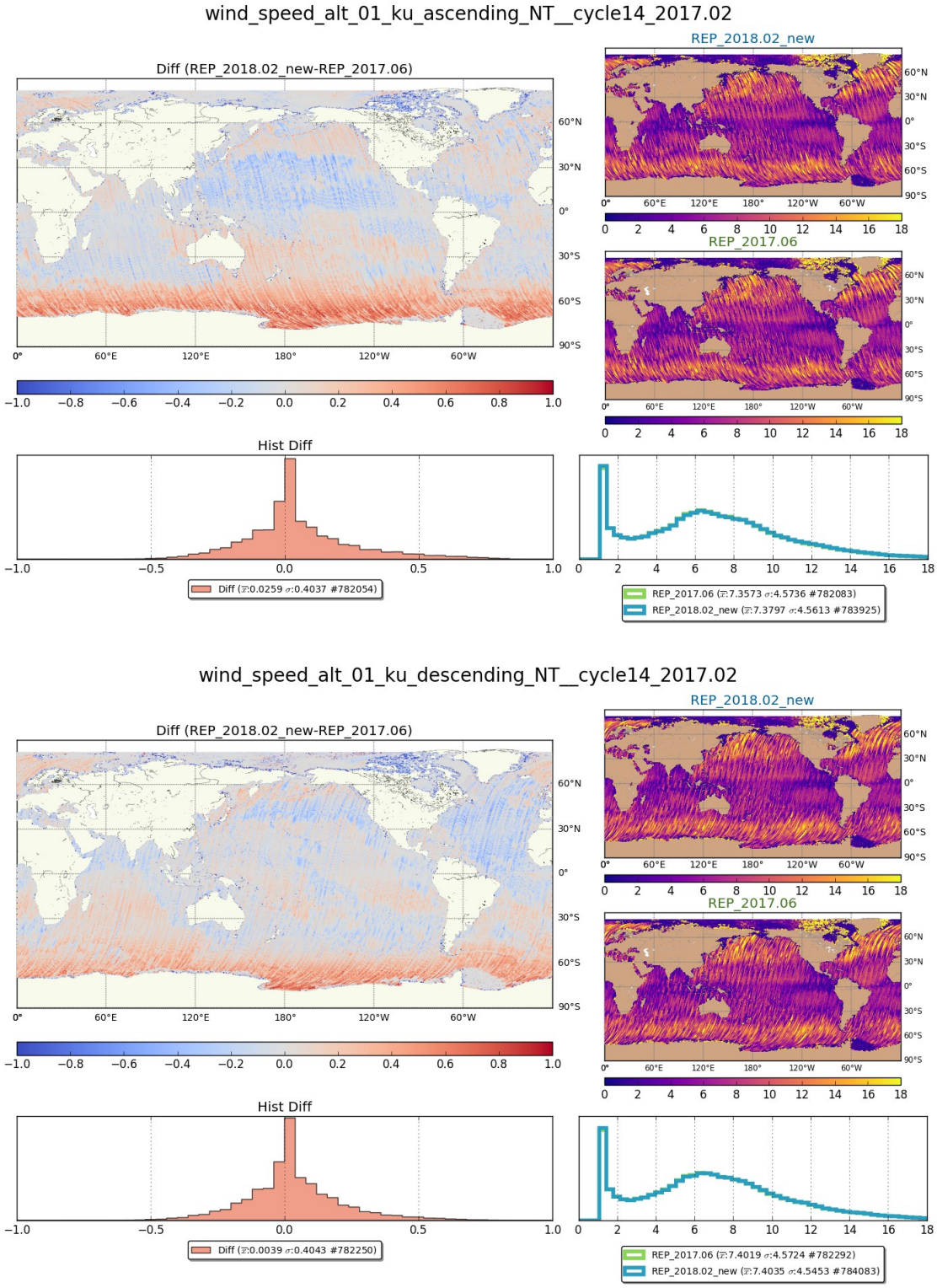

Figure 63 – Wind Speed: Geographical comparison between the current and previous reprocessing

Figure 63 shows the geographical comparison between the previous reprocessing "REP_2017.06" (middle right) and the new one "REP_2018.02_new" (top right). The histograms of both datasets are on the bottom left overlapped.

In the top left, there is the map of differences between both datasets and the histogram of the differences below. No filtering was applied to the datasets on this case. The differences are calculated at 1Hz, in a one-to-one difference.

The top plot shows the Ascending Direction while the bottom shows the Descending one. The Cycle shown here is 14 from 2017/02.

From the time series and the geographical comparison plot, it can be identified that overall the wind speed is very slightly higher with the new PB.

4.3.7 Altimeter Ionospheric Correction

4.3.7.1 SAR vs PLRM comparison

Figure 64 shows a geographical comparison between the altimeter-derived ionospheric corrections as processed in PLRM or SAR mode.

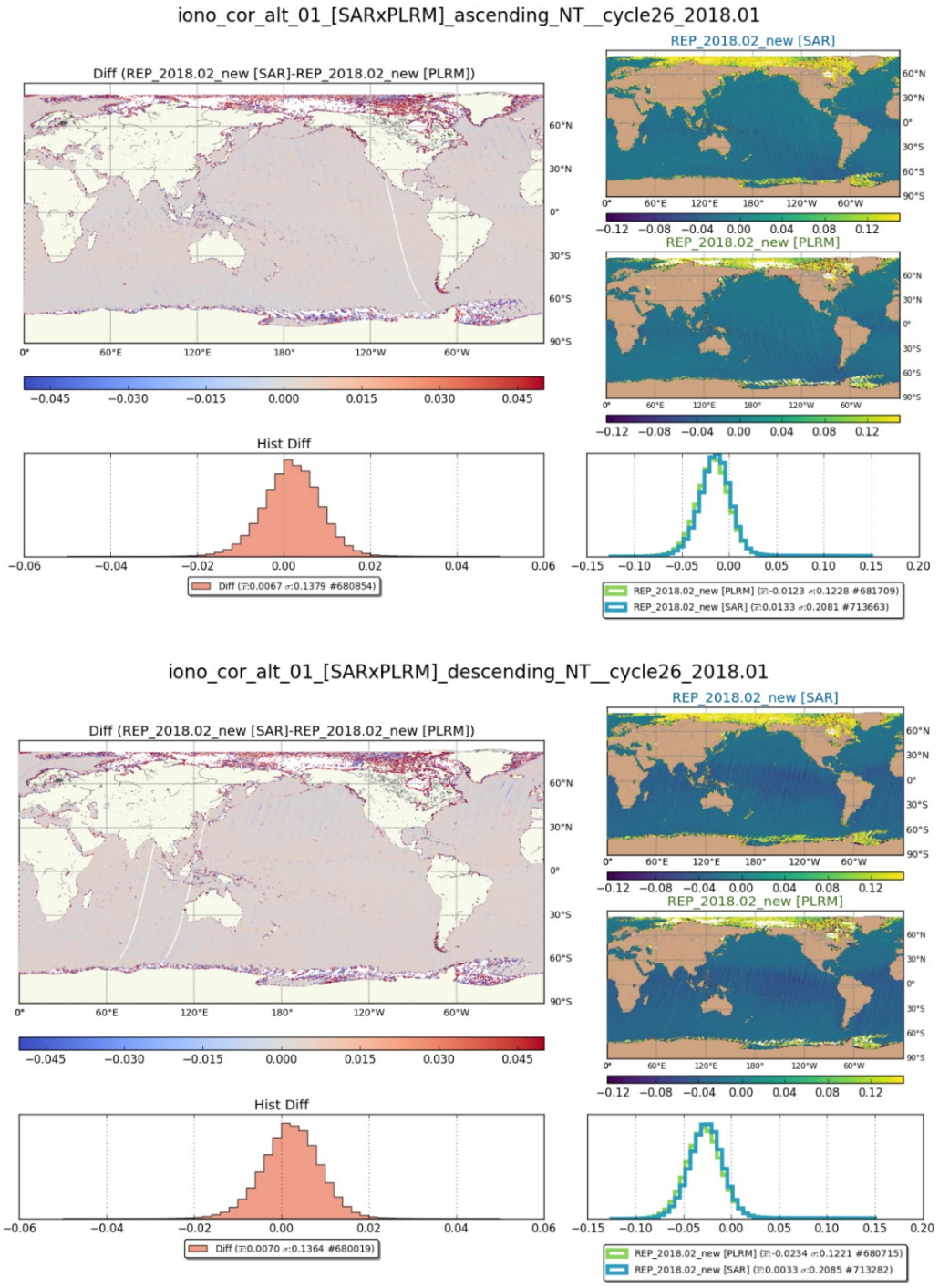

Figure 64 – Ionospheric Correction: Geographical comparison between S3 SAR and PLRM. Ascending (top image), descending (bottom image).

There is a difference of ~7 mm between SAR and PLRM. This result is achieved without data filtering. The relevant differences are observed at high latitudes.

When we consider only the ocean points not covered by sea-ice and after low-pass filtering the ionospheric corrections, the bias between SAR and PLRM ionospheric corrections reduces to ~2 mm (see Figure 65).

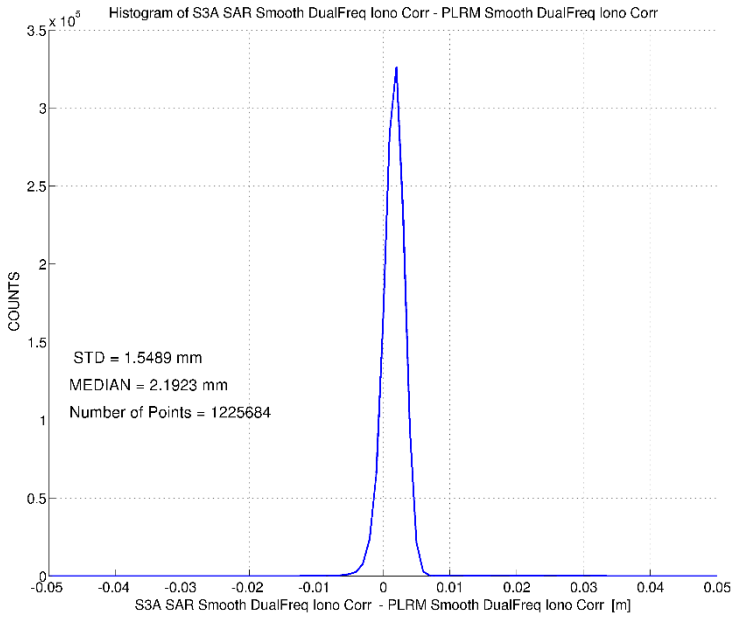

Figure 65 – Histogram of the Difference between SAR Dual Frequency Ionospheric Correction and PLRM Dual Frequency Ionospheric Correction in Cycle 15

4.3.7.2 Comparison with Jason-3

The comparison between S3A and Jason-3 ionospheric correction as derived by the altimetry dual frequency is illustrated in Figure 66.

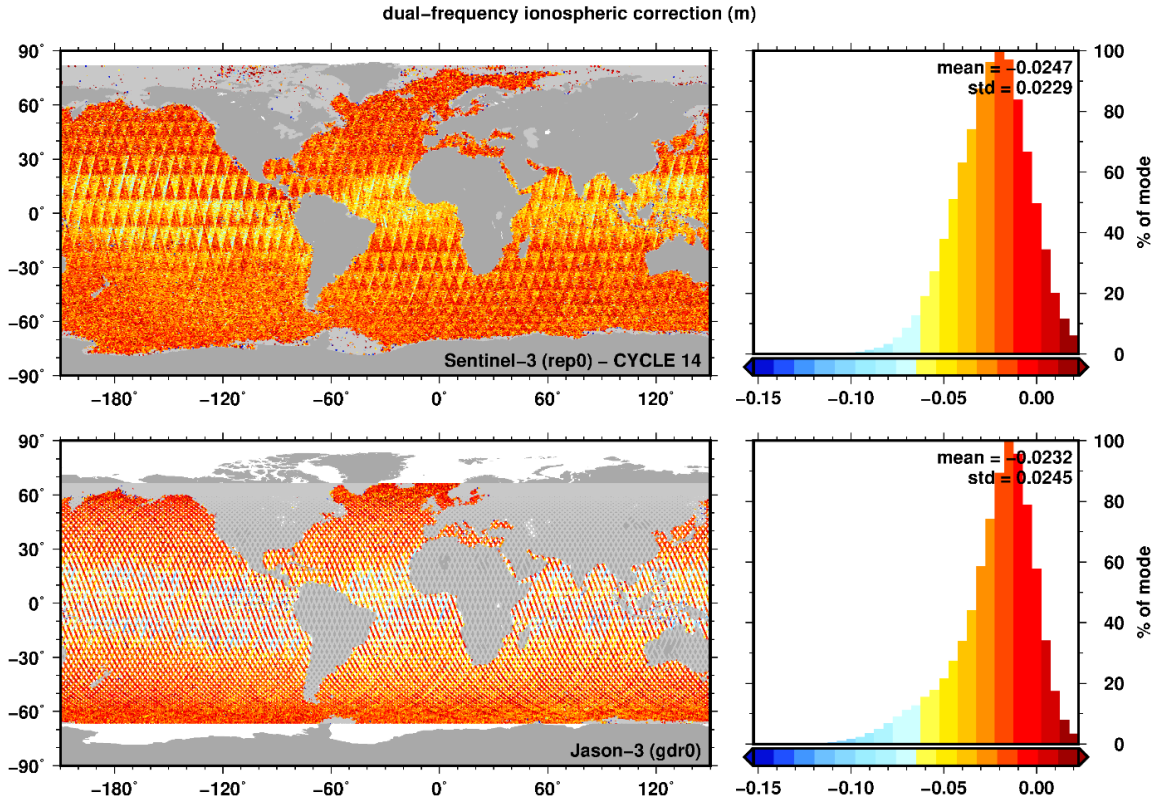

Figure 66 – Ionospheric Correction cross-comparison between S3A (top) and J3 (bottom) for Cycle 14.

The two datasets are consistent, showing a good coherence of the ionospheric correction between S3A and J3.

4.3.7.3 Comparison with GIM Model

Figure 67 show the geographical comparison between the GIM model correction for ionosphere "iono_cor_gim_01_ku" (middle right) and the altimeter derived correction "iono_cor_alt_01_ku" (top right). The histograms of both datasets are on the bottom left overlapped.

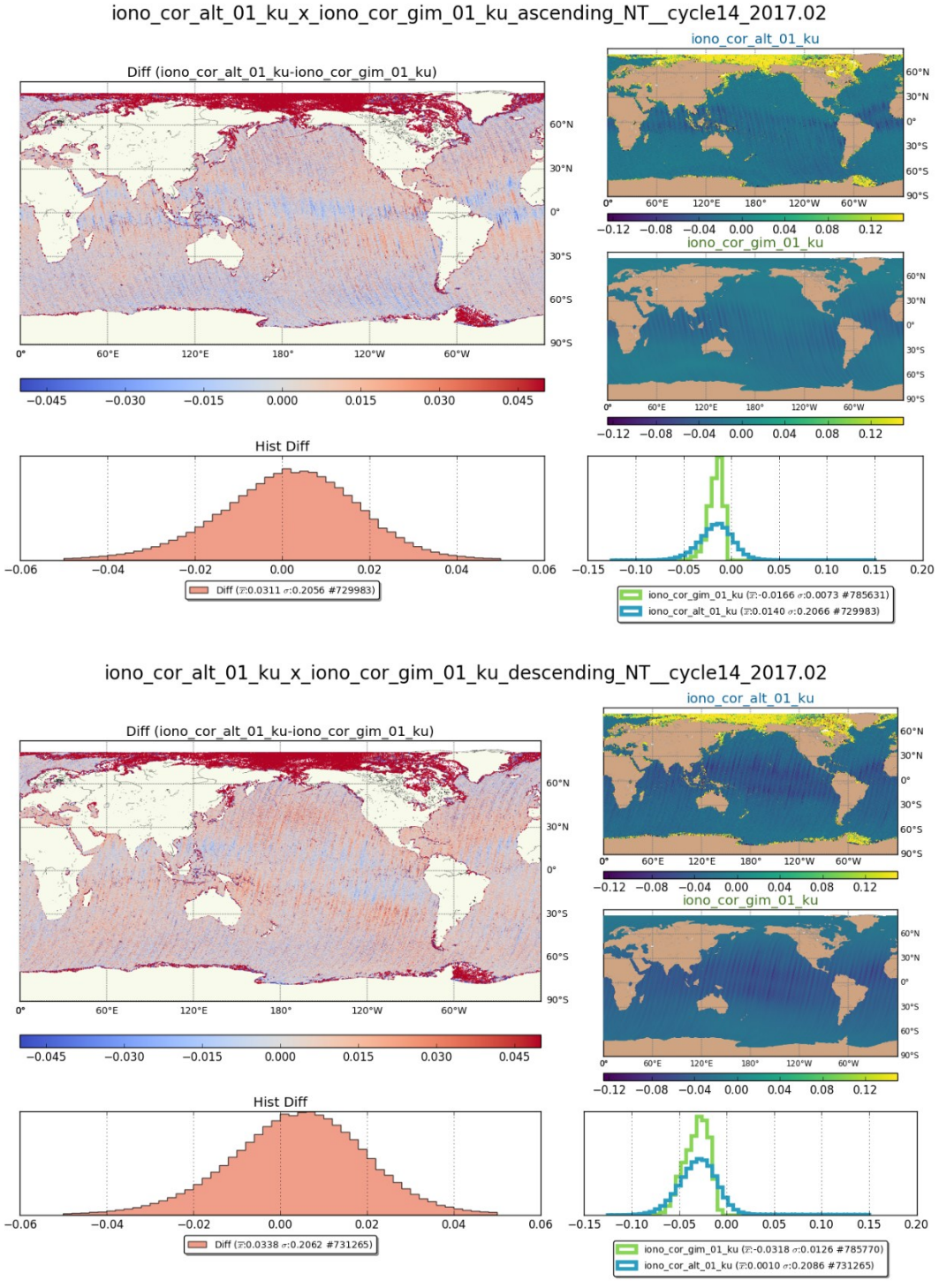

Figure 67 – Ionospheric Correction: Geographical comparison between the altimeter-derived correction and GIM model

In the top left, there is the map of differences between both datasets and the histogram of the differences below. No filtering was applied to the datasets on this case. The differences are calculated at 1 Hz, in a one-to-one difference.

The top plot shows the Ascending Direction while the bottom one the Descending one. The Cycle shown here is 14 from 2017/02.

As expected the major differences between the ionospheric correction from the GIM model and the one derived from the dual frequency altimeter are in the high latitude regions, where sea-ice/ice might interfere in the altimeter processing.

Overall the GIM correction has lower values than the ones from the altimeter, the plot is overall reddish.

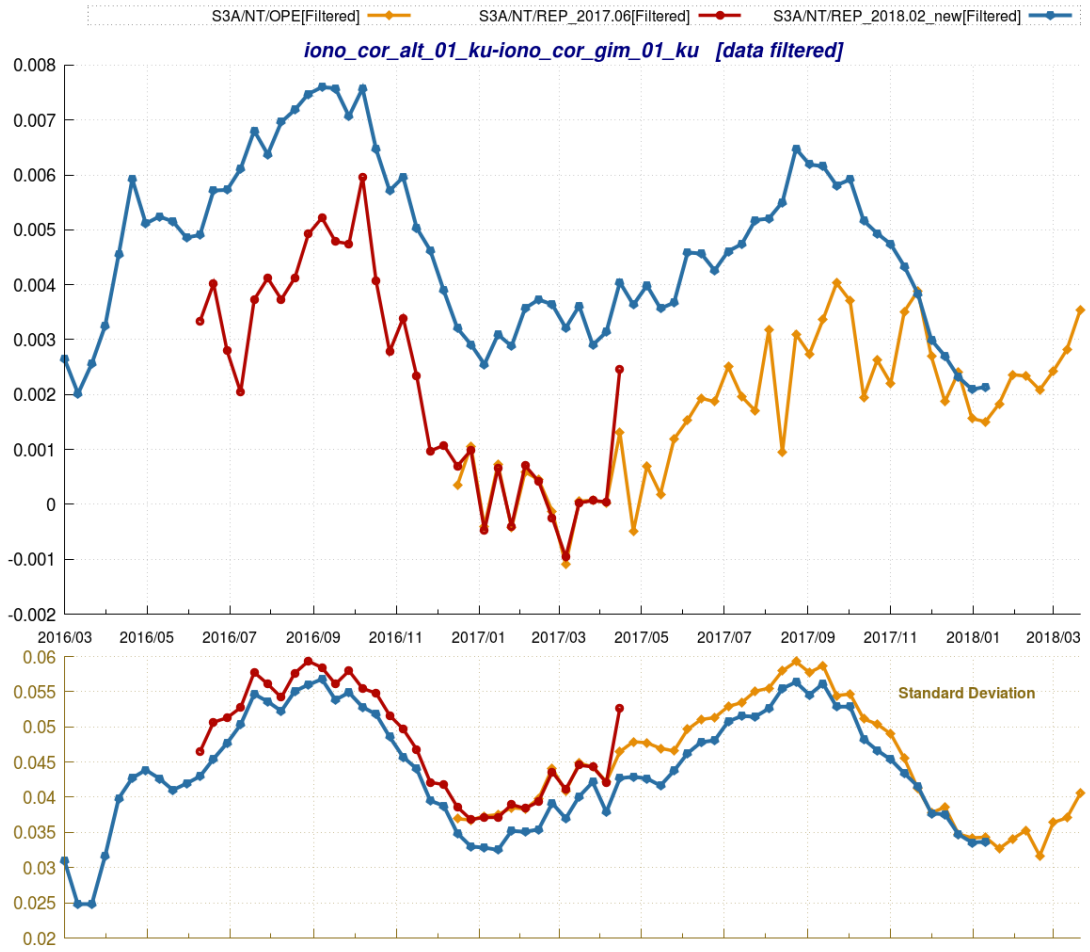

Figure 68 – Ionospheric correction (altimeter versus model): Comparison with previous datasets delivered by EUMETSAT

Figure 68 shows the difference between the altimeter-derived ionospheric correction and the GIM model one. **Notice that the above altimeter derived one is not smoothed**.

The different datasets delivered by EUMETSAT to end users are shown. The blue is the new dataset from the 2018 reprocessing (PB 2.27), the red is the dataset from the previous reprocessing (PB 2.15) and the orange line shows the operational data being generated in NTC with the different PBs over time.

The bottom panel has the standard deviation.

The data is filtered using the STM Tools criteria (see 4.3.1.2) and the aggregated into 10 days (each point corresponds to 10 days of filtered data).

From Figure 68, it is clear that the new reprocessing campaign and processing baseline has improved the consistency between GIM model and altimeter-derived ionospheric correction but now a +2 mm bias with respect GIM model appears. Analysis will make in future to investigate whether the origin of this bias is in the altimeter-derived ionospheric correction or in the GIM model posted in the L2 marine products.

The improvement in the consistency with GIM model is attributed to the new CAL1 and CAL2 calibration scheme for C Band, returning a more accurate C Band ranging.

4.3.7.4 Comparison between SAR and PLRM

Figure 69 and Figure 70 show good agreement between SAR and PLRM ionospheric corrections in mean (Figure 69), and std (Figure 70). Results derived from the SAR mode show a 2 mm bias with respect to those derived in PLRM, being SAR's ionospheric correction higher. S3A PLRM and GIM model results agree, whereas those derived in SAR mode only feature a constant bias identical to the one observed with respect PLRM. The std values are similar between operational modes, and also to GIM. The time series are generated accounting for a 3-day average using the RADS screening criteria. The SAR and PLRM altimeter-derived ionospheric corrections have been smoothed in the time series.

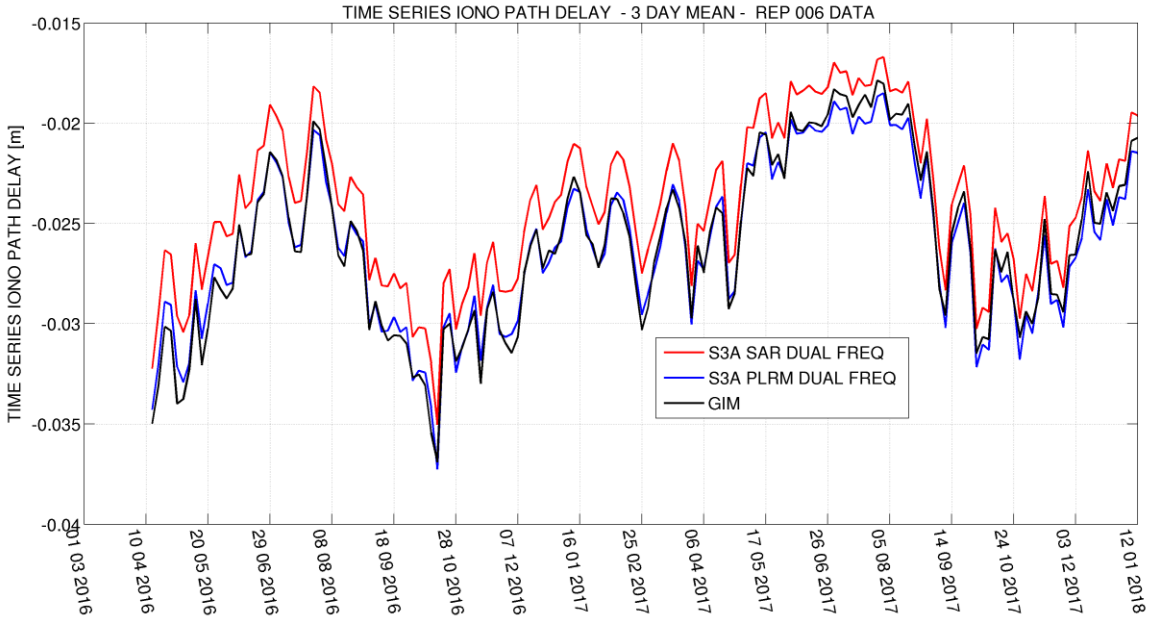

Figure 69 – Time Series of Altimeter-derived Ionospheric Correction Mean for SAR and PLRM mode and Time Series of GIM Ionospheric Model Mean

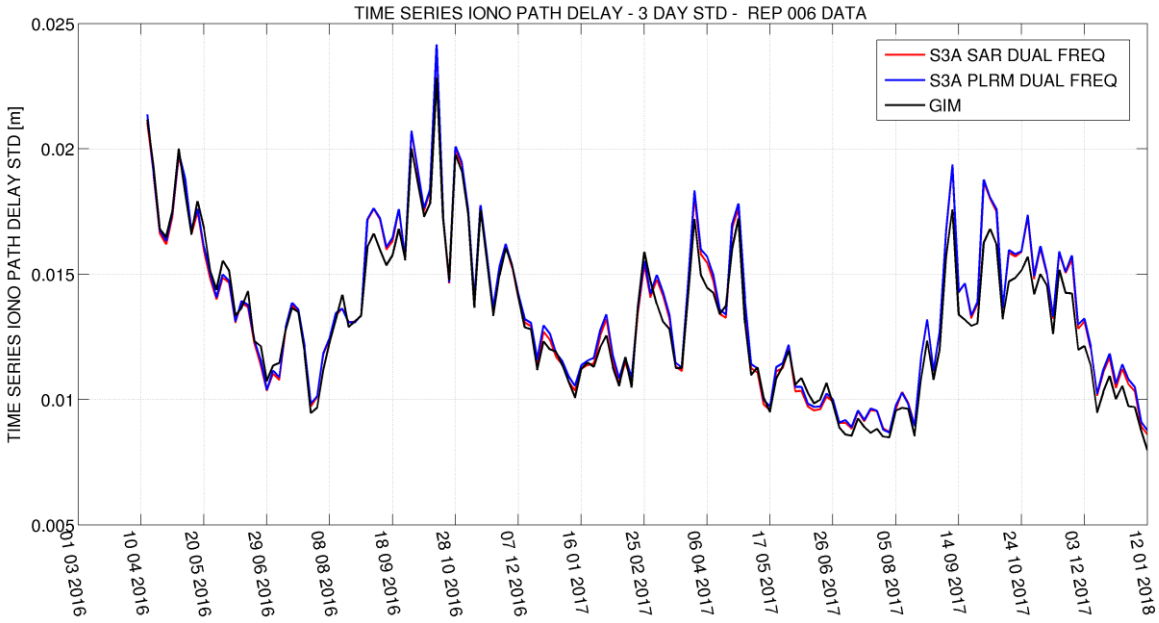

Figure 70 – Time Series of Altimeter-derived Ionospheric Correction STD for SAR and PLRM mode and Time Series of GIM Ionospheric Model STD

4.3.7.5 Altimeter-Derived Ionospheric Correction Drift

The difference between altimeter-derived SAR ionospheric correction and altimeter-derived PLRM ionospheric correction drifts slightly over the time as shown in Figure 71. This drift has been estimated to be –0.27 mm/year for the time period 23 June 2016 to 20 Jan 2018.

The time series have been built with 3-day averaging and using the RADS screening criteria.

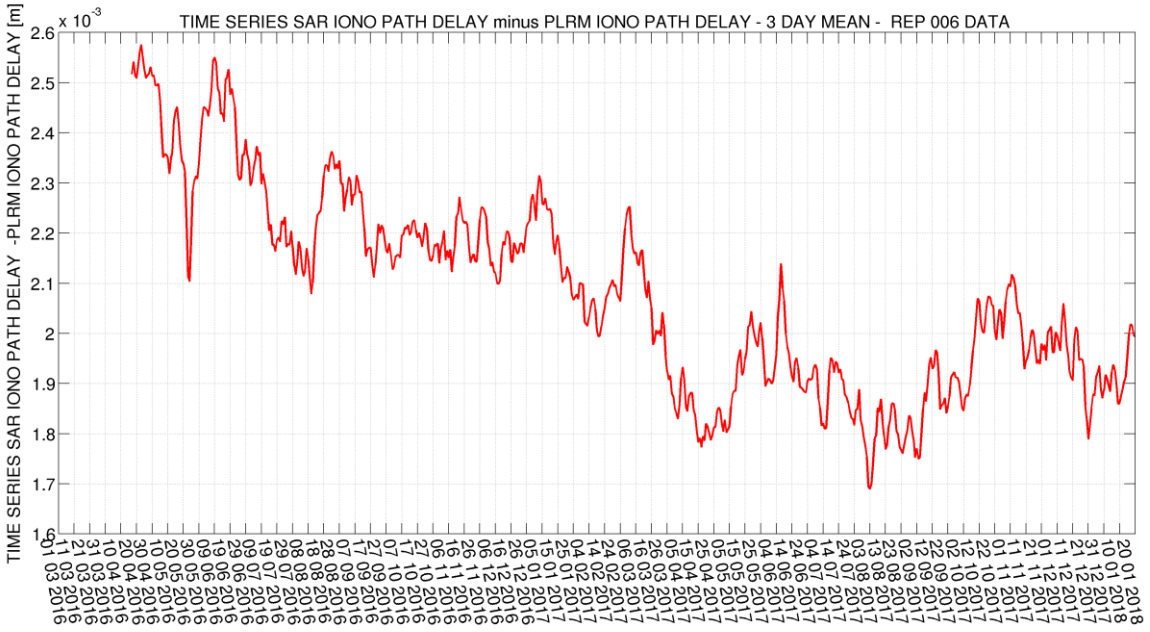

Figure 71 – Time Series of the Difference between altimeter-derived SAR ionospheric correction and altimeter-derived PLRM ionospheric correction. Each point is a 3-day mean.

4.3.7.6 Comparison with previous dataset

Figure 72 shows the different datasets delivered by EUMETSAT to end users and how the altimeter-derived Ionospheric Correction change over time. The blue is the new dataset from the 2018 reprocessing (PB 2.27), the red is the dataset from the previous reprocessing (PB 2.15) and the orange line shows the operational data being generated in NTC with the different PBs over time.

The top panel has the Ionospheric correction variable and the bottom one the standard deviation.

The data is filtered using the STM Tools criteria (see 4.3.1.2) and the aggregated into 10 days (each point corresponds to 10 days of filtered data).

From Figure 72, it is clear that the new reprocessing campaign and processing baseline has improved the global standard deviation and has increased the level of the altimeter-derived ionospheric correction by +2 mm.

The improvement in the global std is attributed to the new CAL1 and CAL2 calibration scheme for C Band returning a more accurate C Band ranging.

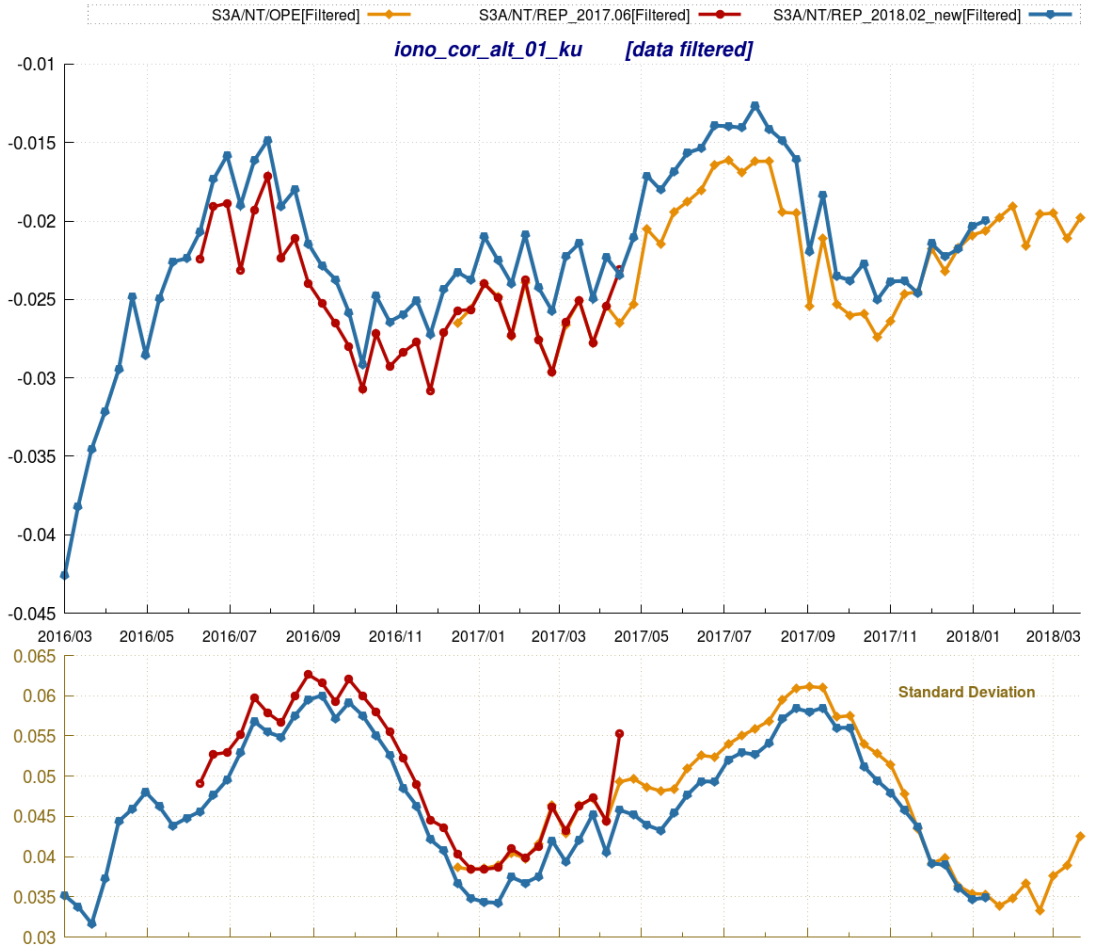

Figure 72 – Ionospheric Correction: Comparison with previous datasets delivered by EUM

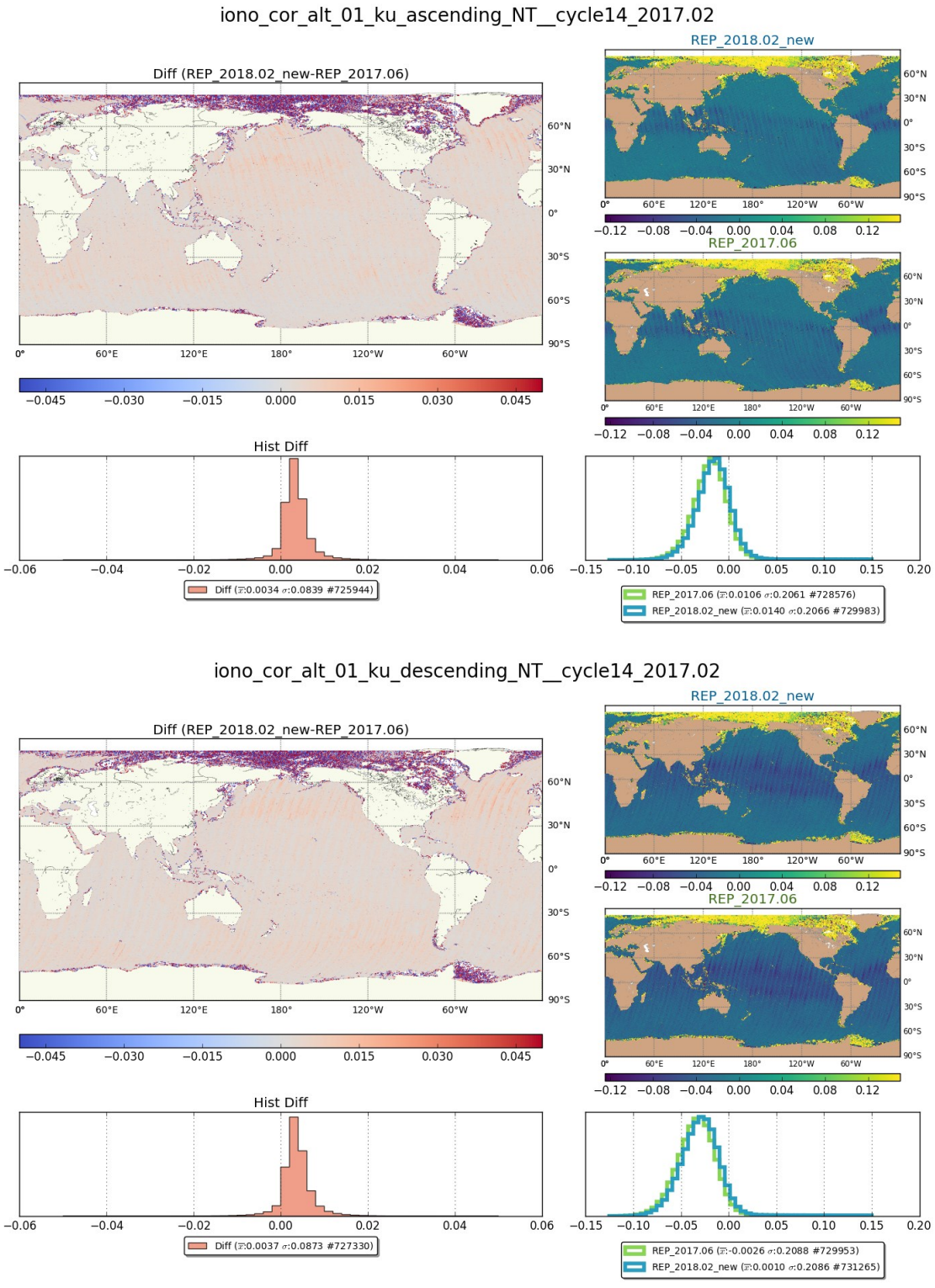

Figure 73 – Ionospheric Correction: Geographical comparison between the current and previous reprocessing

Figure 73 shows the geographical comparison between the previous reprocessing "REP_2017.06" (middle right) and the new one "REP_2018.02_new" (top right). The histograms of both datasets are on the bottom left overlapped.

In the top left, there is the map of differences between both datasets and the histogram of the differences below. No filtering was applied to the datasets on this case. The differences are calculated at 1Hz, in a one-to-one difference.

The top plot shows the Ascending Direction while the bottom one the Descending one. The Cycle shown here is 14 from 2017/02.

4.3.8 Radiometer Wet Tropospheric Correction (WTC)

4.3.8.1 Comparison with Jason-3

The comparison between S3A and Jason-3 radiometer wet tropospheric correction is illustrated in Figure 74.

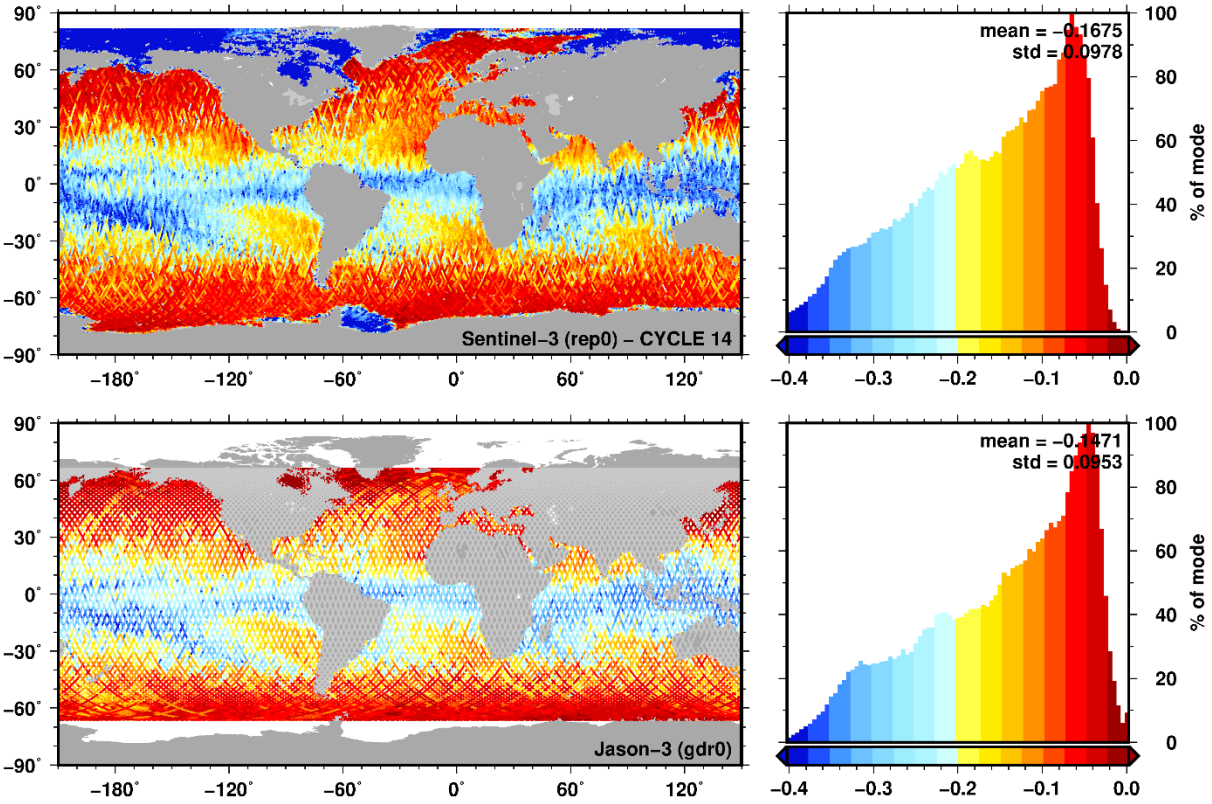

Figure 74 – Radiometer wet tropospheric correction, comparison between Sentinel-3 and Jason-3

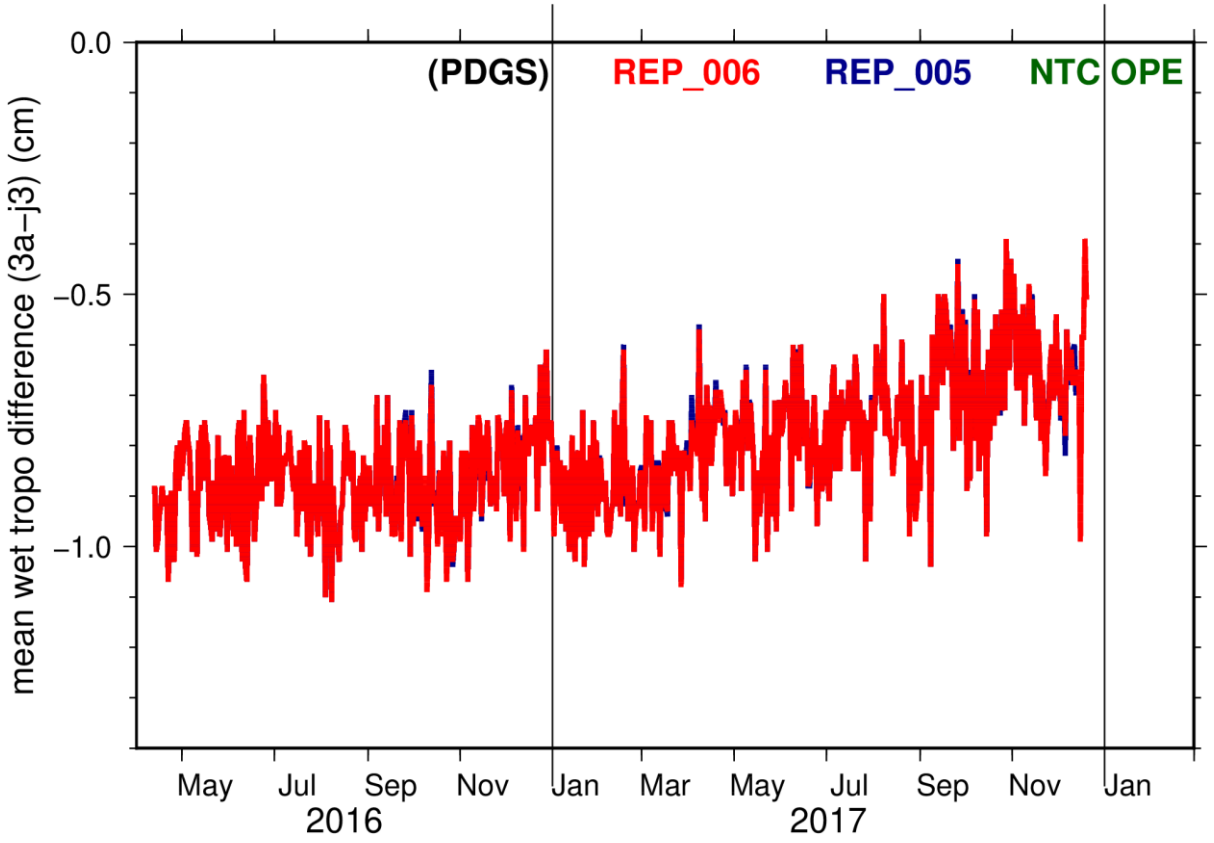

Figure 75 – Radiometer wet tropospheric correction (S3A-J3 xover difference)

There is a trend in the wet tropospheric correction of Jason-3 versus S3A, as can be seen from the Figure 75, where the mean wet tropospheric correction differences between S3A and J3 are plotted over time. These differences increases over time, thus affecting the Sea Surface Height Anomaly. The drift appears to come from an uncompensated drift in the Jason-3 AMR radiometer.

4.3.8.2 Comparison with ECMWF Model

The scatterplot of radiometric wet tropospheric correction (WTC) and the ECMWF wet tropospheric correction (Cycle 15) can be found below. It shows very good consistency (a negligible bias of +0.5 mm, standard deviation of the difference around 1.35 cm and correlation coefficient of 0.99). The scatter cloud is symmetric around the bisector line.

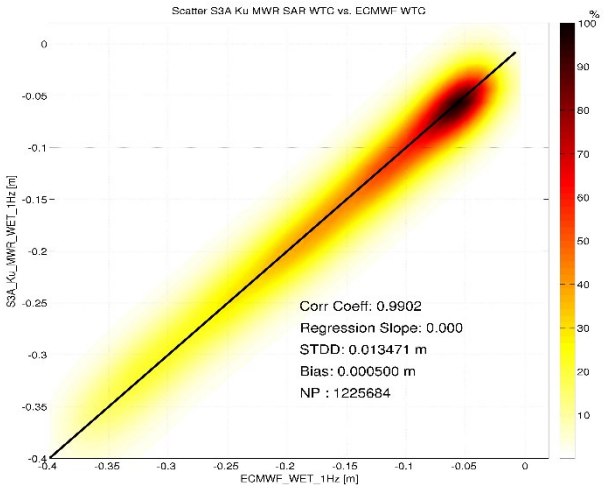

Figure 76 – Scatterplot Radiometer wet range correction versus ECMWF wet range correction, Cycle 15. The colours indicate point density.

Figure 77 shows the geographical comparison between the ECMWF model correction for ionosphere "mod_wet_tropo_cor_meas_altitude_01" (middle right) and the altimeter derived correction "rad_wet_tropo_cor_01_ku" (top right). The histograms of both datasets are on the bottom left overlapped.

In the top left, there is the map of differences between both datasets and the histogram of the differences below. No filtering was applied to the datasets on this case. The differences are calculated at 1Hz, in a one-to-one difference.

As expected the radiometer correction and the modelled one diverge mainly over ice surfaces and coastal zone.

The top plot shows the Ascending Orbit Direction, the bottom one the Descending Orbit Direction. The Cycle shown here is 14 from 2017/02.

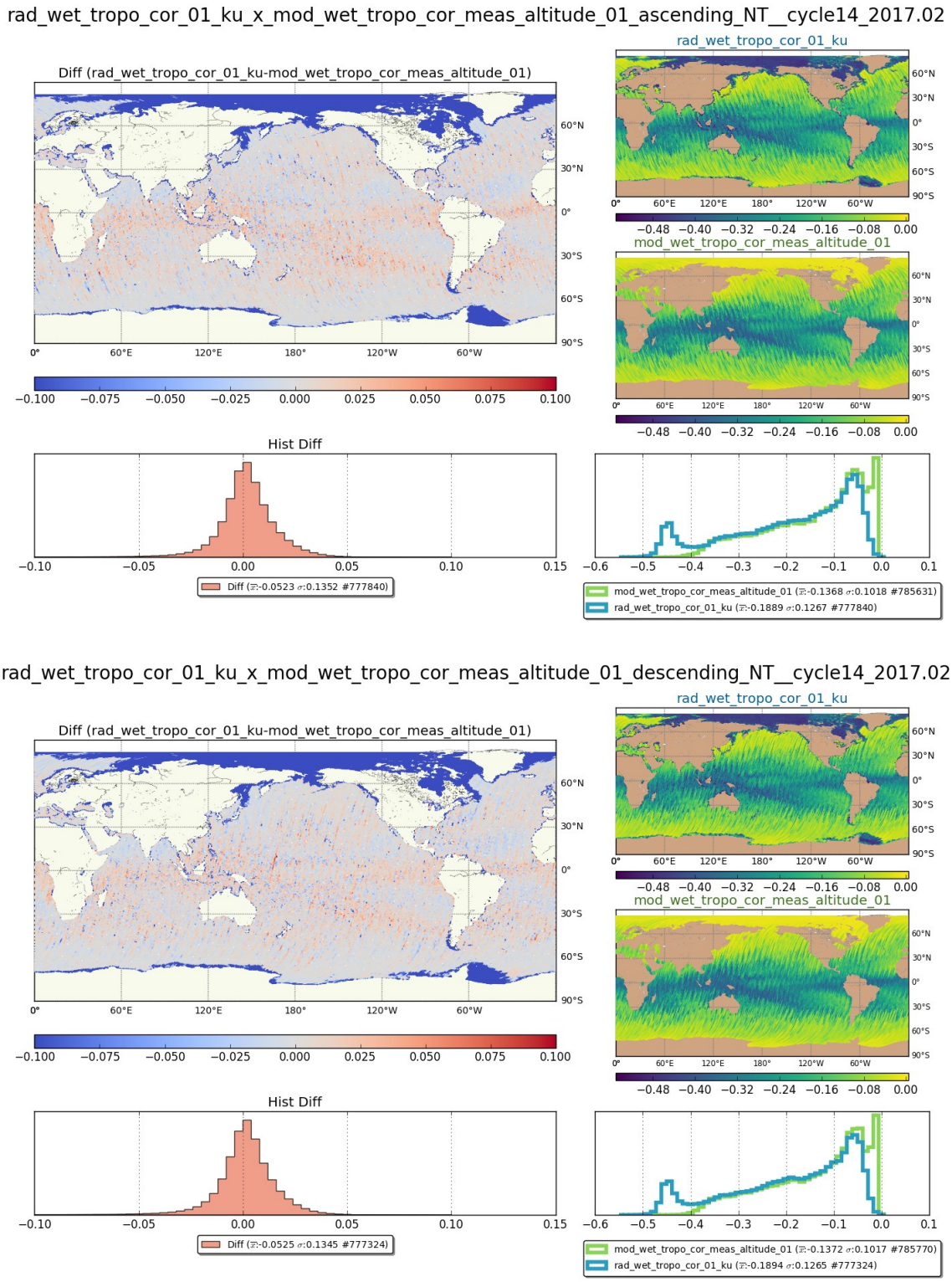

Figure 77 – Radiometer wet tropospheric correction: Geographical comparison between the radiometer derived correction and ECMWF model

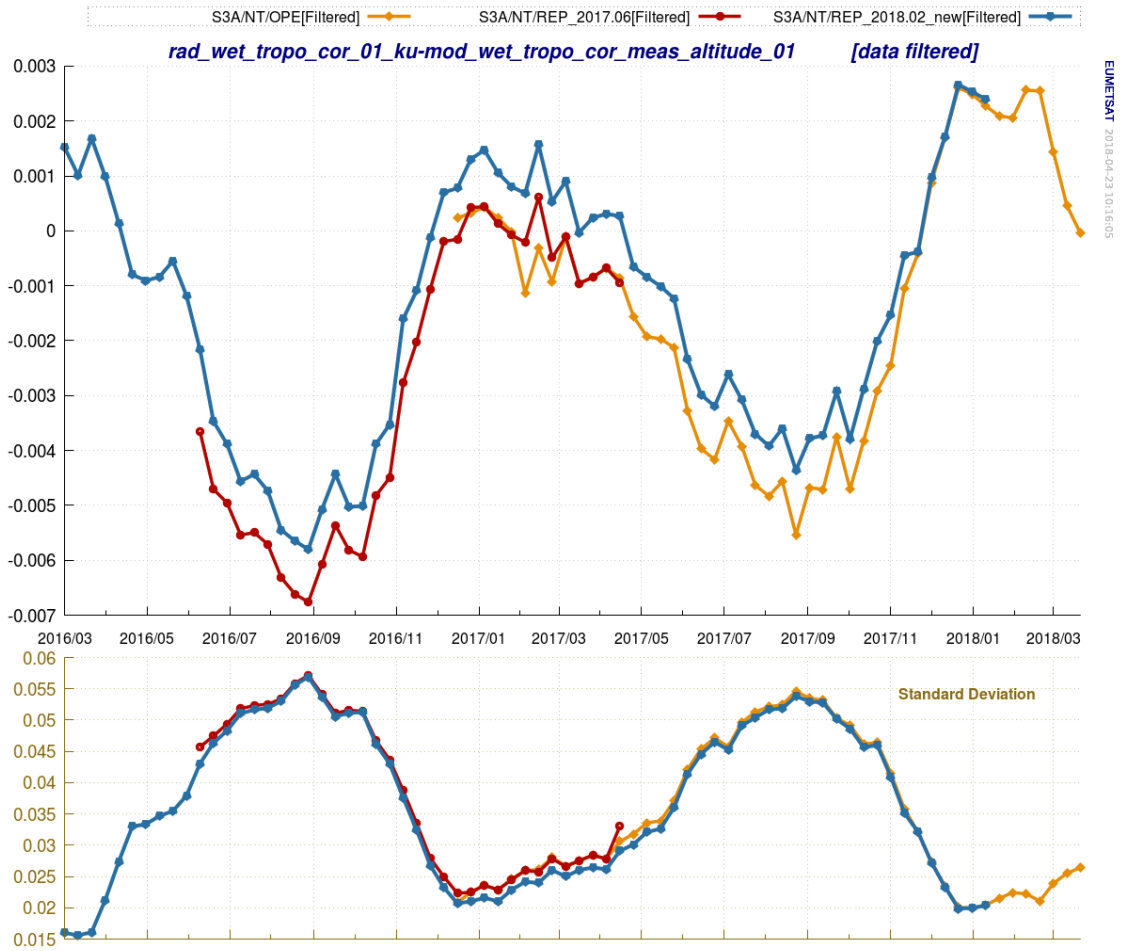

Figure 78 – Radiometer wet tropospheric correction (radiometer versus model): Comparison with previous datasets delivered by EUMETSAT

Figure 78 shows the difference between the radiometer derived wet tropospheric correction and the ECMWF model one. The different datasets delivered by EUMETSAT to end users are shown. The blue is the new dataset from the 2018 reprocessing (PB 2.27), the red is the dataset from the previous reprocessing (PB 2.15) and the orange line shows the operational data being generated in NTC with the different PBs over time.

The bottom panel has the standard deviation.

The data is filtered using the STM Tools criteria (see Section 4.3.1.2) and the aggregated into 10 days (each point corresponds to 10 days of filtered data).

4.3.8.3 Comparison with Previous datasets

Figure 79 shows the different datasets delivered by EUM to end users and how the Radiometer Wet Tropospheric Correction change over time. The blue is the new dataset from the 2018 reprocessing (PB 2.27), the red is the dataset from the previous reprocessing (PB 2.15) and the orange line shows the operational data being generated in NTC with the different PBs over time.

The top panel has the Wet Tropospheric Correction variable and the bottom one the standard deviation.

The data is filtered using the STM Tools criteria and the aggregated into 10 days (each point corresponds to 10 days of filtered data).

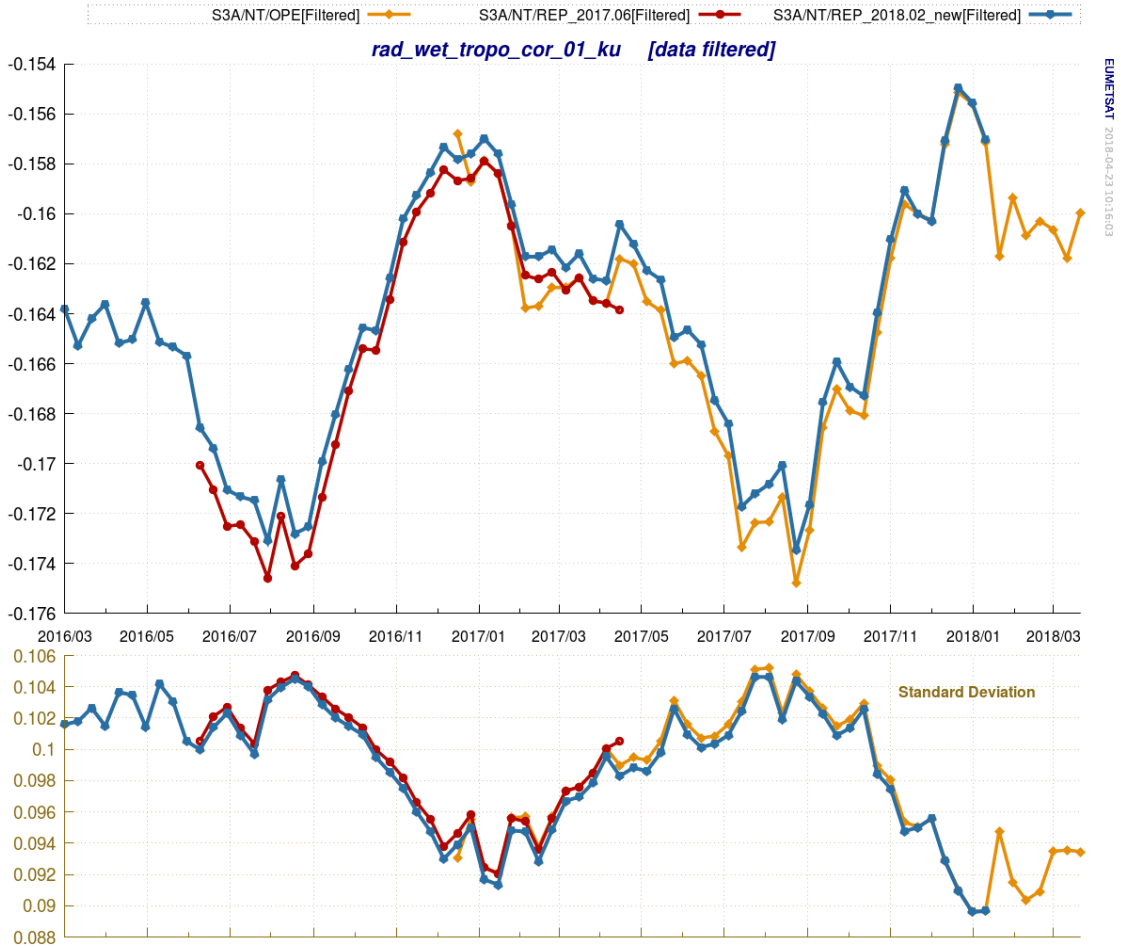

Figure 79 – Radiometer Wet Tropospheric Correction: Comparison with previous datasets delivered by EUM

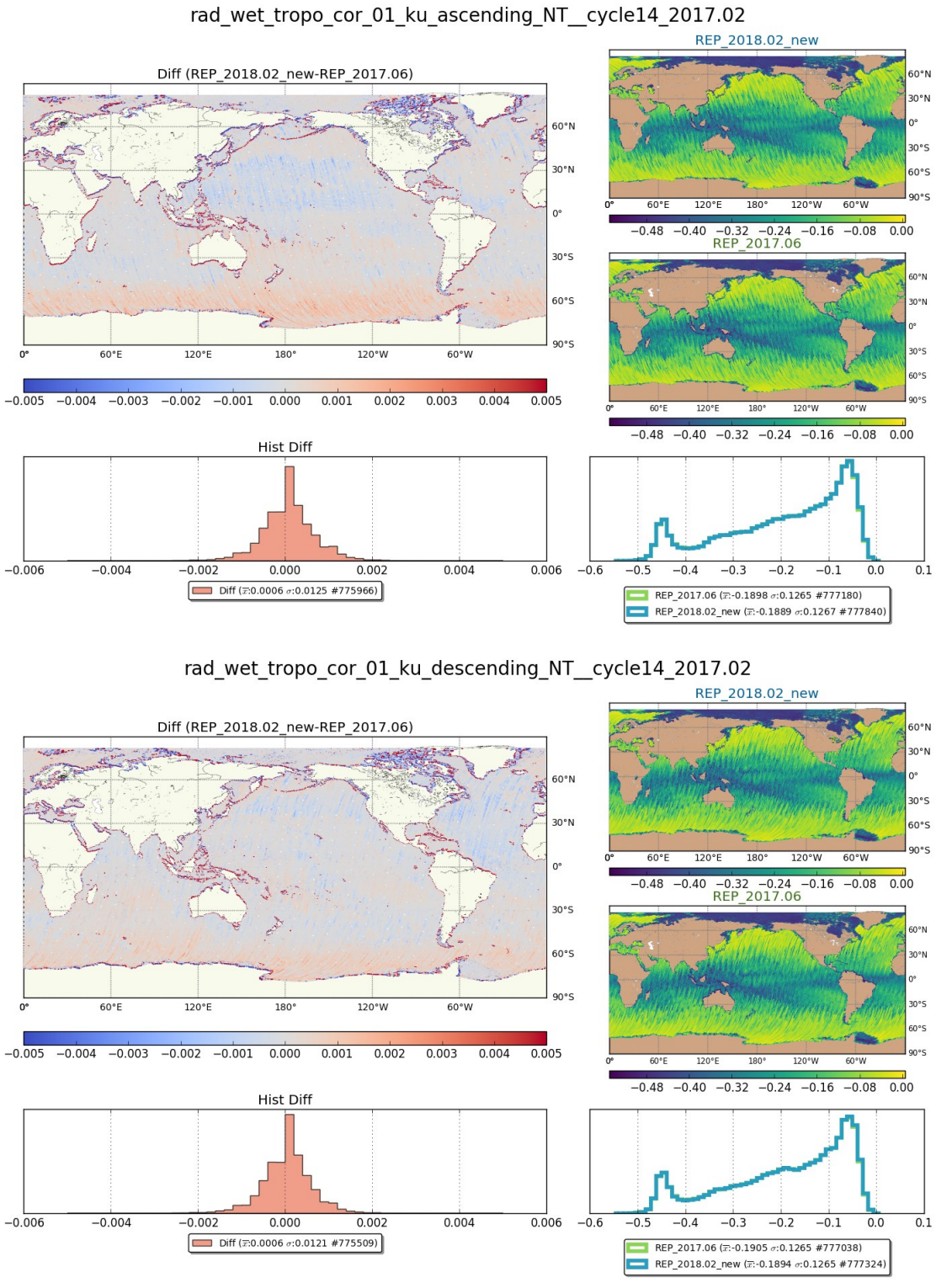

Figure 80 – Radiometer Wet Tropospheric Correction: Geographical comparison between the current and previous reprocessing

The above images show the geographical comparison between the previous reprocessing "REP_2017.06" (middle right) and the new one "REP_2018.02_new" (top right). The histograms of both datasets are on the bottom left overlapped.

In the top left it is the map of differences between both datasets and the histogram of the differences below. No filtering was applied to the datasets on this case. The differences are calculated at 1Hz, in a one-to-one difference.

The top plot shows the Ascending the bottom one Descending. The Cycle shown here is 14 from 2017/02.

4.3.8.4 S3A MWR Wet Tropospheric Correction Drift

The difference between SAR MWR and ECMWF WTC has not a significant drift over time for the time period 23 June 2016 to 20 Jan 2018 (see Figure 81). The drift has been estimated to be only 0.07 mm/year

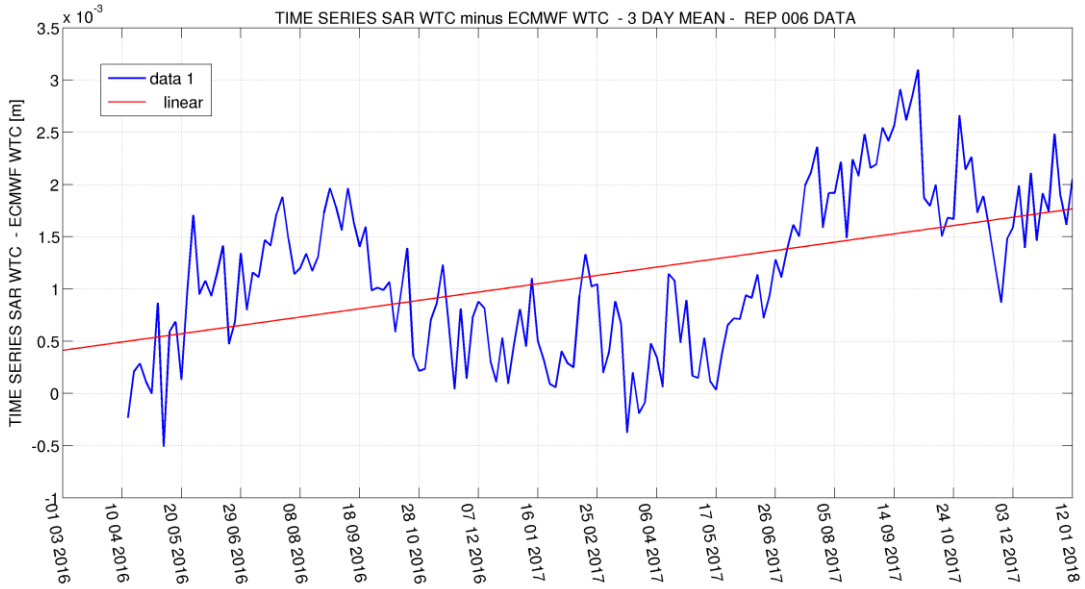

Figure 81 – Time Series of the Mean of the Difference between SAR WTC and ECMWF WTC. 3 Day mean is used.

4.4 Scientific validation over sea ice

The scientific validation of the Level 2 reprocessed dataset over sea ice has been not carried out in the validation Technical Note since the sea ice algorithms in the Processing Baseline 2.27 are not yet tuned over these specific thematic applications (see Product Notice relative to Processing Baseline 2.27).

Evolutions are planned to be implemented in the next processing baselines which are expected to bring Sentinel-3 on par with CryoSat-2 in the measurement of the sea-ice freeboard.

For the time being, the users are discouraged to use the freeboard measurements in the reprocessed marine L2 data for sea-ice thematic applications.

5 Long Term Monitoring Calibrations

The calibrations of the STM chain are stored in Long Term Monitoring files, 4 for SRAL and 3 for MWR. To do the checks, the final (cumulative) LTM file was read and the time differences between each calibration analysed. The content of the calibration files was also analysed and no unexpected result was found. Details can be found in the following Sections. The LTM files were analysed from 2016-03-01 until 2018-01-20.

5.1 SR_1_CA1SAX (CAL1 SAR)

The filename verified in this Section is:

```
S3A_SR_1_CA1SAX_20000101T000000_20180215T203213_20180227T034802_____________
________LR1_R_AL____.SEN3
```

5.1.1 Time difference

The temporal differences between the different CAL measurements in the LTM file were analysed.

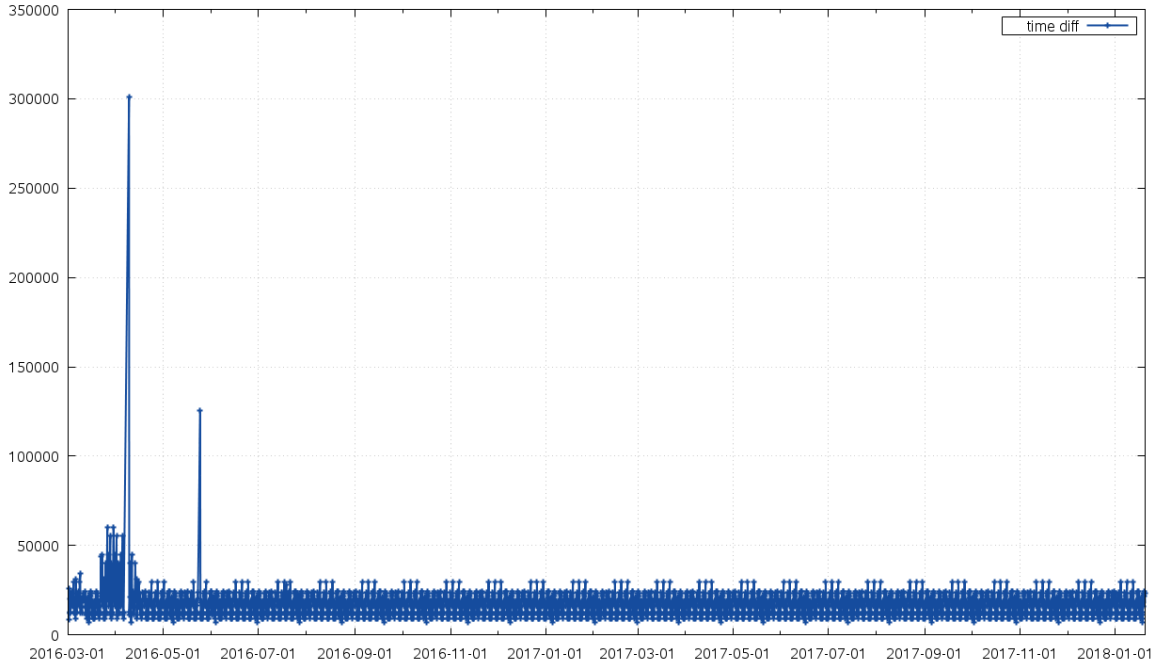

Figure 82 – Time difference between consecutive CAL measurements in the SR_1_CA1SAX LTM file.

A large gap can be seen in the initial period (see Figure 82), a zoom in of the period is shown in the image below.

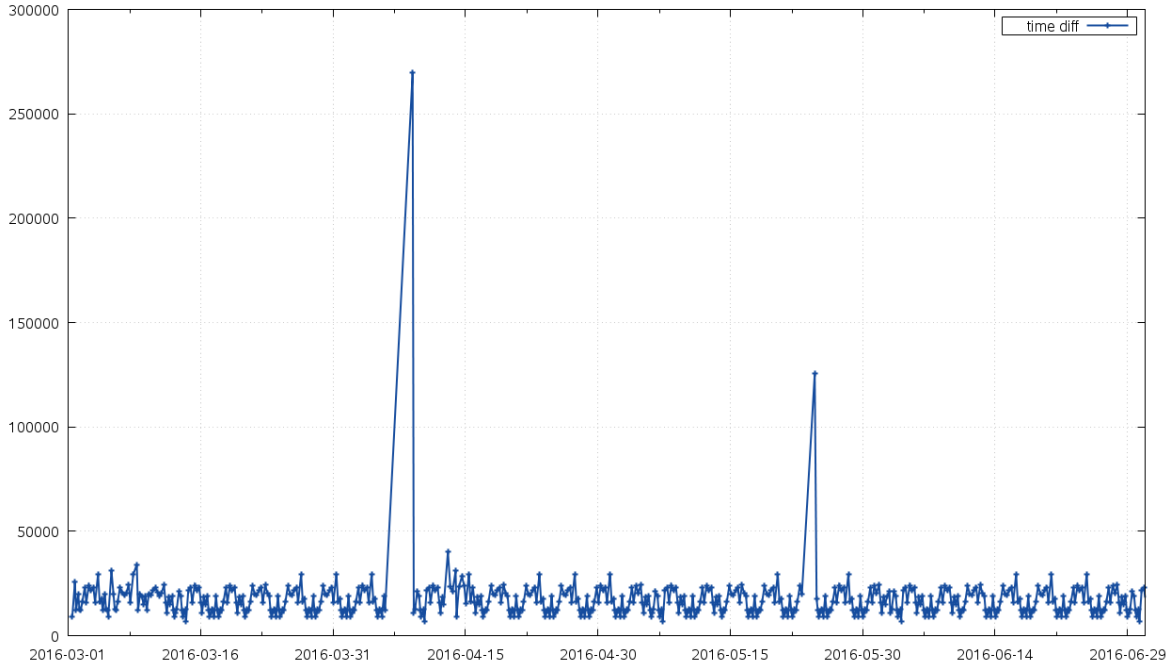

Figure 83 – Time difference between consecutive SR_1_CA1SAX Cal, zoom in initial period (2016-03-01 until 2016-07-01)

This gap in calibrations was due to a special operation on-going at the time (2016-EST021), between 6 April 2016 00:00:00 and 8 April 2016 23:59:59 UTC Time. The gap in May 2016 is expected to be related to the uplink of the OLTC (see Section 4.3.2.6).

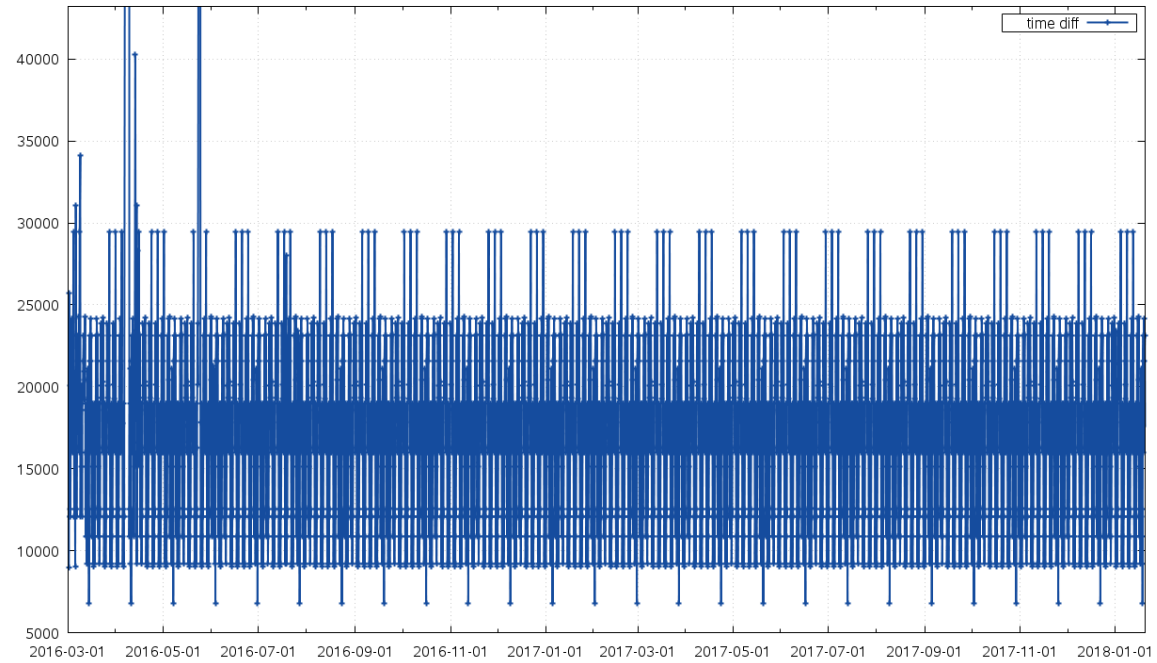

Figure 84 – Time difference between consecutive CAL measurements in the SR_1_CA1SAX LTM file, capped at 12 hours.

If the time difference plot is capped at 12 hours it is possible to see that besides the early mission part, there are no calibrations with more than 8 hours difference (30000 seconds = 8.33 hours).

5.1.2 Content

The CAL1 Point target response (PTR) power for Ku band shows a decrease as previously identified (see Figure 85). With this PB, an averaged CAL2 filter is applied to the CAL1 waveform, instead of just one single CAL2, thus making the CAL1 PTR power less nosy.

The current decay rate has been improving overtime, as can be seen from the less steep slope in CA1SAX ptr_pow_ku in the last three months with respect the first months in global SAR mode.

The CAL1 PTR power decay in Ku Band is compensated in the IPF processing chain.

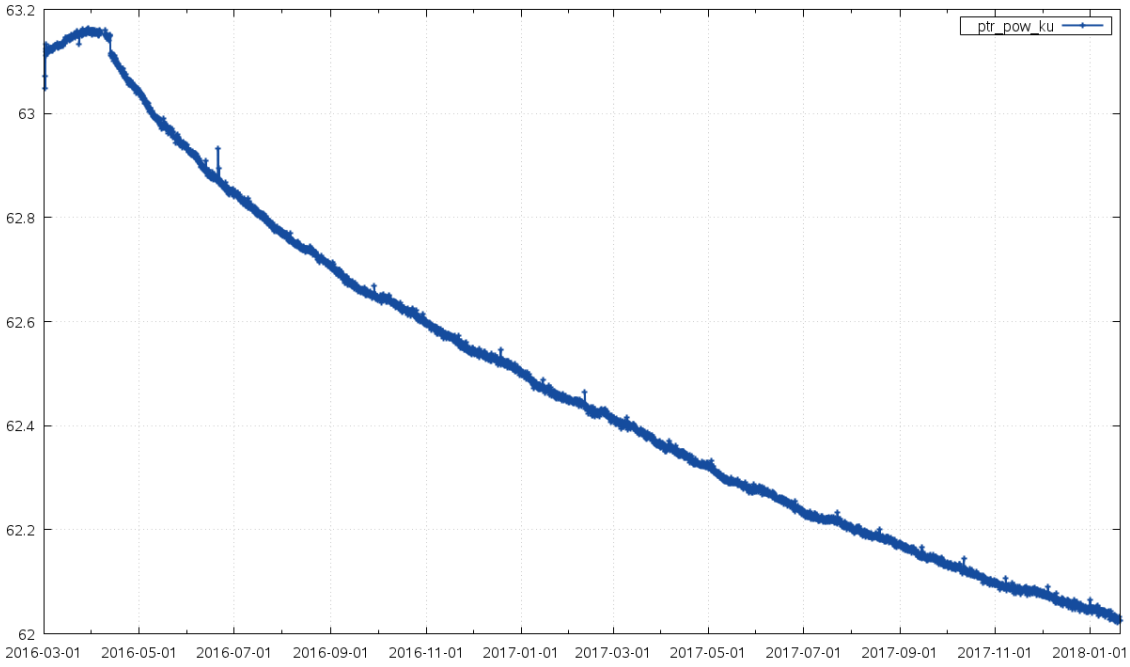

Figure 85 – CA1SAX ptr_pow_ku (dB)

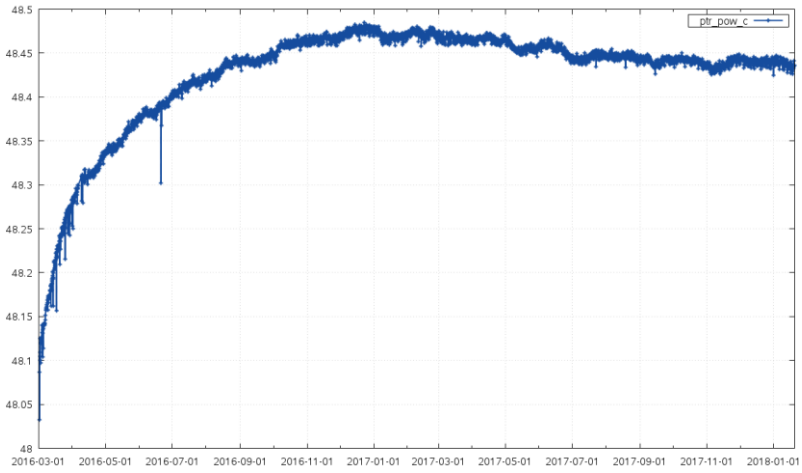

Figure 86 – CA1SAX ptr_pow_c (dB)

Figure 86 shows the CAL1 PTR power in C band, as calculated over the mission time. The new Processing Baseline now uses a Ku Band CAL2 filter (averaged) to be applied to CAL1 PTR in C band. This allows to finally decrease the level of noise and monitor better the C band PTR power profile. Please, notice a change of trend in CA1SAX ptr_pow_c around February 2017: after that time, the CAL1 PTR power in C band is decreasing instead of increasing.

The CAL1 PTR power decay in C Band is compensated in the IPF processing chain.

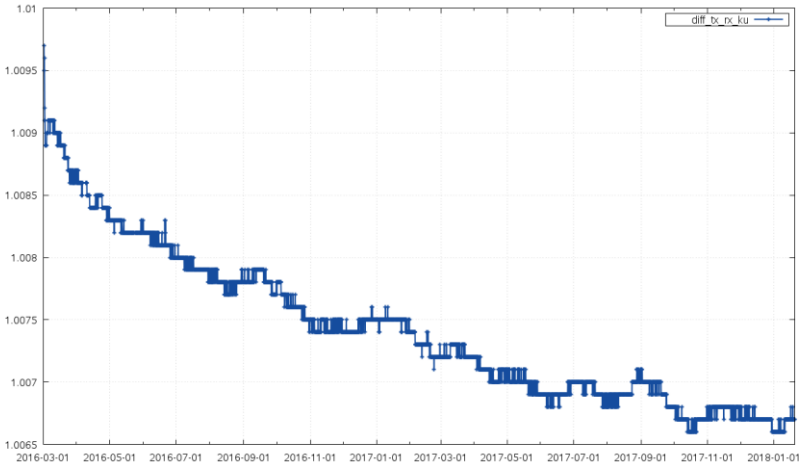

Figure 87 – CA1SAX diff_tx_rx_ku (m)

Figure 87 illustrates the CAL1 PTR range delay (difference of travel between Tx and Rx lines) in Ku band, as calculated over the mission time. We can notice how CA1SAX diff_tx_rx_ku was particularly steep in the early mission phase whereas now is slowly stabilizing over the time. Further, CA1SAX diff_tx_rx_ku, as stored in the LTM products, features a digitation noise on top of the measurement. The origin of this digitation noise will be investigated further on.

The CAL1 PTR range delay drift in Ku Band is compensated in the IPF processing chain.

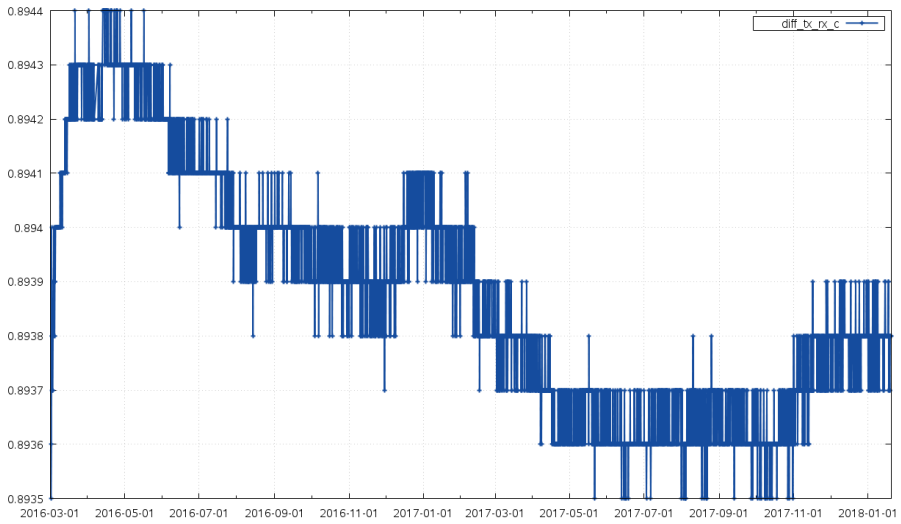

Figure 88 – CA1SAX diff_tx_rx_c (m)

Figure 88 shows the CAL1 PTR range delay (difference of travel between Tx and Rx lines) in C band, as calculated over the mission time. It shall be noted that CA1SAX diff_tx_rx_c is noisier than CA1SAX diff_tx_rx_ku (as an effect of the only 2 C Band pulses in the burst), as well as it shows to be affected by digitalization noise.

The CAL1 PTR range delay drift in C Band is compensated in the IPF processing chain.

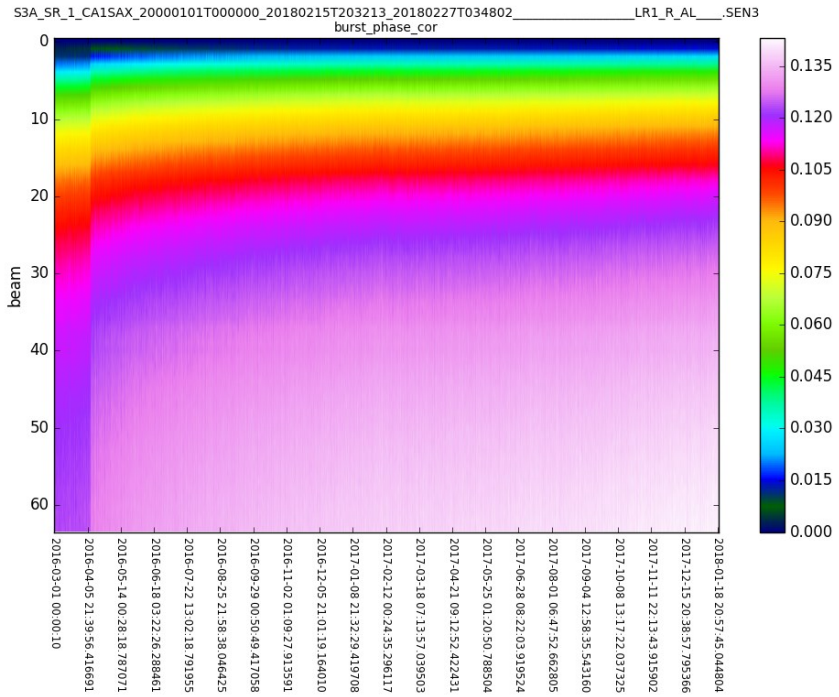

Figure 89 – CA1SAX burst_phase_cor (radian) - Complete reprocessing period

Figure 89 shows the inter-burst phase correction (in radian) applied to each burst over the mission time. It shall be noted that there is a discontinuity in the correction in early April 2016, highlighted in Figure 90 that shows a zoom in around that time.

The discontinuity occurs at the time that the instrument is definitively switched from LRM into SAR mode (2016-04-12). Notice that there is gap in the calibration between 2016-04-06 and 2016-04-09 (see Section 5.1.1).

The calibration burst corrections are correctly compensated in the IPF processing chain and the Figure 90 is just to highlight the change at sensor level.

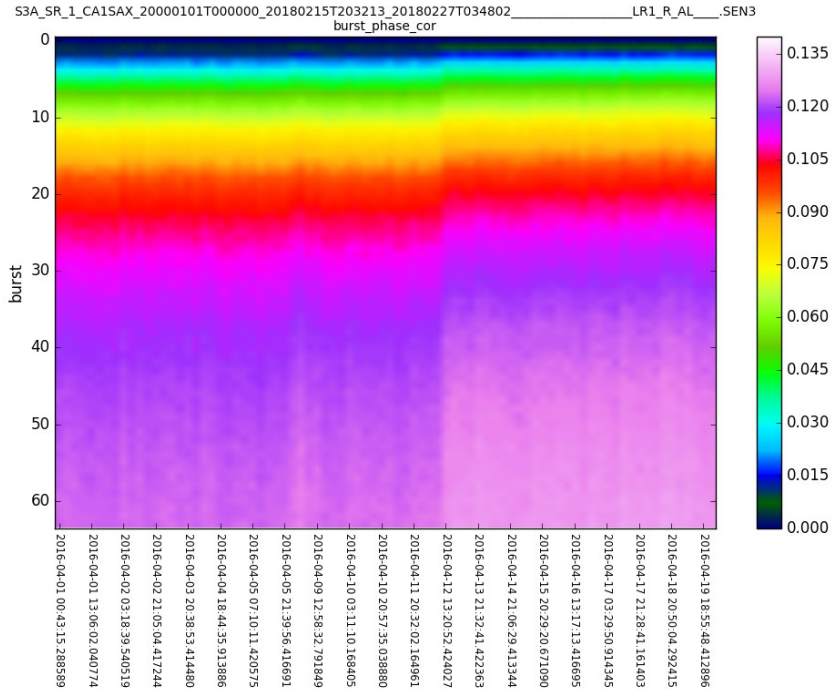

Figure 90 – CA1SAX burst_phase_cor (radian) – Zoom in April 2016

It is possible that a discontinuity could create a very minor degradation around the date 2016-04-12, because of the averaging of different burst corrections (before and after the discontinuity time) in the average time window, as can be seen in Figure 91 The averaged inter-burst phase correction per burst pulse differs in the LRM (blue) and SAR (green) periods, being lower in the LRM period.

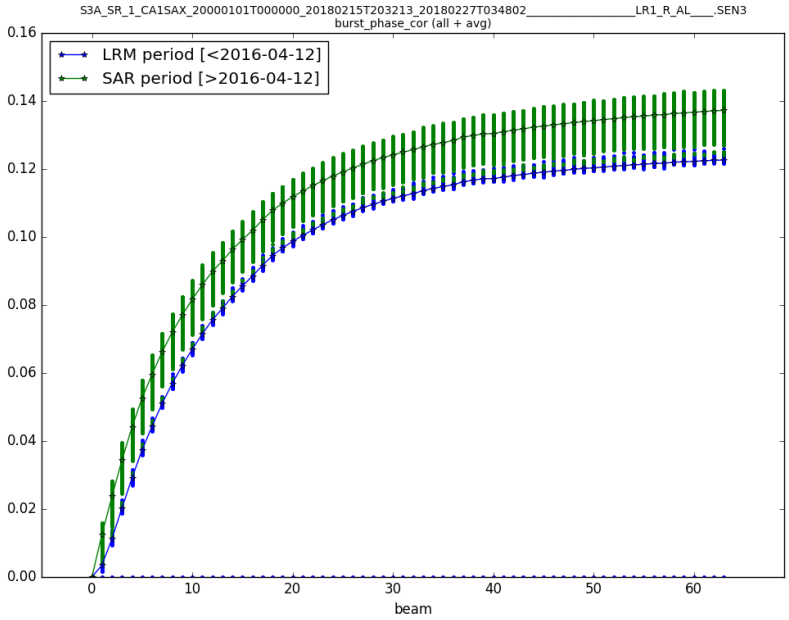

Figure 91 – Averaged burst_phase_cor for SAR and LRM time periods

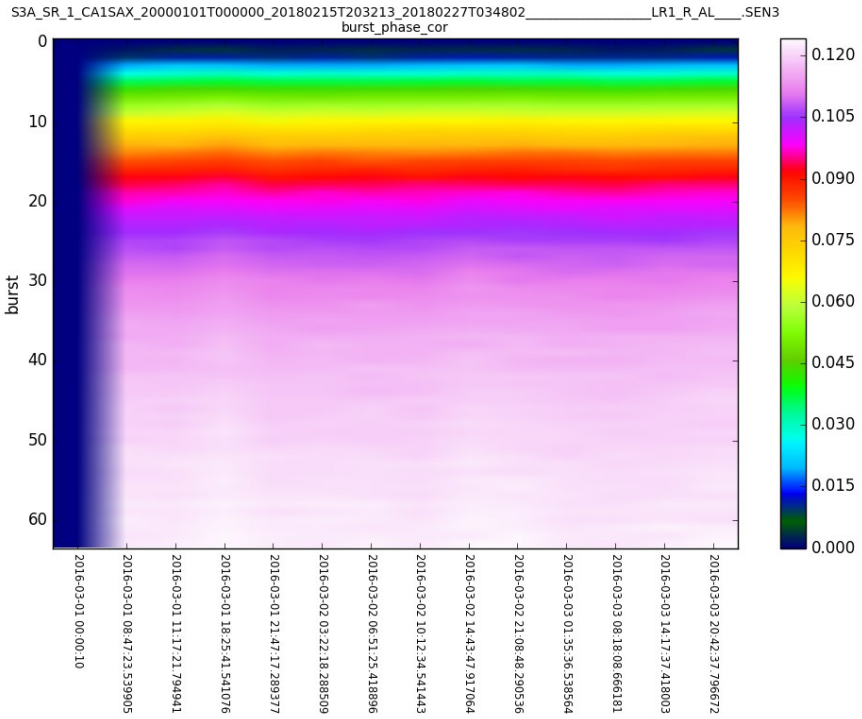

Figure 92 – CA1SAX burst_phase_cor (FFT power unit) – Zoom in March 2016

To be noted that the initial inter burst phase correction was set to 0 to all burst, as per on-ground value, Figure 92.

Figure 93 – CA1SAX burst_power_cor (FFT power units) - Complete reprocessing period

Figure 93 shows the inter-burst power correction applied at each burst. It can be seen that there is discontinuity in the correction in early April 2016 (2016-04-12), like for the phase correction.

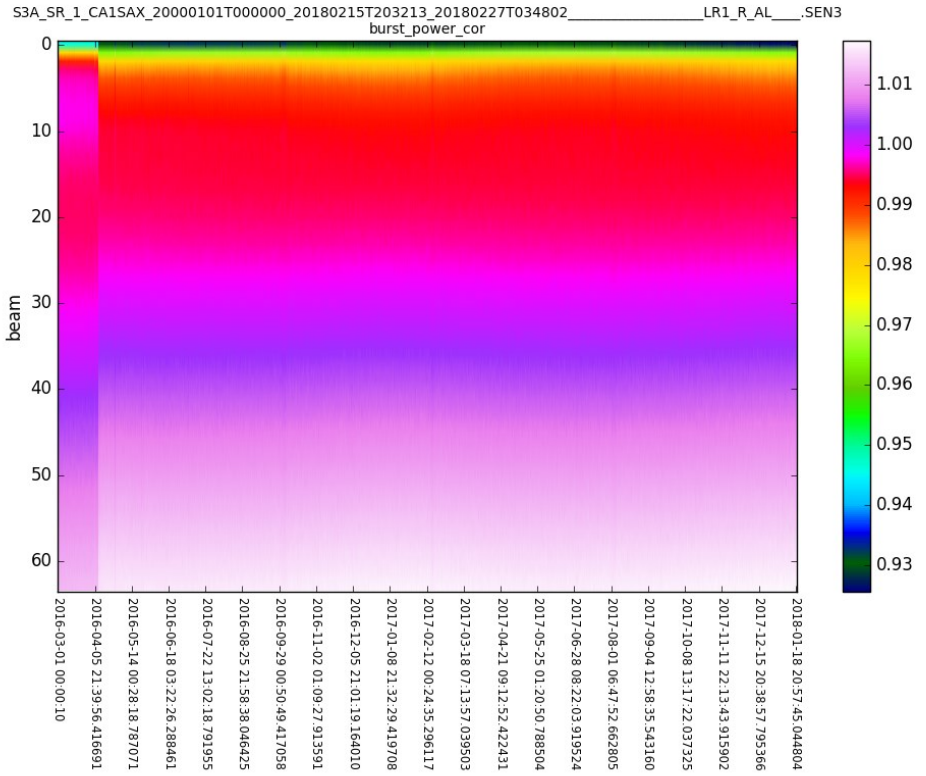

An average value of the correction was calculated for each pulse of the burst, separating between the LRM (blue) and SAR (periods). This average is represented in Figure 94. It can be seen that the shape is different, unlike for the phase where it appeared to be just a jump in the values.

It is possible that a discontinuity could create a very minor degradation around the date 2016-04-12, because of the averaging of different burst corrections (before and after the discontinuity time) in the average time window.

In the plot, the first value of the LTM set on-ground to the value of 1 is also shown.

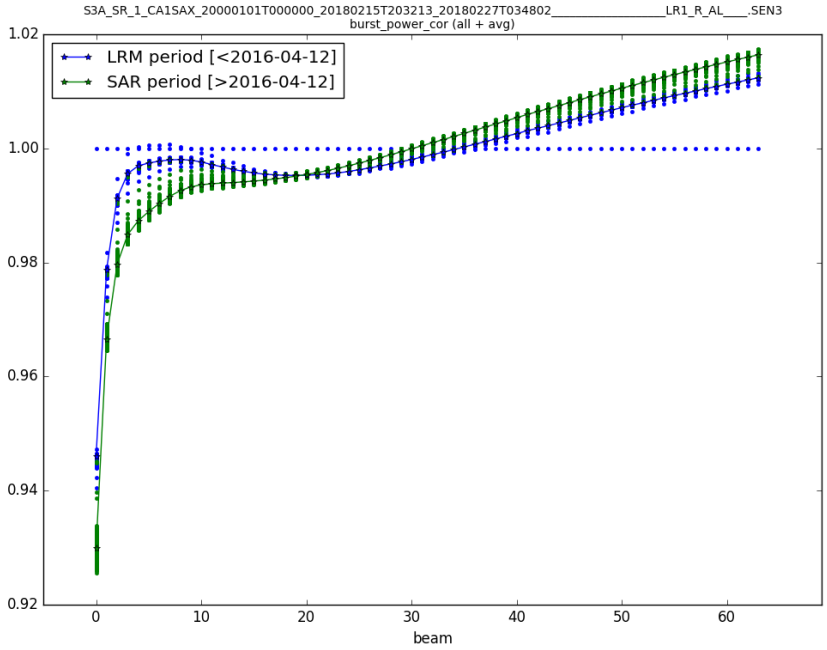

Figure 94 – Averaged burst_power_cor for SAR and LRM time periods (FFT power unit)

The following variables are always 0 in the file and those are not plotted in this document:

- *flag_diff_tx_rx_c*
- *flag_diff_tx_rx_ku*
- *flag_ptr_power_c*
- *flag_ptr_power_ku*

5.1.3 PTR Width

Although not part of the LTM file, the Ku PTR Range Width variation was also monitored. The IPF is currently not correcting for this variation.

It can be seen in Figure 95 that the PTR's shape has changed on 12 April 2016 (change in PTR width) and also on 22 May 2016 (again change in PTR width). Since that period, the PTR width is more stable. The PTR width variation is about -0.5 mm/year

The PTR Width in Figure 95 has been computed from an in-house prototype.

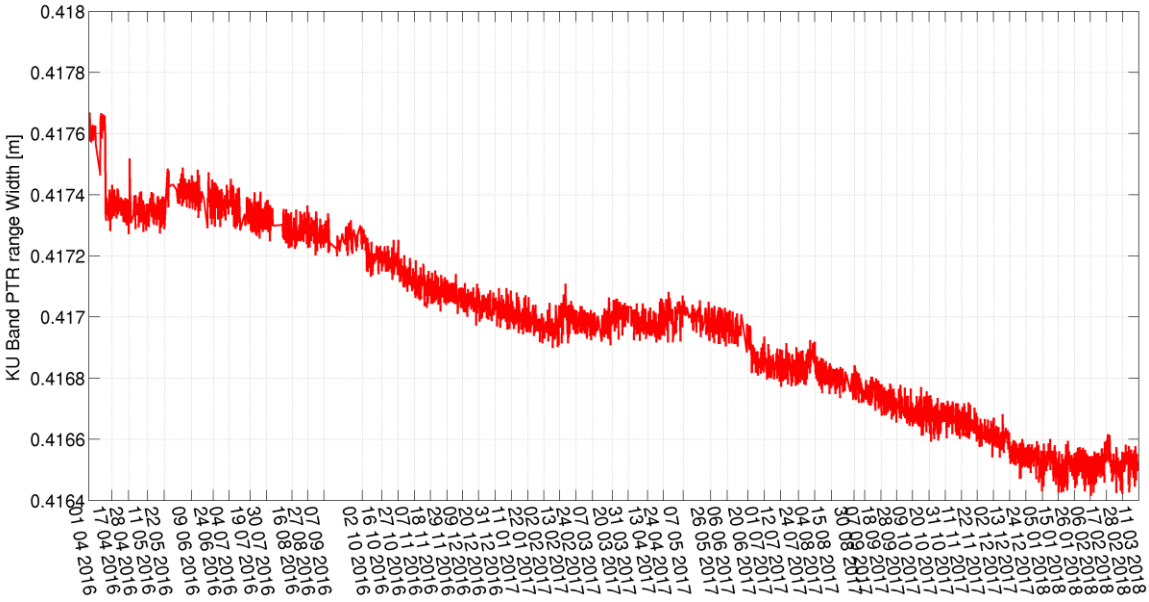

Figure 95 – Ku Band PTR width time series

5.2 SR_1_CA1LAX (CAL1 LRM)

The filename verified was the following:

```
S3A_SR_1_CA1LAX_20000101T000000_20180215T203206_20180227T034802_____________
_______LR1_R_AL____.SEN3
```

5.2.1 Time difference

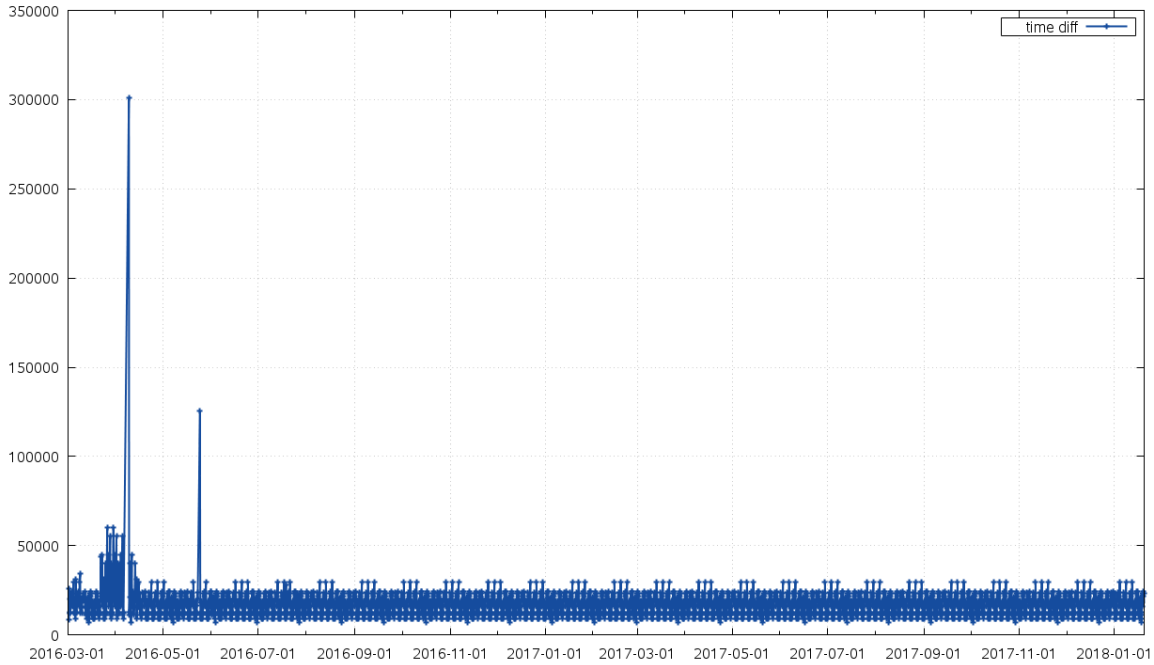

Figure 96 – Time difference between consecutive CAL measurements in the SR_1_CA1LAX LTM file.

The gaps are the same as reported for SR_1_CA1SAX (see 5.1).

The temporal gaps occur only in the beginning of the mission.

5.2.2 Content

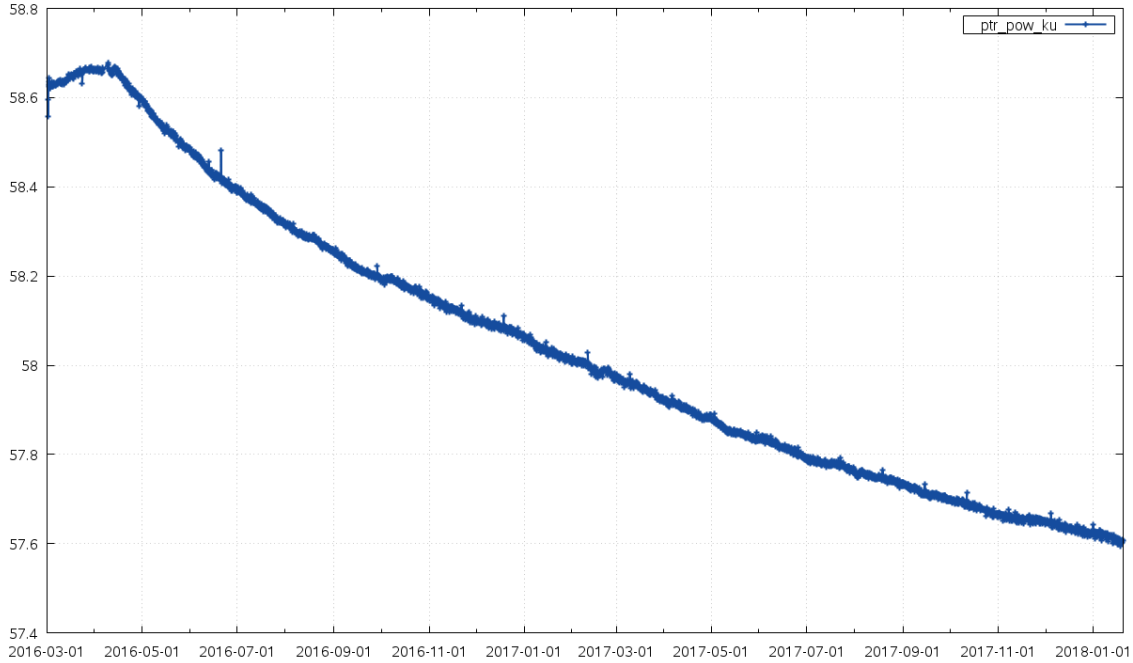

Figure 97 – CA1LAX ptr_pow_ku

The trend is similar to the one of CA1SAX (Figure 85), but the values are different.

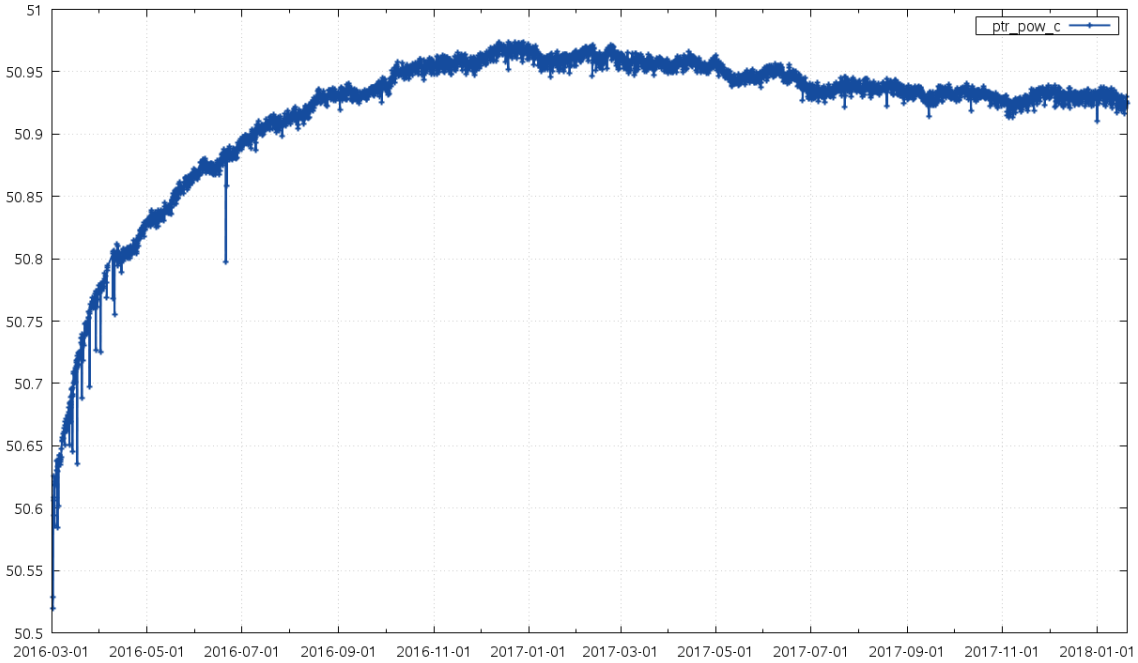

Figure 98 – CA1LAX ptr_pow_c

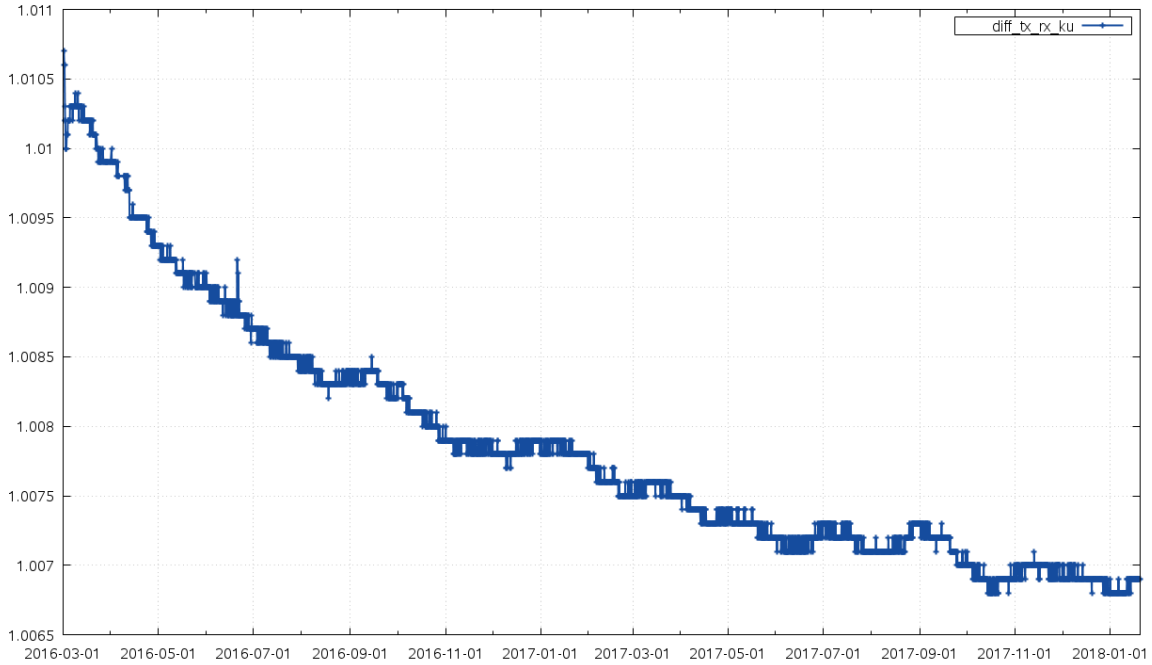

Figure 99 – CA1LAX diff_tx_rx_ku

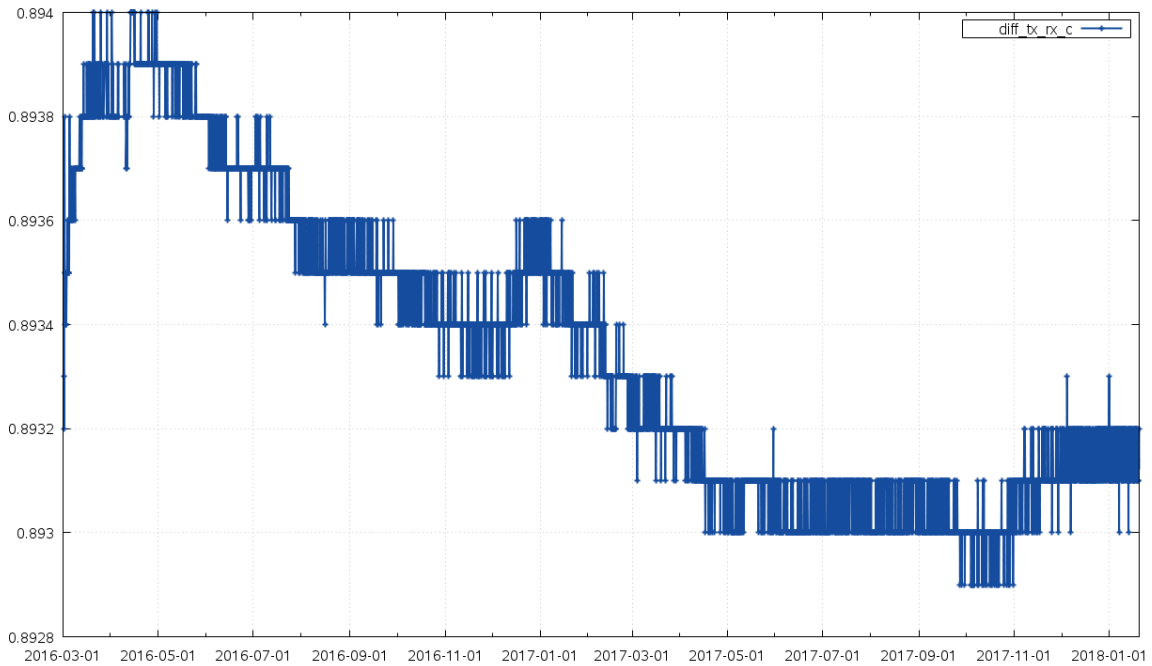

Figure 100 – CA1LAX diff_tx_rx_c

The following variables are always 0 in the file and those are not plotted in this document:

- *flag_diff_tx_rx_c*
- *flag_diff_tx_rx_ku*
- *flag_ptr_power_c*
- *flag_ptr_power_ku*

5.3 SR_1_CA2CAX (CAL2 C-Band)

The filename verified was the following:

```
S3A_SR_1_CA2CAX_20000101T000000_20180215T203219_20180227T034802_____________
_______LR1_R_AL____.SEN3
```

5.3.1 Time difference

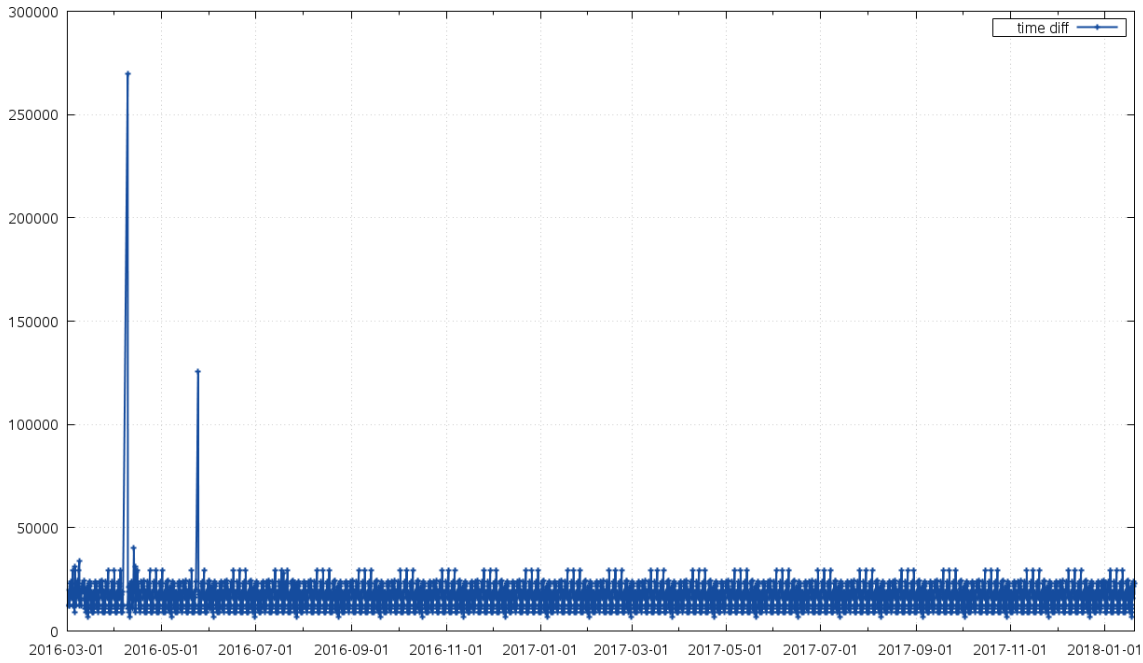

Figure 101 – Time difference between consecutive CAL measurements in the SR_1_CA2CAX LTM file.

The gaps are the same as reported for SR_1_CA1SAX (see 5.1).

5.3.2 Content

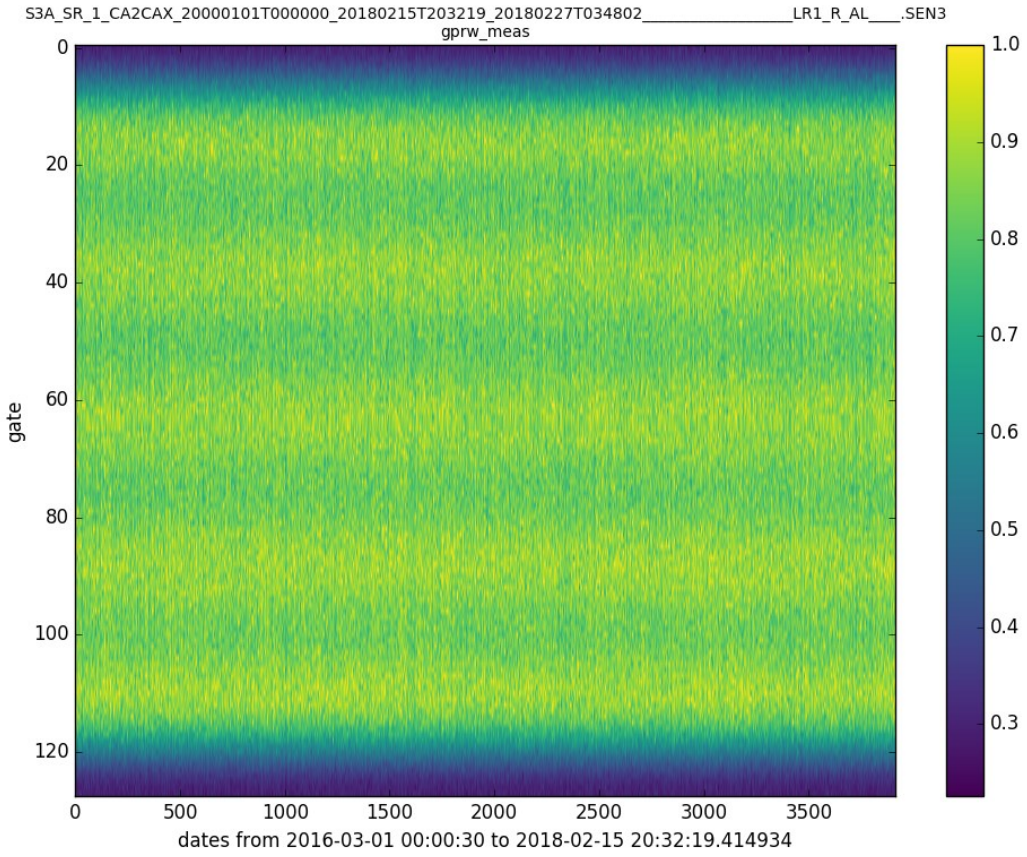

Figure 102 – gprw_meas (CAL2) for CA2CAX

The above image shows the CAL2 correction, as part of CA2CAX.

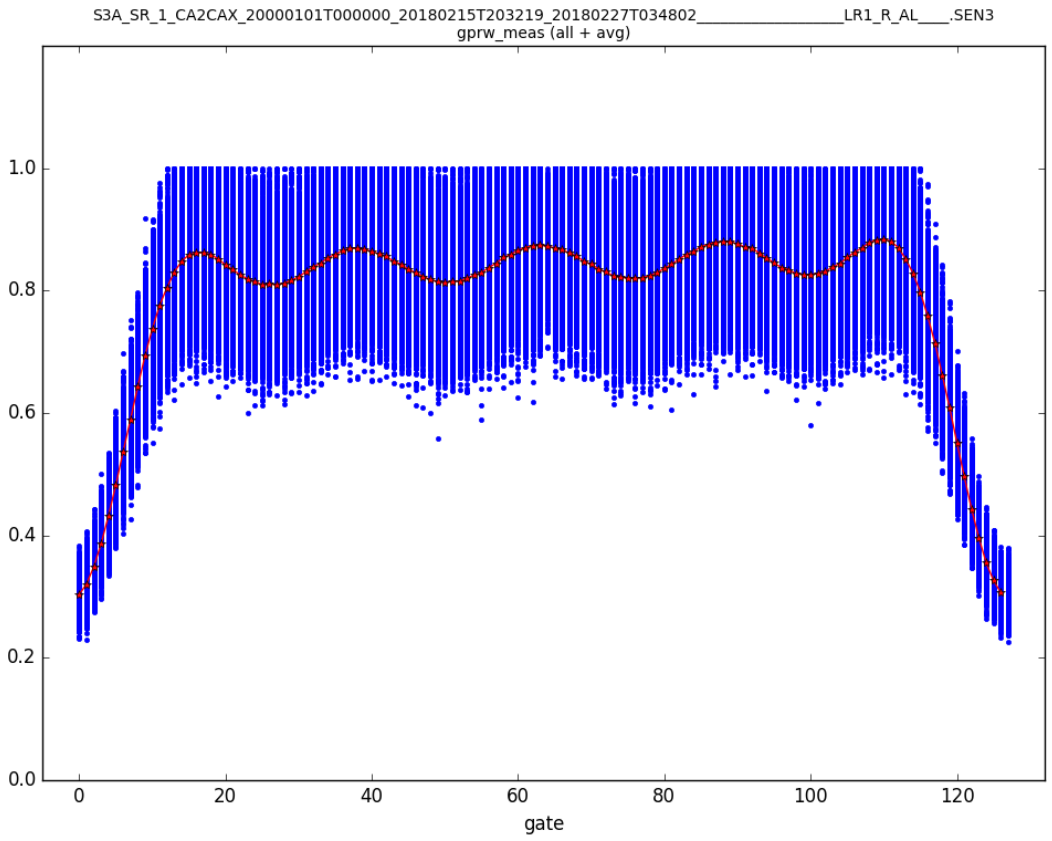

Figure 103 – Average gprw_meas (CAL2) for CA2CAX

The above image shows all C-band CAL2 correction values (in blue). The averaged value for each gate is represented in red. The average uses all measurements for that gate.

Note that C Band CAL2 is no longer used in the processing, but the Ku Band CAL2 filter is used instead, following industry recommendation.

5.4 SR_1_CA2KAX (CAL2 Ku-Band)

The filename verified was the following:

```
S3A_SR_1_CA2KAX_20000101T000000_20180215T203219_20180227T034802_____________
_______LR1_R_AL____.SEN3
```

5.4.1 Time difference

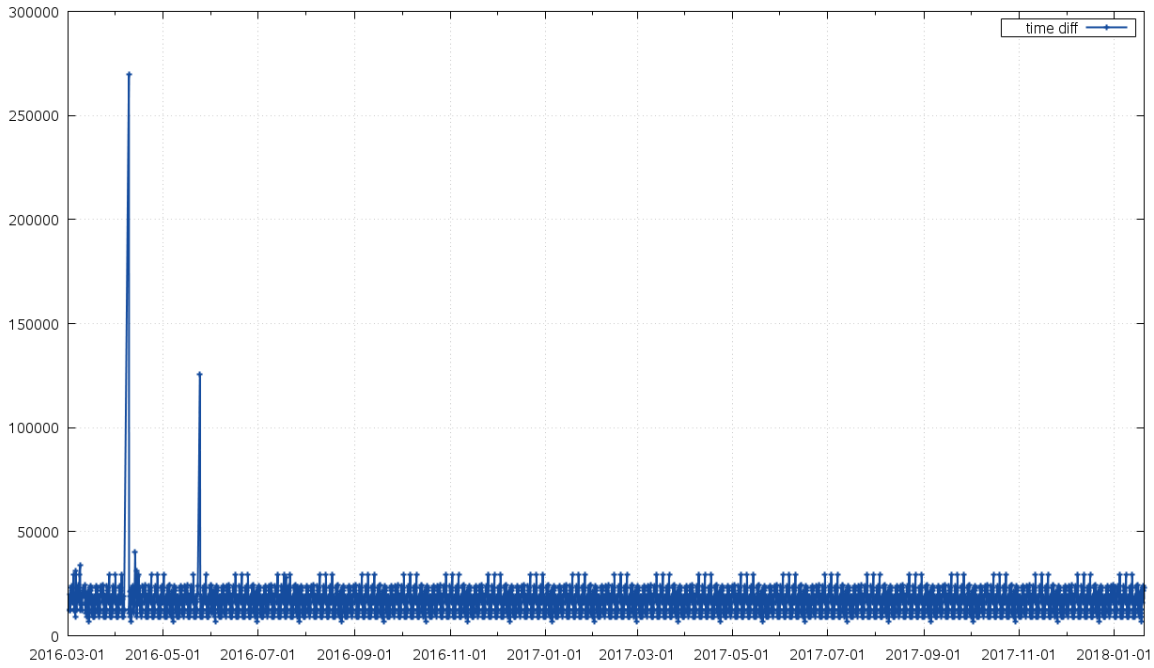

Figure 104 – Time difference between consecutive CAL measurements in the SR_1_CA2KAX LTM file.

The gaps are the same as reported for SR_1_CA1SAX (see 5.1).

5.4.2 Content

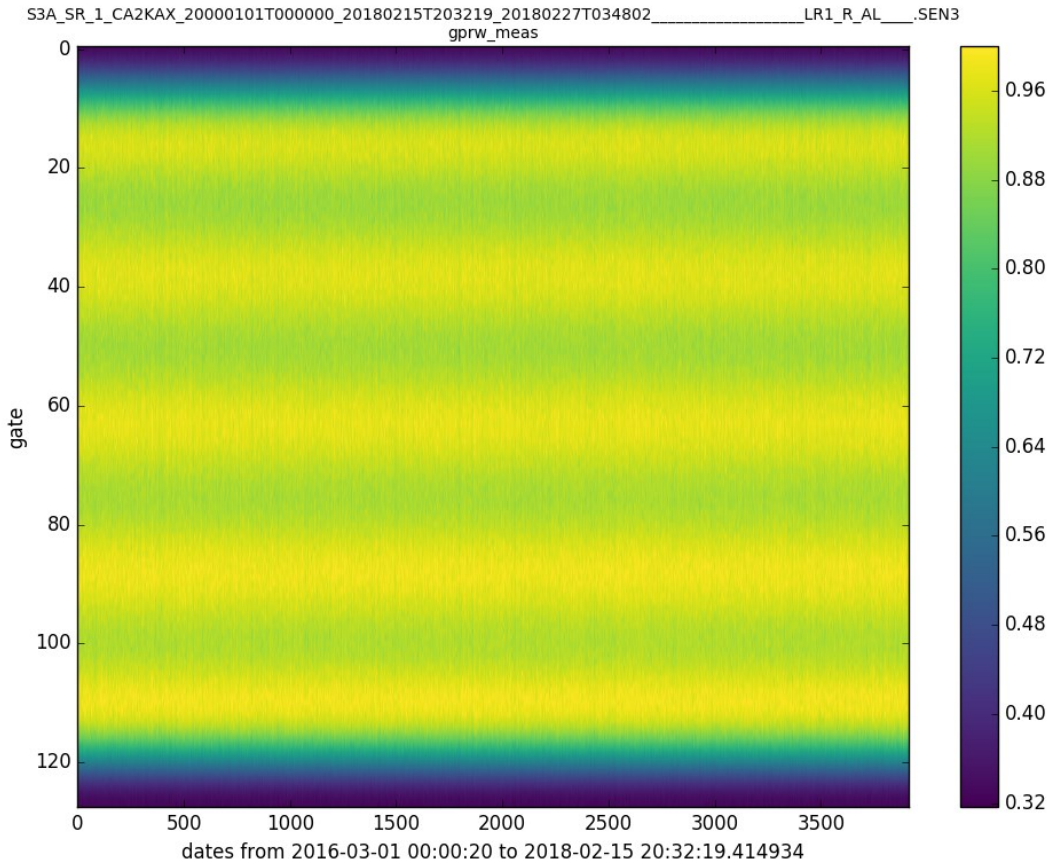

Figure 105 – gprw_meas (CAL2) for CA2KAX

The above image shows the CAL2 correction, as part of CA2KAX.

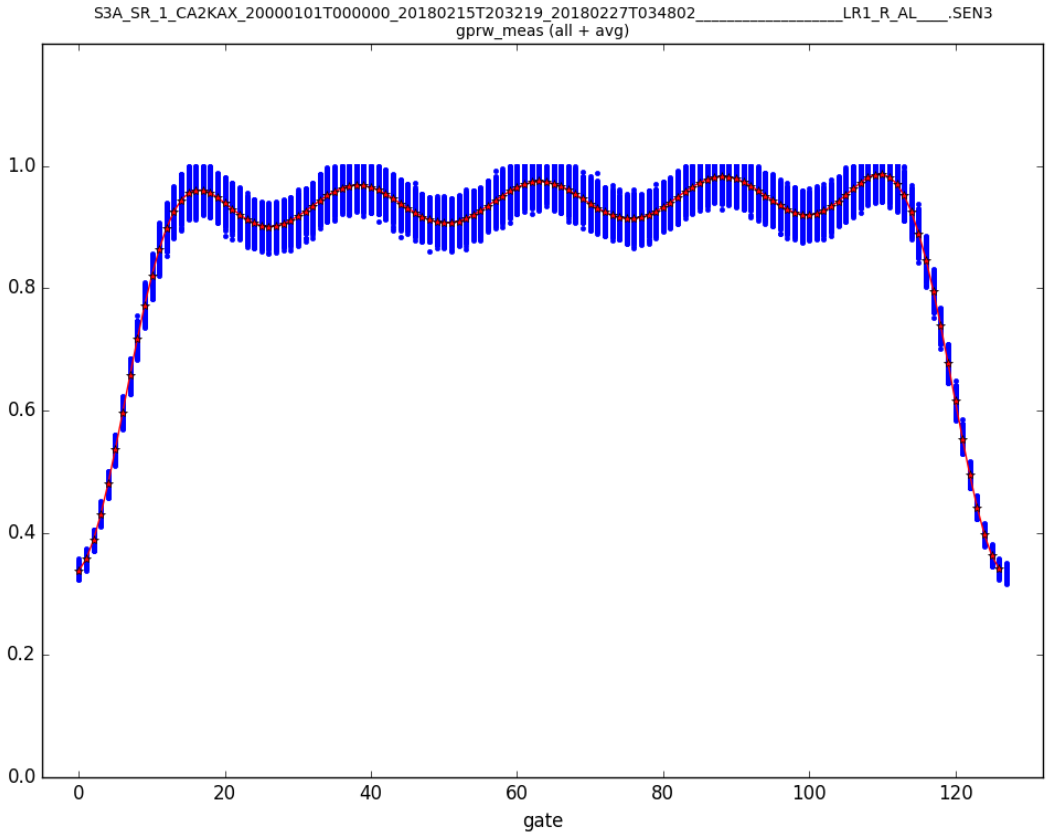

Figure 106 – Average gprw_meas (CAL2) for CA2KAX

The above image shows all Ku-band CAL2 correction values (in blue). The averaged value for each gate is represented in red. The average uses all measurements for that gate.

The Ku band is much less noisy than the C band, as can be seen by comparing Figure 106 (Ku band) and Figure 102 (C band). This is expected because in one burst there are 64 Ku Band pulses and only 2 C Band pulses.

5.5 MW_1_NIR_AX

The filename verified was the following:

```
S3A_MW_1_NIR_AX_20000101T000000_20180212T232603_20180228T144120_____________
_______LR1_R_AL____.SEN3
```

5.5.1 Time difference

In the beginning of the mission the calibration scheme was different, this can be seen in Figure 107.

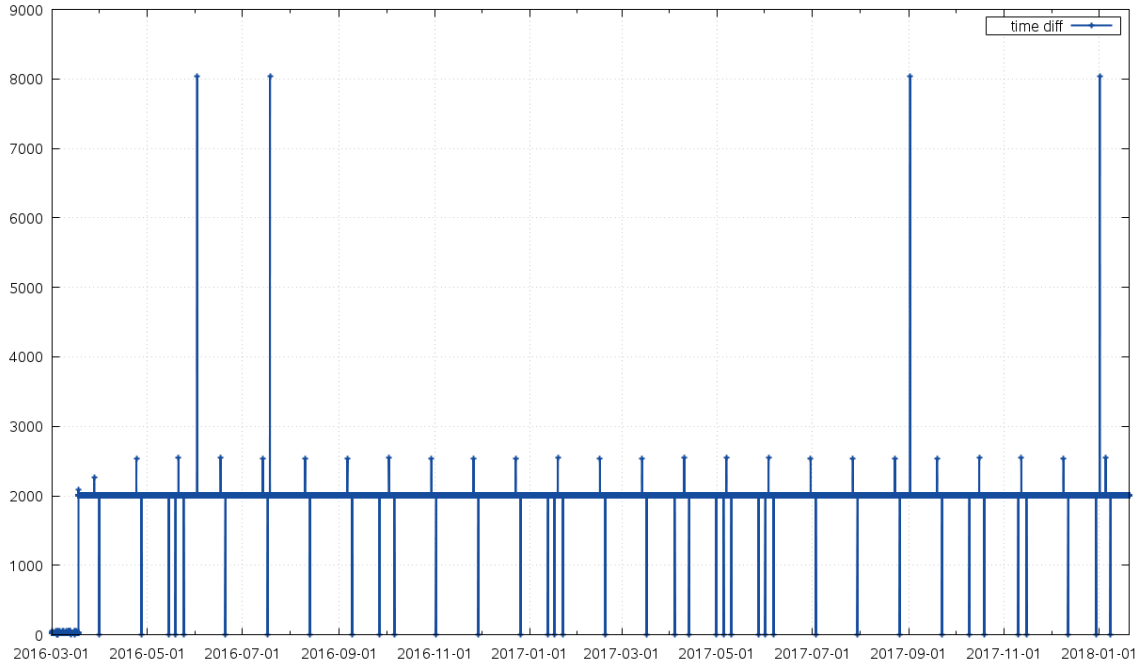

Figure 107 – Time difference between consecutive CAL measurements in the MW_1_NIR_AX LTM file.

The expected time difference between consecutive calibrations in the current calibration scheme (valid up to 2018-03-01 08:19 UTC Time) is about 2000 seconds (i.e. 3 calibration sequences per orbit).

There are 4 clear outliers corresponding to the missing dumps (see Section 8.2), as well as cases where the radiometer calibration was performed in rapid succession.

5.5.2 Content

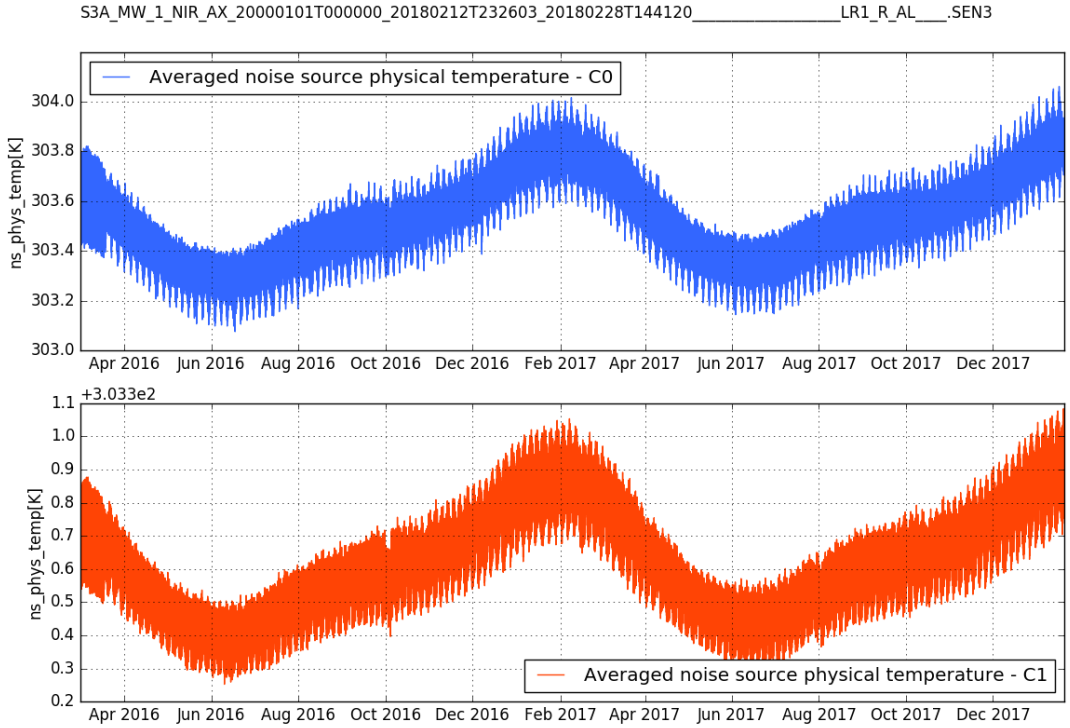

Figure 108 – ns_phys_temp for both channels (MW_1_NIR_AX)

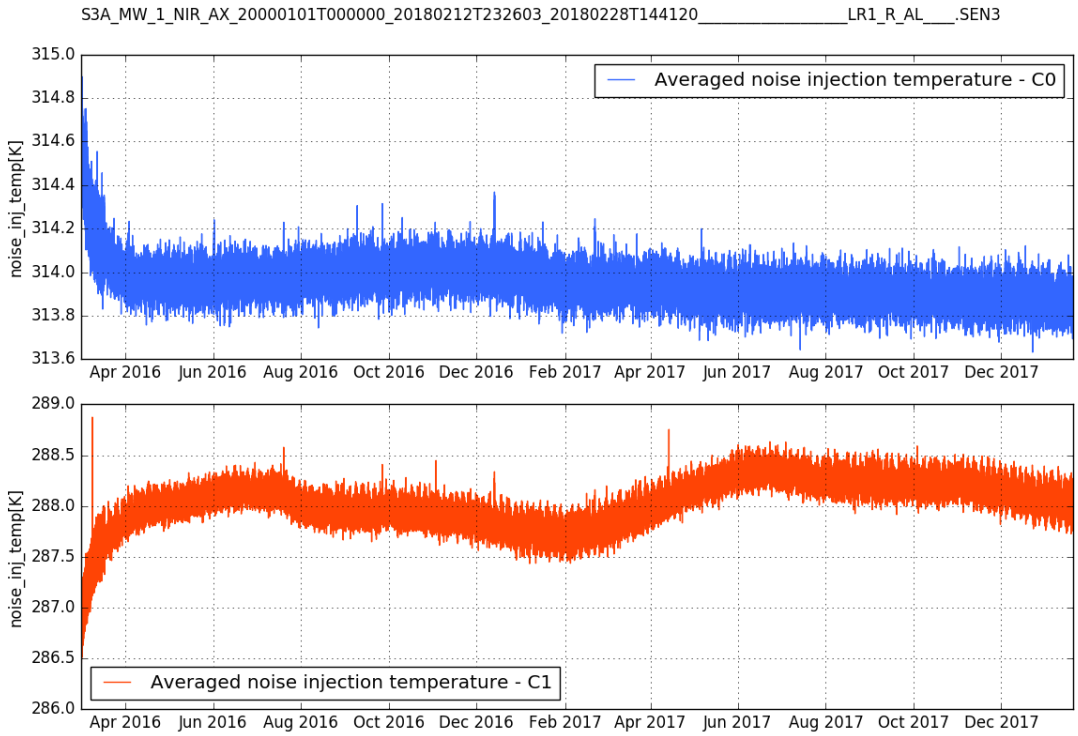

Figure 109 – noise_inj_temp for both channels (MW_1_NIR_AX)

5.6 MW_1_MON_AX

The filename verified was the following:

```
S3A_MW_1_MON_AX_20000101T000000_20180212T235751_20180228T144120_____________
_______LR1_R_AL____.SEN3
```

5.6.1 Time difference

The MWR monitoring generally occurs at intervals of 27.5 or 55.0 seconds. The large gaps are due to missing dumps (see Section 8.2). Excluding this period from the plot there are a few small outliers, but nothing that should impact the data quality.

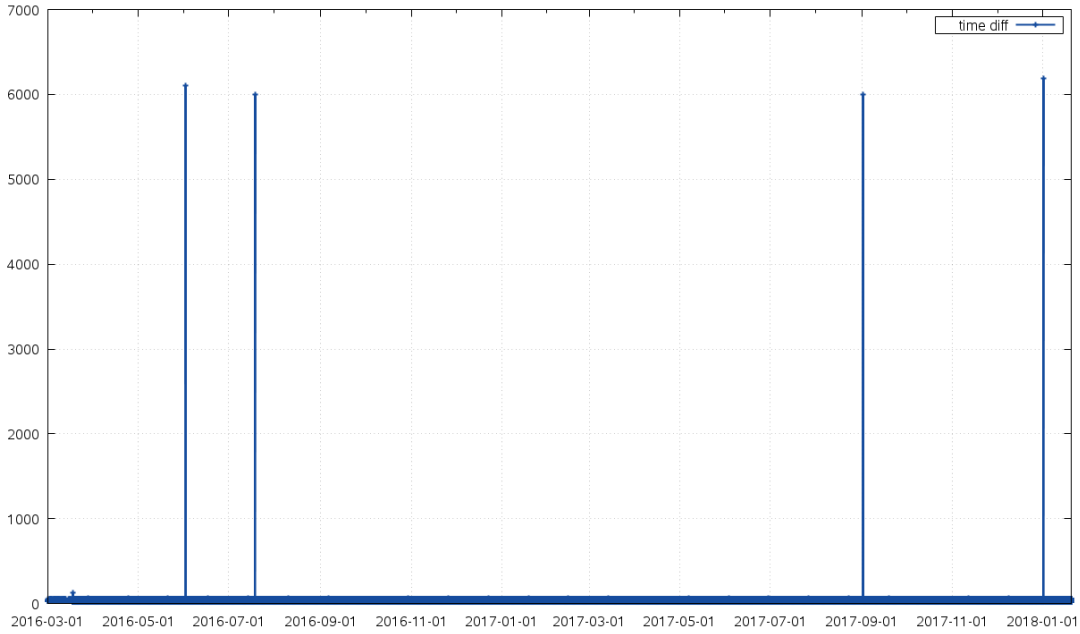

Figure 110 – Time difference between consecutive CAL measurements in the MW_1_MON_AX LTM file.

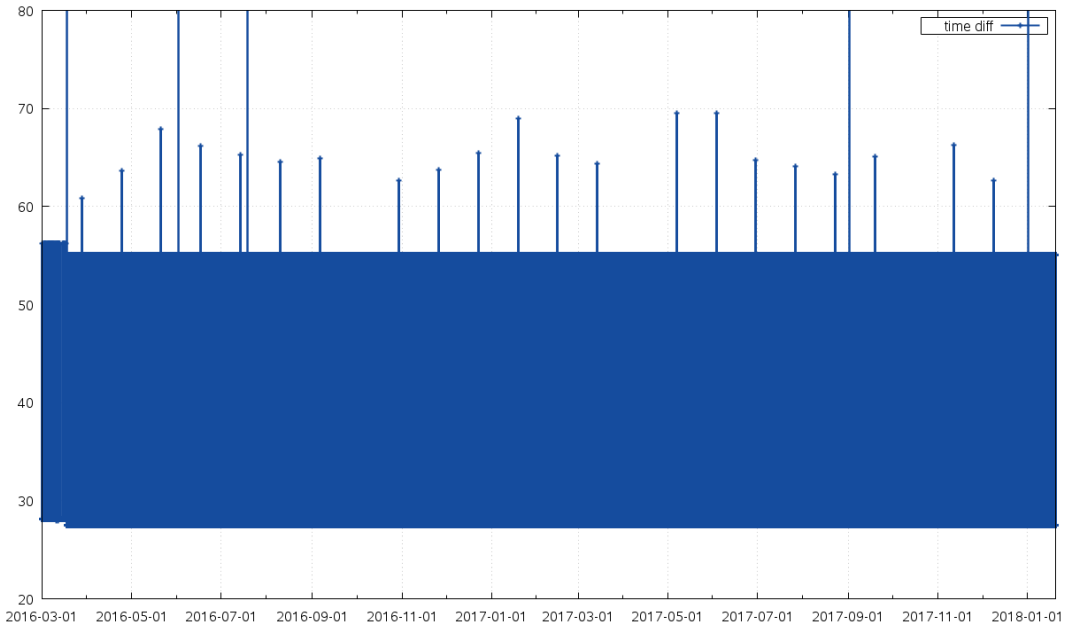

Figure 111 – Time difference between consecutive CAL measurements in the MW_1_MON_AX LTM file capped to 80 seconds.

5.6.2 Content

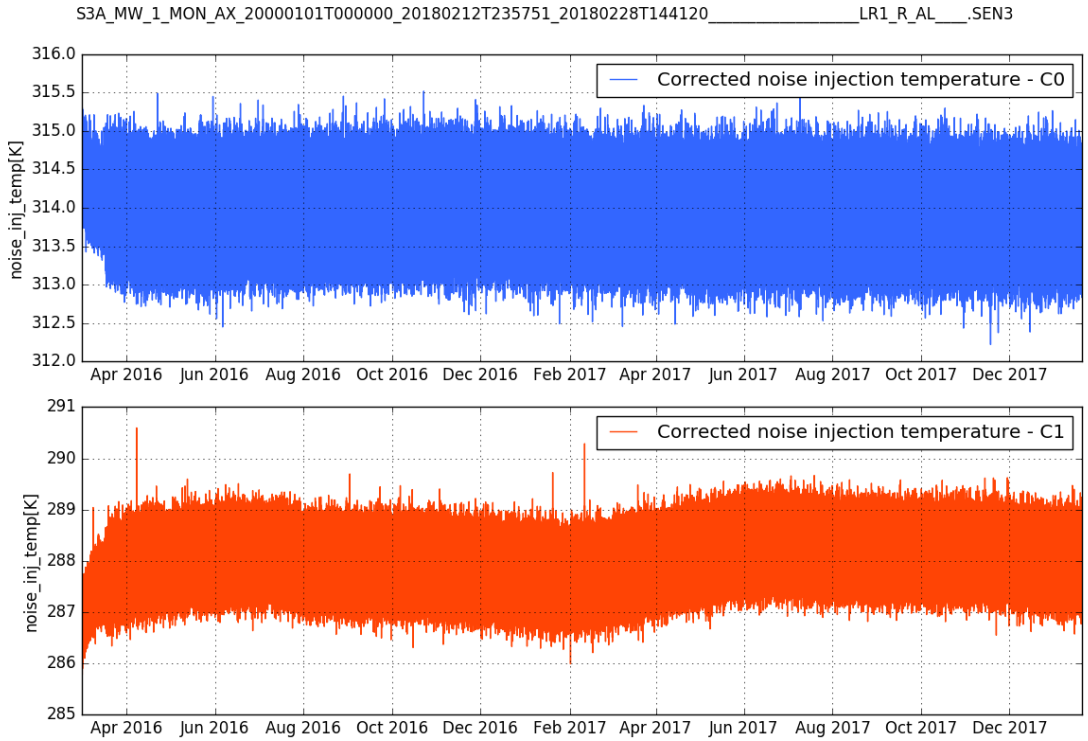

Figure 112 – noise_inj_temp for both channels (MW_1_MON_AX)

The values are within the expected range.

5.7 MW_1_DNB_AX

The filename verified was the following:

```
S3A_MW_1_DNB_AX_20000101T000000_20180212T232607_20180228T144120_____________
_______LR1_R_AL____.SEN3
```

5.7.1 Time difference

The plot is quite similar to the one from MW_1_NIR_AX, taking place normally at 2000 second intervals, however on this case there are no calibrations with very small time difference.

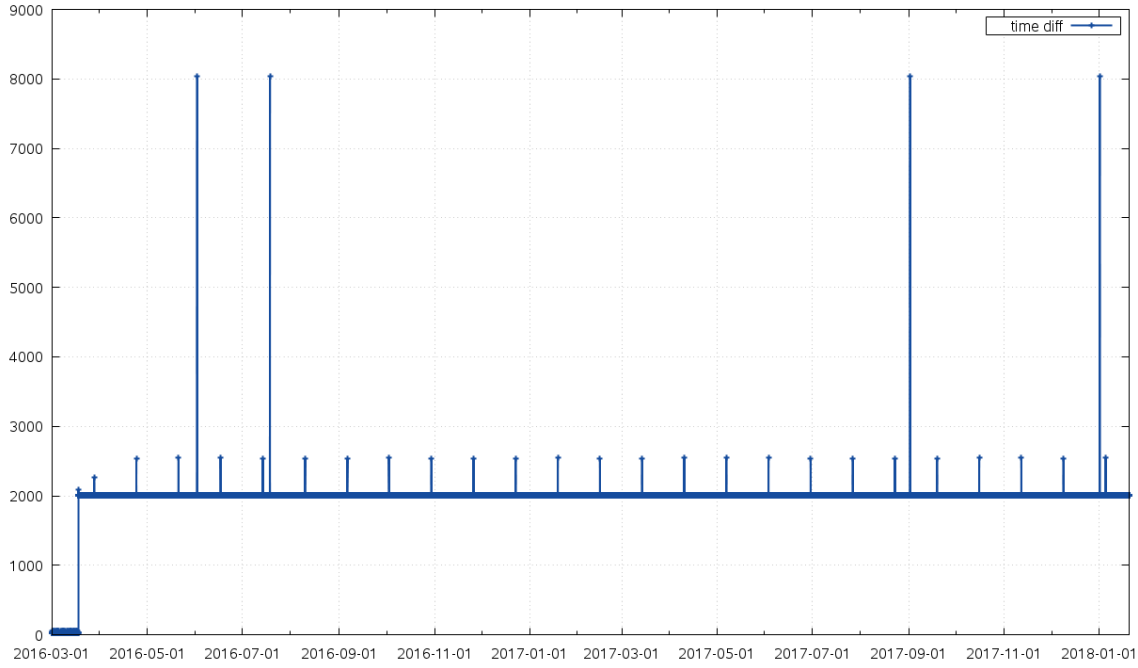

Figure 113 – Time difference between consecutive CAL measurements in the MW_1_DNB_AX LTM file.

5.7.2 Content

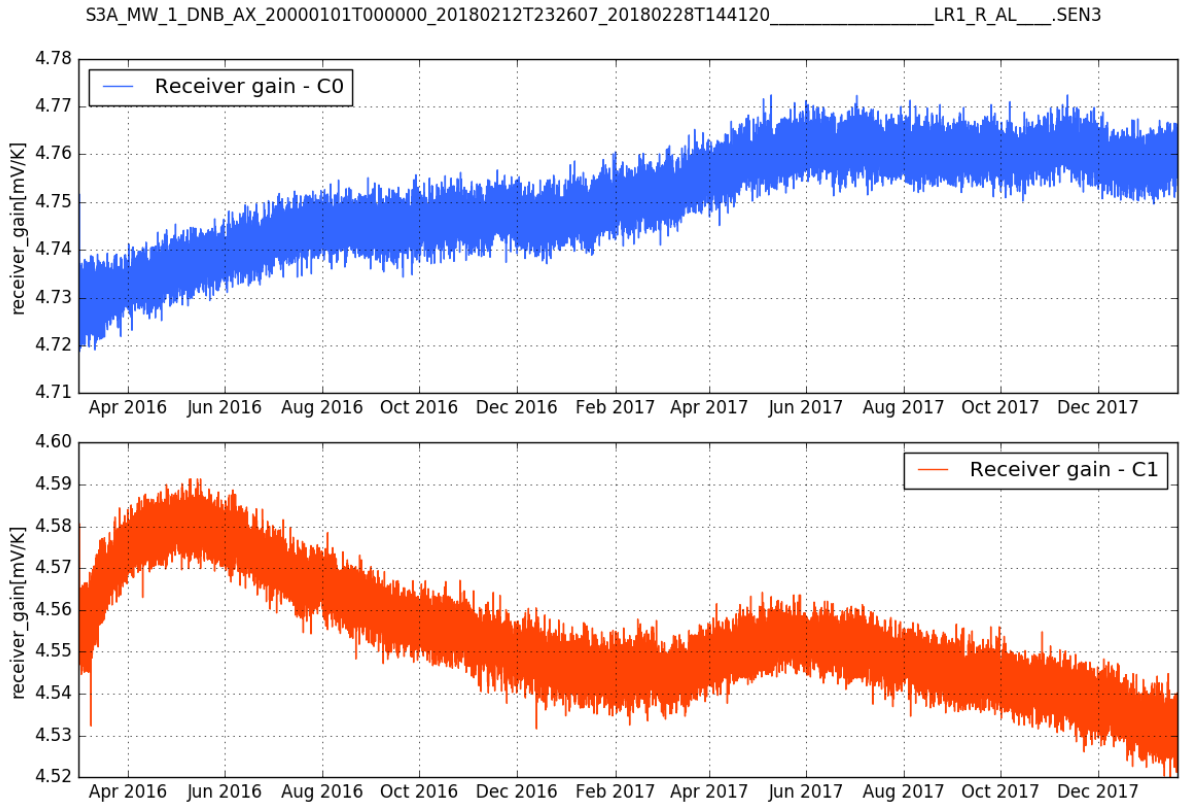

Figure 114 – receiver_gain for both channels (MW_1_DNB_AX)

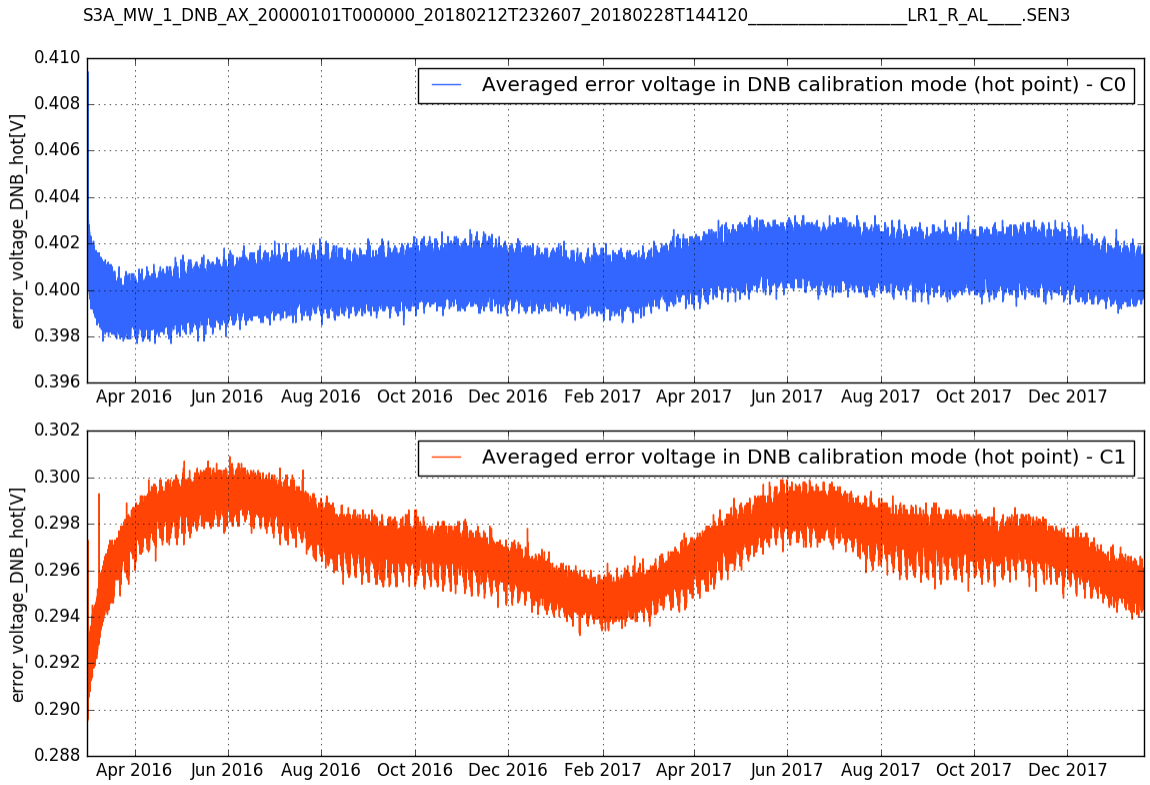

Figure 115 – error_voltage_DNB_hot for both channels (MW_1_DNB_AX)

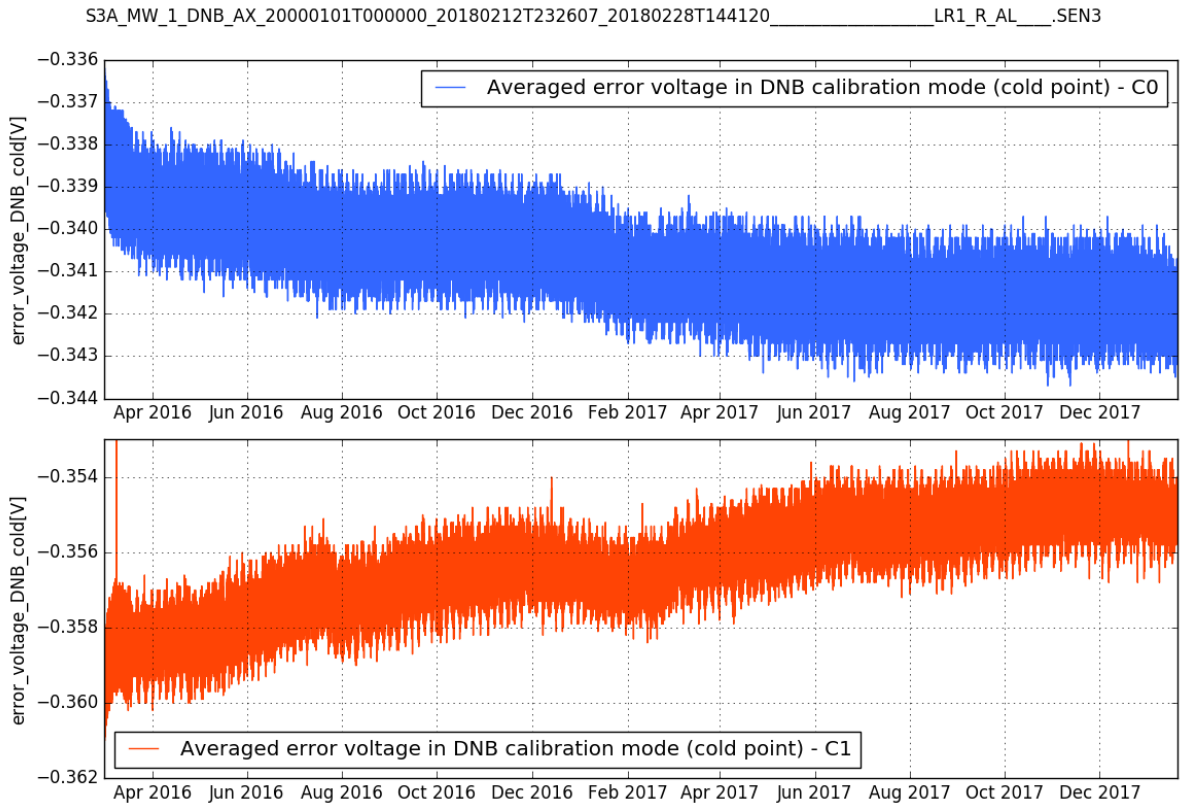

Figure 116 – error_voltage_DNB_cold for both channels (MW_1_DNB_AX)

The values are within the expected range.

6 SRAL L0

6.1 Consolidation

Due to differences on the orchestration software between the Operational PDGS platform and the Reprocessing platform, the same mechanism could not be used to generate exactly the same start/stop time for each consolidated product.

The mechanism used in the reprocessing platform was based on the provision of a list of start/stop times to be used in the consolidation of the SRAL L0 granules into SRAL L1 passes. These times were derived from an internal ORF (Orbit Revolution File) generated by RSP division at EUM.

In order to generate non-overlapping products, the time that the satellite was passing closest to the poles was truncated and added .500000 for the start of the pass and .499999 for that end of the pass. This ensures that the first and the last 1-Hz measurement in the file, which are always at xxx.000000 seconds, have always half a second of 20-Hz measurements on either side of the 1-Hz time tag, so that the 1-Hz average can be properly generated.

This method for setting the start and end times of the pass files (as is used for the reprocessing) is more accurate than the one currently being used in the Operational platform.

This type of consolidation was not performed for the regular operational data, not even at NTC latency. This means that in case of the operational data:

- The STC and NTC files that were supposed to be split in ascending and descending passes do not exactly run from and to the rollover points; the times can be up to 10 seconds off.
- The quality of the 20-Hz and 1-Hz measurements degrades at the start and end of each original 600-second granule.

Both these issues are resolved in the reprocessed data.

6.2 Data gaps

There are several gaps in the dataset at Level 0. These gaps were due to several reasons, mainly to On-Board anomalies, Satellite/Ground-Station downlink problems, archive, or transmission issues. These gaps correspond to minuscule number of data loss when comparing to the overall data availability.

Any gaps within Level 0 files and those between Level 0 files larger than 500 seconds are reported in the following table. These gaps result from the SAFE manifest (xdfumanifest.xml) analysis that reports internal gaps. The external gaps (gaps between products) were analysed considering into the start/stop times of the L0 products.

Table 2 – Data gaps at L0 - summary table

Gap ID	*sensing start*	*sensing stop*	*comment*	*Gap duration (seconds)*
GAP_SR0_001	20160301T111211	20160301T112401	Missing L0 – under investigation	710
GAP_SR0_002	20160301T120301	20160301T121451	Missing L0 – under investigation	710

GAP_SR0_003	20160314T230326	20160315T000451	Missing L0 – under investigation	3685
GAP_SR0_004	20160428T203057	20160428T211024	Data Lost – SRAL set in standby mode[10]	2367
GAP_SR0_005	20160504T214432	20160504T215426	Missing L0 – under investigation	594
GAP_SR0_006	20160511T050854	20160511T061651	Data Lost – Partial dump received[10]	4077
GAP_SR0_007	20160515T034347	20160515T041218	Missing L0 – under investigation	1711
GAP_SR0_008	20160515T092846	20160515T094046	Missing L0 – under investigation	720
GAP_SR0_009	20160518T124109	20160518T131811	Data Lost – Data not received due to DPEF issue**Error! Bookmark not defined.**	2223
GAP_SR0_010	20160519T060500	20160519T061346	Data Lost – SRAL set in standby mode[10]	526
GAP_SR0_011	20160519T165925	20160519T175126	Data Lost – Spacecraft anomaly[10]	3121
GAP_SR0_012	20160523T074901	20160523T093226	Data Lost – SRAL OLTC EEPROM patch upload[10]	6205
GAP_SR0_013	20160524T123220	20160524T125007	Data Lost – SRAL OLTC EEPROM patch upload**Error! Bookmark not defined.**	1067
GAP_SR0_014	20160525T221042	20160525T224940	Data Lost – SRAL OLTC EEPROM patch upload**Error! Bookmark not defined.**	2339
GAP_SR0_015	20160601T203453	20160601T221557	Data Lost – Missing dump[10]	6064
GAP_SR0_016	20160603T035111	20160603T041947	Missing L0 – under investigation	1715
GAP_SR0_017	20160610T152808	20160610T155310	Missing L0 – under investigation	1502
GAP_SR0_018	20160611T034348	20160611T041218	Data Lost - SRAL SpW ASIC anomaly[10]	1711
GAP_SR0_019	20160616T074720	20160616T081527	Data Lost - SRAL SpW ASIC anomaly	1686
GAP_SR0_020	20160617T185640	20160617T193507	Limitation – Missing L0	2307

[10] As reported in the daily/weekly EUM PDGS operations reports.

GAP_SR0_021	20160618T080733	20160618T081635	Limitation – Missing L0	542
GAP_SR0_022	20160618T235839	20160619T000751	Data Lost - SRAL SpW ASIC anomaly (TBC)	553
GAP_SR0_023	20160621T021943	20160621T023736	Data Lost - SRAL SpW ASIC anomaly[11]	1073
GAP_SR0_024	20160621T070309	20160621T071327	Data Lost - SRAL SpW ASIC anomaly[11]	618
GAP_SR0_025	20160621T083043	20160621T084153	Data Lost - SRAL SpW Anomaly[11]	670
GAP_SR0_026	20160623T082335	20160623T093020	Data Lost (on-board operations[12])	4005
GAP_SR0_027	20160623T171532	20160623T172751	Data Lost – Several Downlink issues	739
GAP_SR0_028	20160718T115651	20160718T133638	Data not received[13]	5987
GAP_SR0_029	20160728T073549	20160728T091652	Limitation – Missing L0	6063
GAP_SR0_030	20160808T124223	20160808T143158	Data not received[14]	6575
GAP_SR0_031	20170706T173419	20170706T174411	Data not received[15]	592
GAP_SR0_032	20170901T143708	20170901T162625	Data Lost - Data not acquired[16]	6557
GAP_SR0_033	20170919T093934	20170919T094934	Missing L0 – under investigation	600
GAP_SR0_034	20180101T033518	20180101T052018	Data Lost – Missing dump[17]	6300

[11] As reported in the daily/weekly EUM FCT operations reports.

[12] It was applied on the 2016-06-23 a patch to the on-board software that prevented future occurrences of the SRAL SpW anomaly.

[13] AR EUM/Sen3/AR/2009: S3A X-band Dump for orbit #2179 not received

[14] AR EUM/Sen3/NCR/2096: Missing L0PP: orbits 2479-2478 [12:52-14:32] no measurement L0PP received for OLCI, SLSTR, SRAL

[15] EUM/Sen3/AR/3411: EUM MAR PDGS has not received any OLCI, SLSTR and SRAL

[16] EUM/Sen3/AR/3622: X-Band data and HKTM files for orbit #8027 were not acquired. DATA LOSS, not delayed

[17] EUM/Sen3/AR/4006: No L0PP granules and HKTM file received for orbit #9760

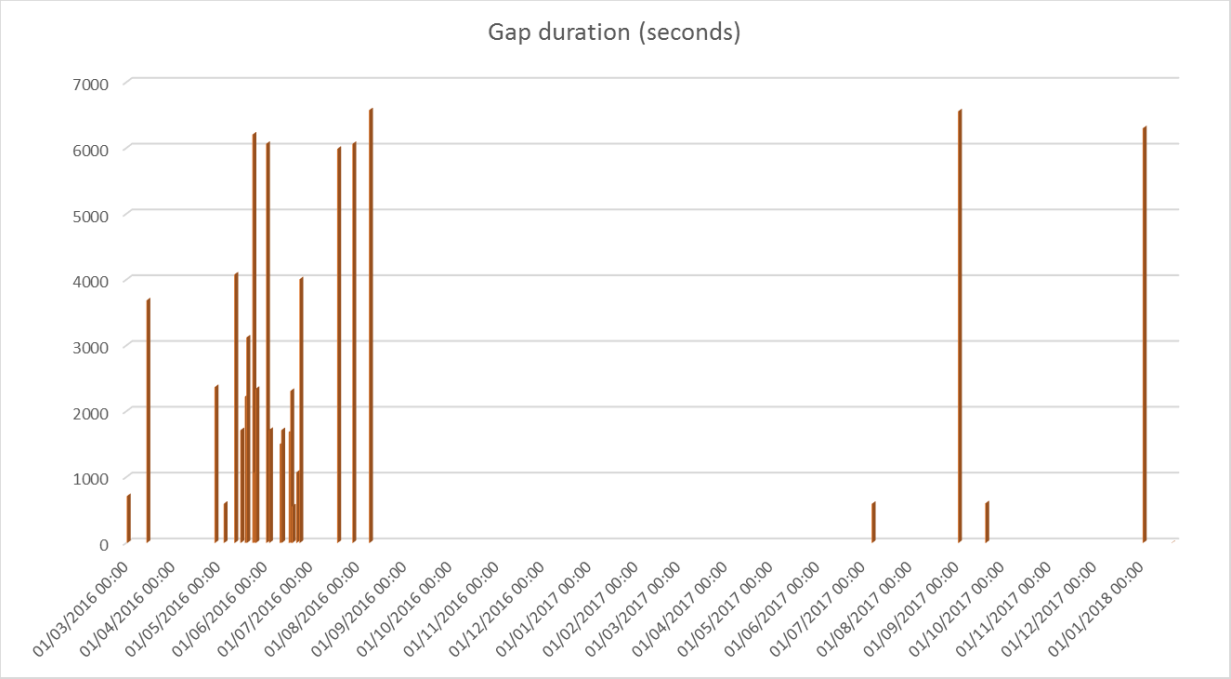

Figure 117 – SRAL L0 Gaps over time

7 SRAL L1

7.1 Data completion and Processing Baseline check

The L1 products (L1A, L1B, L1B-S) have the same start/stop time as the input consolidated L0 products.

The first L1B from the dataset is:

```
S3A_SR_1_SRA____20160301T092017_20160301T093000_20180202T230137_0583_0
01_221______LR1_R_NT_003.SEN3
```

The last one:

```
S3A_SR_1_SRA____20180120T230931_20180121T000000_20180302T063750_3029_0
27_058______LR1_R_NT_003.SEN3
```

The L1A and L1B-S following the same start/stop times as L1B.

There are several data gaps in the SRAL L1 data, for more details about the gaps check Section 7.3.

All the L1 files were confronted with the L1 Processing Baseline (IPF version and static ADF) and all were correctly produced, in this regard. The same tools were used as currently used to monitor the Processing Baseline in the S3 PDGS.

7.2 Content verification

Ten days of SRAL L1B data products in February and April 2017 were verified in term of data content.

In specific, it was verified that the field nb_stack_20_ku (number of Doppler beams in the stack) is properly set to 180 (as expected) over open ocean (see Figure 119). Further, the number of beams in the stack (nb_stack_20_ku) maintains the value of 180 at north and south roll-over points (i.e. at transition between two pole-to-pole passes). See in this regard Figure 118.

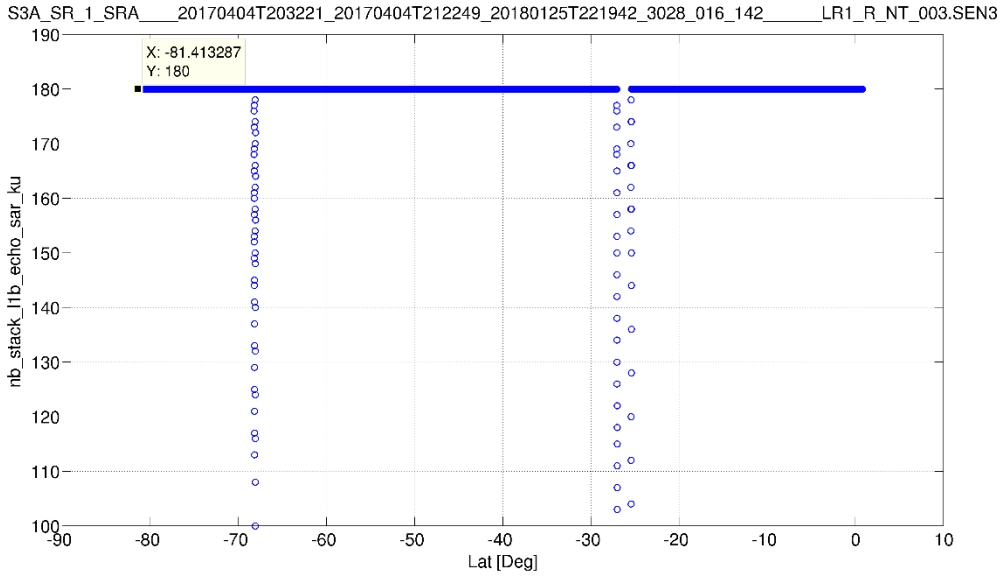

Figure 118 – nb_stack_20_ku versus Latitude in one product

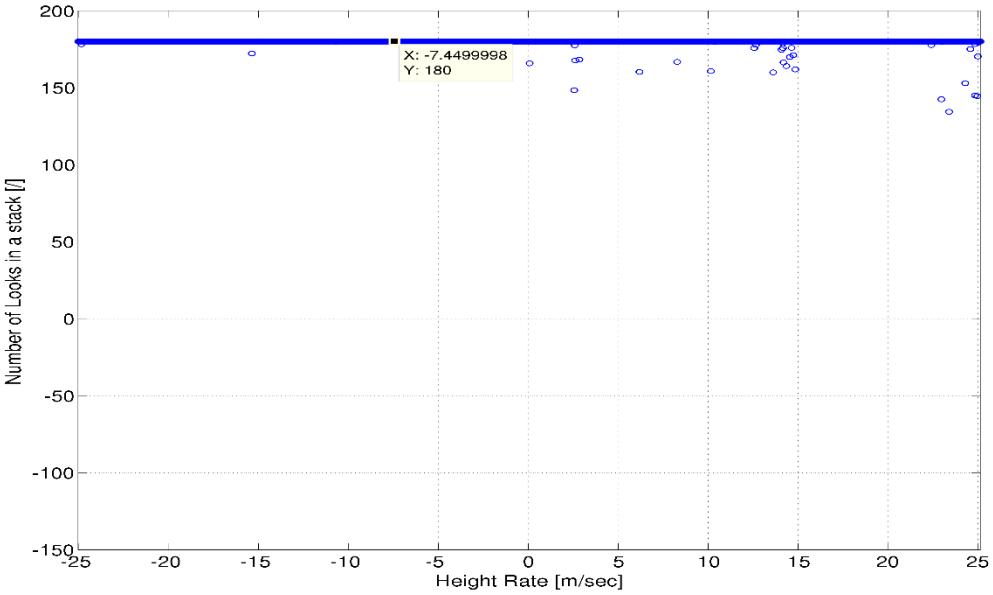

Figure 119 – Number of Beams in the stack (nb_stack_20_ku) over Open Ocean. The value is set nominally to 180.

Further, sporadic samples of L1A and L1B-S data products were opened and content inspected: no anomaly was found. In Figure 120, we show a sample of Doppler Beam Stack (top) and the consistency between the waveform computed from a L1B-S Stack (after decompression) and as stored in the L1B-S product (bottom).

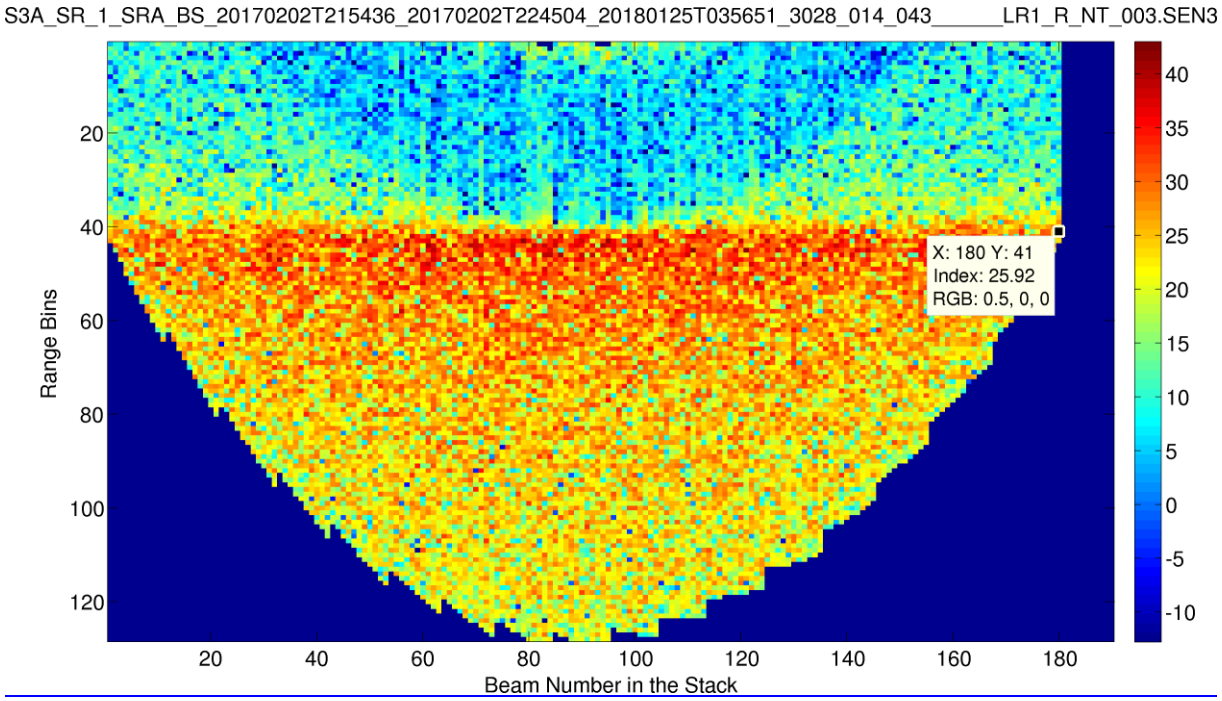

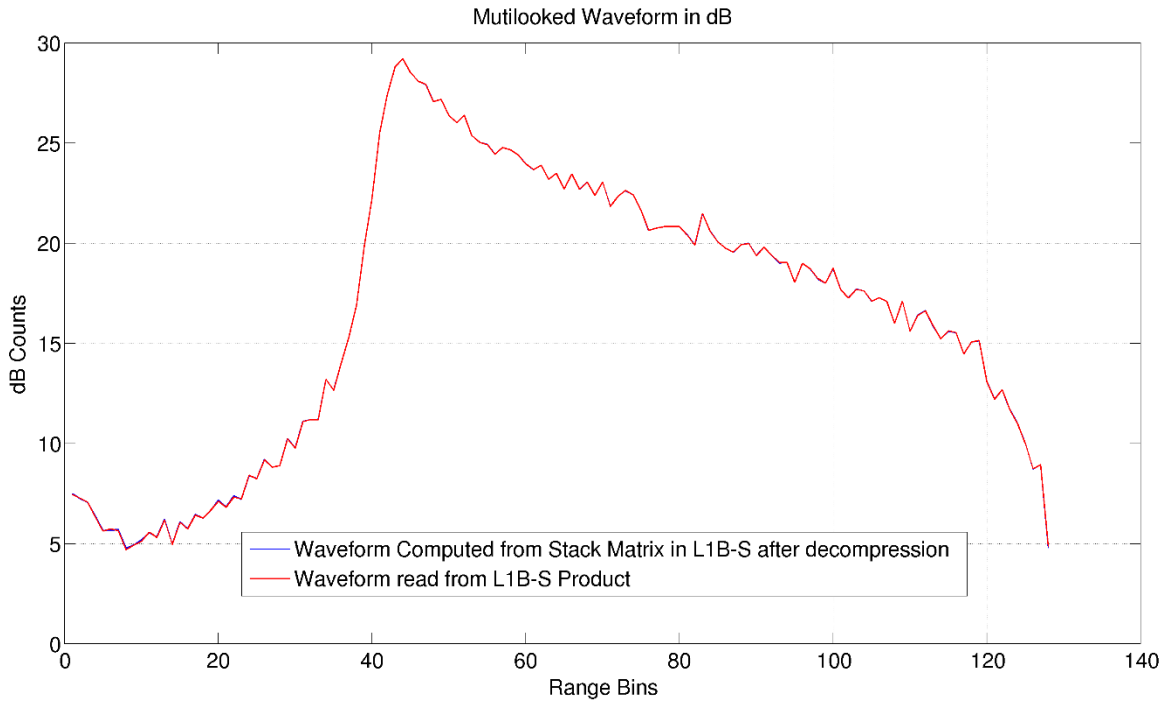

Figure 120 – Doppler Beam Stack after decompression (top) and SAR waveform computed from the Stack and read from the L1B-S product (bottom)

7.3 Data gaps

The Level 1 gaps internal or between files larger than 500 seconds are reported in the following table. These gaps result from the SAFE manifest (xdfumanifest.xml) analysis that reports internal gaps. The external gaps (between products) were analysed considering into the start/stop times of the L1 products.

Table 3 – Data gaps at L1 - summary table

Gap ID	*sensing start*	*sensing stop*	*comment*	*Missing seconds (includes all gaps reported in the file(s))*
GAP_SR1_001	20160301T111101	20160301T120129	Related to gap *GAP_SR0_001* - L1 Product Internal gap	886
GAP_SR1_002	20160301T120130	20160301T125200	Related to gap *GAP_SR0_002* - L1 Product Internal gap	805
GAP_SR1_003	20160308T112957	20160308T122025	S3A Calibration operations - L1 Product Internal gap	1222
GAP_SR1_004	20160308T122026	20160308T131055	S3A Calibration operations - L1 Product Internal gap	1289
GAP_SR1_005	20160308T131056	20160308T140125	S3A Calibration operations - L1 Product Internal gap	1218
GAP_SR1_006	20160308T140126	20160308T145154	S3A Calibration operations - L1 Product Internal gap	1314
GAP_SR1_007	20160308T145155	20160308T154224	S3A Calibration operations - L1 Product Internal gap	1384
GAP_SR1_008	20160314T230326	20160315T000451	Related to gap *GAP_SR0_003*	3685
GAP_SR1_009	20160416T190359	20160416T203429	IPF Failure	5430
GAP_SR1_010	20160418T034220	20160418T061350	IPF Failure	9089
GAP_SR1_011	20160420T102426	20160420T111455	Under investigation - L1 Product Internal gap	652
GAP_SR1_012	20160427T044941	20160427T054012	IPF Failure	3030
GAP_SR1_013	20160428T202255	20160428T211323	Related to gap *GAP_SR0_004*- L1 Product Internal gap	2476
GAP_SR1_014	20160430T024040	20160430T033110	IPF Failure	3029
GAP_SR1_015	20160504T210749	20160504T215817	Related to gap *GAP_SR0_005* - L1 Product Internal gap	693
GAP_SR1_016	20160511T050848	20160511T061651	Related to gap *GAP_SR0_006*	4083

GAP_SR1_017	20160515T034225	20160515T043254	Related to gap *GAP_SR0_007* - L1 Product Internal gap	1742
GAP_SR1_018	20160515T092843	20160515T094047	Related to gap *GAP_SR0_008*	724
GAP_SR1_019	20160518T122948	20160518T132016	Related to gap *GAP_SR0_009* - L1 Product Internal gap	2235
GAP_SR1_020	20160519T060458	20160519T061346	Related to gap *GAP_SR0_010*	528
GAP_SR1_021	20160519T165925	20160519T175126	Related to gap *GAP_SR0_011*	3121
GAP_SR1_022	20160523T074901	20160523T093226	Related to gap *GAP_SR0_012*	6205
GAP_SR1_023	20160524T122646	20160524T131439	Related to gap *GAP_SR0_013* - L1 Product Internal gap	1190
GAP_SR1_024	20160525T220355	20160525T225424	Related to gap *GAP_SR0_014*- L1 Product Internal gap	2351
GAP_SR1_025	20160601T203453	20160601T221557	Related to gap *GAP_SR0_015*	6064
GAP_SR1_026	20160603T034953	20160603T044022	Related to gap *GAP_SR0_016* - L1 Product Internal gap	1784
GAP_SR1_027	20160610T150501	20160610T155530	Related to gap *GAP_SR0_017* - L1 Product Internal gap	1534
GAP_SR1_028	20160611T034225	20160611T043254	Related to gap *GAP_SR0_018* - L1 Product Internal gap	1743
GAP_SR1_029	20160616T072459	20160616T081527	Related to gap *GAP_SR0_019* - L1 Product Internal gap Data Lost - SRAL SpW ASIC anomaly[18,19]	1696
GAP_SR1_030	20160617T184543	20160617T193611	Related to gap *GAP_SR0_020* - L1 Product Internal gap Limitation – Missing L0 granule[20]	2351
GAP_SR1_031	20160618T080733	20160618T081635	Related to gap *GAP_SR0_021* - Limitation – Missing L0 granule [20]	544
GAP_SR1_032	20160618T232229	20160619T001258	Related to gap *GAP_SR0_022* - L1 Product Internal gap Limitation – Missing L0 granule[20]	587
GAP_SR1_033	20160621T015206	20160621T024234	Related to gap *GAP_SR0_023* - L1 Product Internal gap	1119

[18] As reported in the daily/weekly EUM FCT operations reports.

[19] Due to the way the consolidation is performed at L0, some of the SRAL SpW ASIC anomalies are only visible at L1

[20] Due to the way the consolidation is performed at L0, some gaps due to internal granules being missing are only visible at L1, the start/stop time of the missing input granules is not part of the job-order, as they were not available.

			Data Lost - SRAL SpW ASIC anomaly[18,19]	
GAP_SR1_034	20160621T065504	20160621T074532	Related to gap *GAP_SR0_024* - L1 Product Internal gap Data Lost - SRAL SpW ASIC anomaly[18,19]	716
GAP_SR1_035	20160621T083023	20160621T084153	Related to gap *GAP_SR0_025* - Data Lost - SRAL SpW Anomaly[18]	690 seconds
GAP_SR1_036	20160623T082335	20160623T093020	Related to gap *GAP_SR0_026* - Data Lost - on-board operations[12]	4005 seconds
GAP_SR1_037	20160623T142737	20160623T174937	Related to GAP_SR0_027 plus several downlink issues and IPF Failure	12119 seconds
GAP_SR1_038	20160718T115651	20160718T133638	Related to gap *GAP_SR0_028* - Data not received[13]	5987 seconds
GAP_SR1_039	20160728T073549	20160728T091652	Related to gap *GAP_SR0_029* - Limitation – Missing L0 granule[20]	6063 seconds
GAP_SR1_040	20160808T124223	20160808T143158	Related to gap *GAP_SR0_030* Data not received[14]	6575 seconds
GAP_SR1_041	20170706T165914	20170706T174942	Related to gap *GAP_SR0_031* - L1 Product Internal gap	609 seconds
GAP_SR1_042	20170901T143708	20170901T162625	Related to gap *GAP_SR0_032*	6557
GAP_SR1_043	20170919T093018	20170919T102047	Related to gap *GAP_SR0_033*- L1 Product Internal gap	605
GAP_SR1_044	20171114T110928	20171114T125028	Downlink issue[21] and IPF Failure	6059
GAP_SR1_045	20180101T033518	20180101T052018	Related to gap *GAP_SR0_032*	6300

[21] PDGSANOM-2652: CGS2:SG23: S3A: sequencing errors recorded on both channels on DFEP3 & DFEP 6

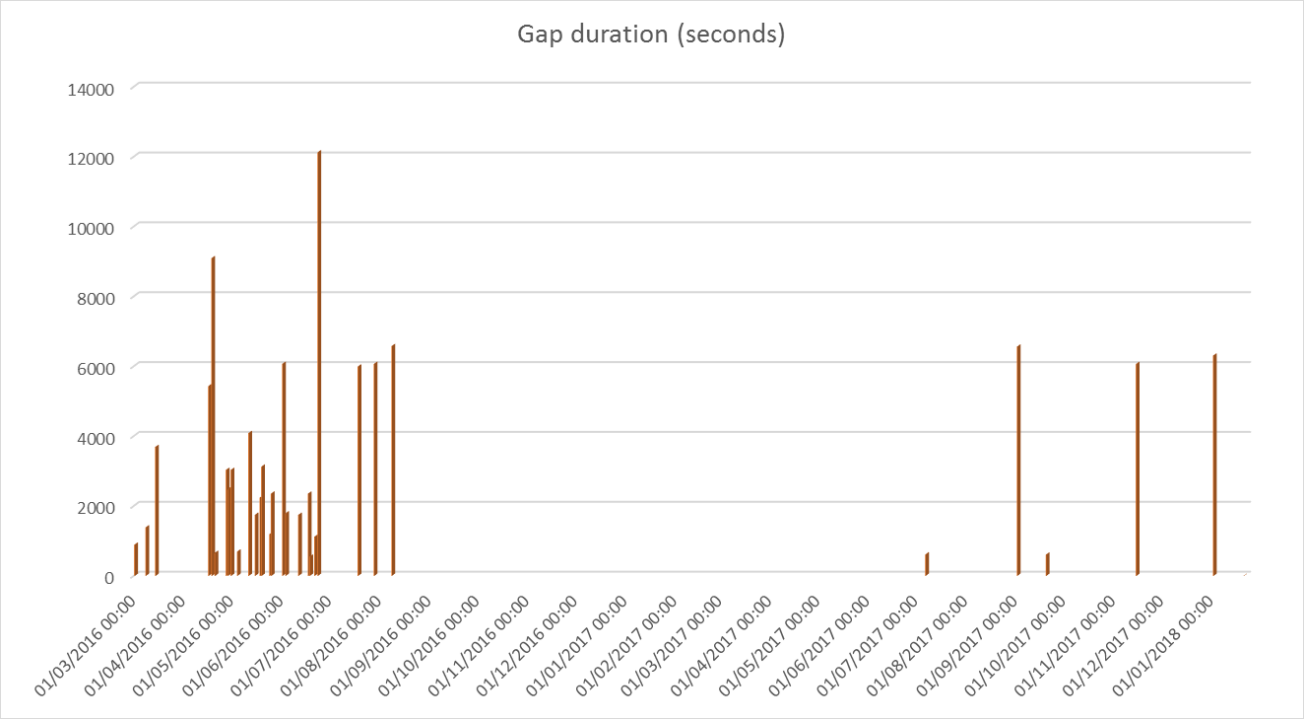

Figure 121 – SRAL L1 Gaps over time

8 MWR L1

8.1 Data completion and Processing Baseline check

The reprocessed period was since the turn-on of the instrument on 2016-02-29 to 2018-01-20.

The first MWR L1 from the dataset is:

```
S3A_MW_1_MWR____20160229T140647_20160229T154500_20180119T073345_5892_0
01_210______LR1_R_NT_003.SEN3
```

The last one:

```
S3A_MW_1_MWR____20180120T235405_20180121T013621_20180312T181903_6135_0
27_059______LR1_R_NT_003.SEN3
```

There are several data gaps in the MWR L1 data, for more details about the gaps check Section 8.2. All the L1 files were confronted with the L1 Processing Baseline (IPF version and static ADF) and all were correctly produced, in this regard. The same tools were used as currently used to monitor the Processing Baseline in the S3 PDGS.

8.2 Data gaps

There are four missing dumps from the satellite/ground station. And correspond to the following periods:

- 2016-06-01 20:34 → 2016-06-01 22:15 (see[22]) [6064 seconds]
- 2016-07-18 10:16 → 2016-07-18 11:56 (see[13]) [5987 seconds]
- 2017-09-01 14:46 → 2017-09-01 16:26 (see[16]) [5980 seconds]
- 2018-01-01 03:37 → 2018-01-01 05:20 [6145 seconds]

Besides these, there are no other gaps larger than 100 seconds.

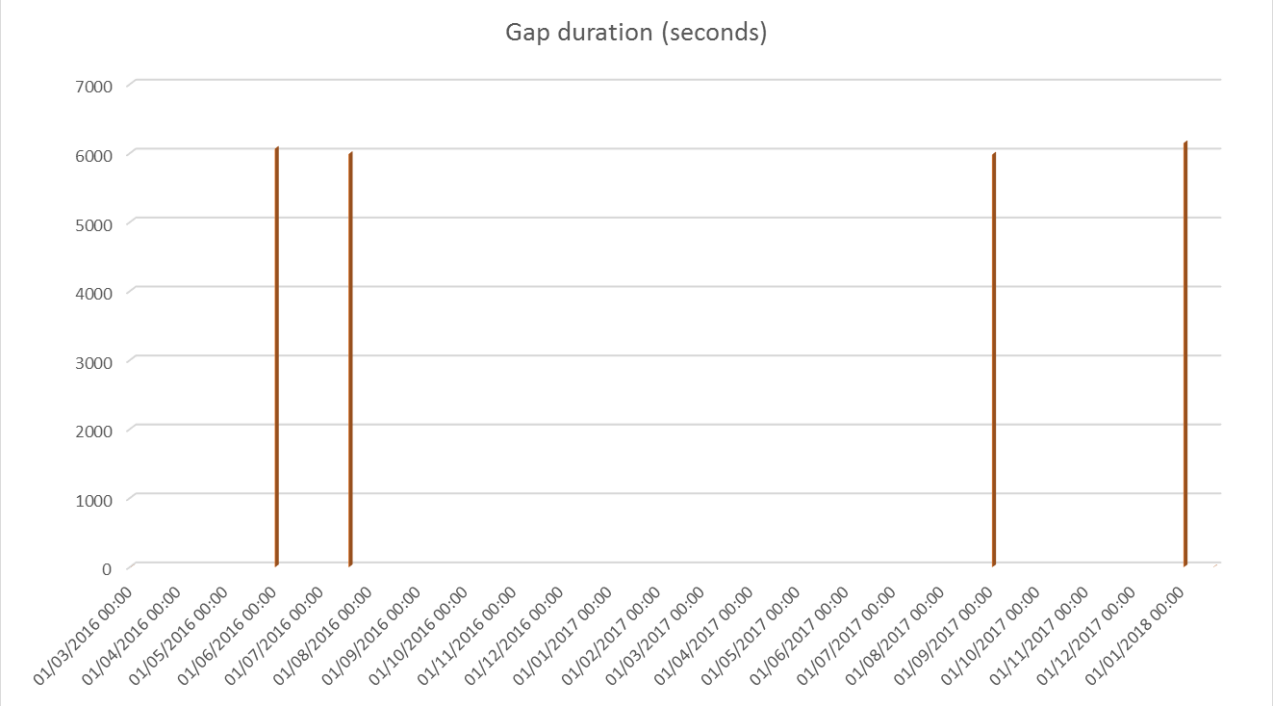

Figure 122 – MWR L1 Gaps over time

[22] As reported on the electronic log of operations available in DMTool (ID: 854229).

9 Overall Conclusions

In general, the new reprocessing showed the good quality for Sentinel-3A altimetry data. There is a better agreement with models and/or other missions, Jason-3 (J3), than with the previous reprocessed dataset. Having a longer time series, almost two years of S3A data, processed with the same consistent baseline showed to be very fruitful to better characterize the S3A data. These longer series also allowed to find some trends in the dataset, such as the SAR mode versus PLRM mode that over time show a small drift.

The initial phase of the dataset is characterized by some issues that lasted until 23 June 2016 (end of Cycle 5) and are no longer present since then. More information can be found in Section 4.3.2. General users are recommended to start using the Sentinel-3 SRAL data from Cycle 6 on-wards.

The Sea Surface Height Anomaly (**SSHA**) of S3 is now closer to the J3 one, in term of absolute bias, and the standard deviation is also reduced. The new dataset allows for the ocean signals, at large and medium scale, to be better retrieved.

The long time series allowed for a relative drift to be found between the SSHA measurements processed in SAR mode and PLRM mode, investigation is on-going regarding the full characterization and correction of the drift. More details can be found in Section 4.3.2.

The Significant Wave Height (**SWH**) retrieved from this reprocessing is now more consistent between SAR and PLRM mode, but a relative drift in time can be seen now. This can explain part of the relative drift seen in SSHA, as the SWH is input to the Sea State Bias correction used to calculate SSHA. The SAR mode SWH is quite consistent with ECWMF's modelled waves, but a discrepancy at lower wave heights, below 1.5 meters has been identified and work on the fix is on-going. For more details we refer to Section 4.3.4.

The **Sigma0** (backscatter) and **Wind Speed** of the new reprocessing have improved with respect to the previous one. The sigma0 is now more accurate at very small scales and the dependency with orbit altitude is significantly mitigated. This allows for a better coherence between the values retrieved in SAR and PLRM mode, and significantly improved the wind speed retrieved from the altimeter in SAR mode. When compared to the ECMWF model, the wind speed values matched very well. For more details we refer to Section 4.3.5 (Sigma0) and 4.3.6 (Wind Speed).

The **Ionospheric correction** derived from the dual-frequency altimeter ranges was significantly improved as the result of an enhancement in the treatment of the C-band range calibration. The correction is now more consistent with the GPS-derived GIM model. However, there is a still a bias between the altimeter-derived correction and the GIM one, and SAR and PLRM solutions drift over time, owing to a relative drift of the SAR and PLRM range measurements. A detailed analysis of the ionospheric correction can be found in section 4.3.7.

The **Radiometer Wet Trophosperic correction** from this reprocessing shows no bias when compared to the modelled wet tropospheric correction derived from ECMWF meteorological fields. In addition, the standard deviation of the difference has significantly decreased compared to the previous reprocessing data set. More details can be found in Section 4.3.8.

At Level 1, we highlight the updated calibration scheme that generated less noisy calibrations and improved the data quality (see Section 5). This reprocessing allowed to show that the PTR width is changing over time and that this may need to be taken into account in a future reprocessing.

The global mean sea level seen by Sentinel-3A follows the trend seen by other altimeters, as can be seen in the Figure 123 and Figure 124.

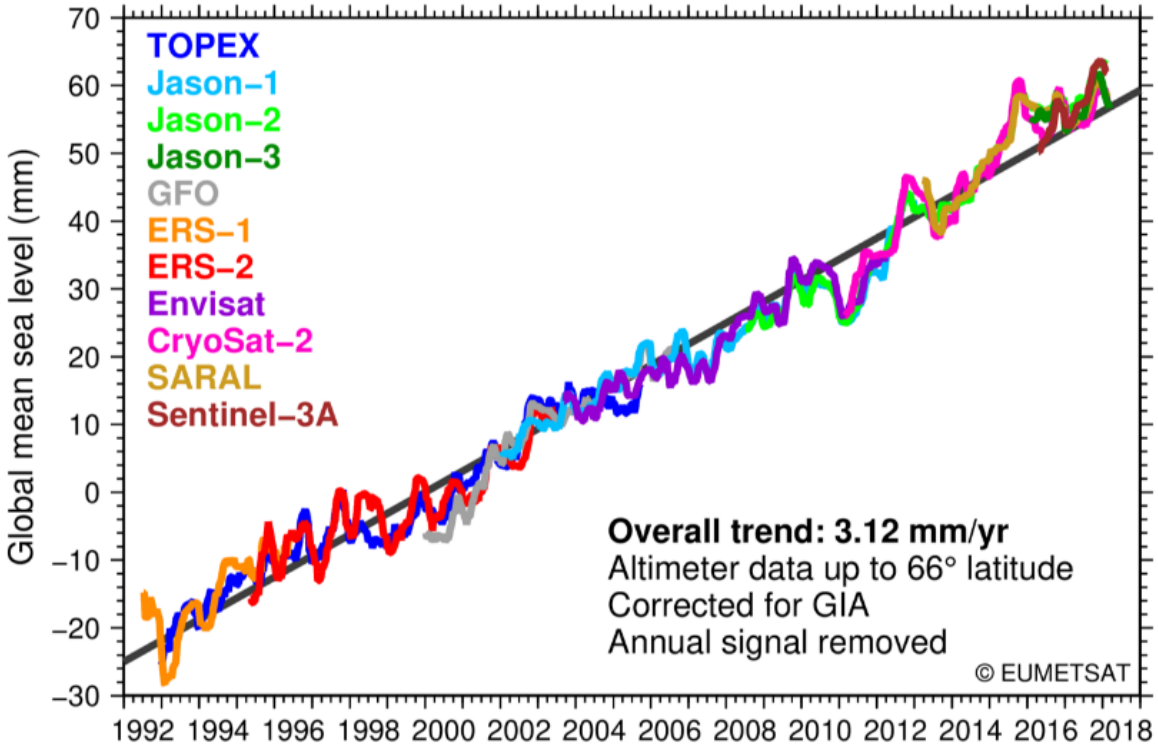

Figure 123 – Global mean sea level since 1992.

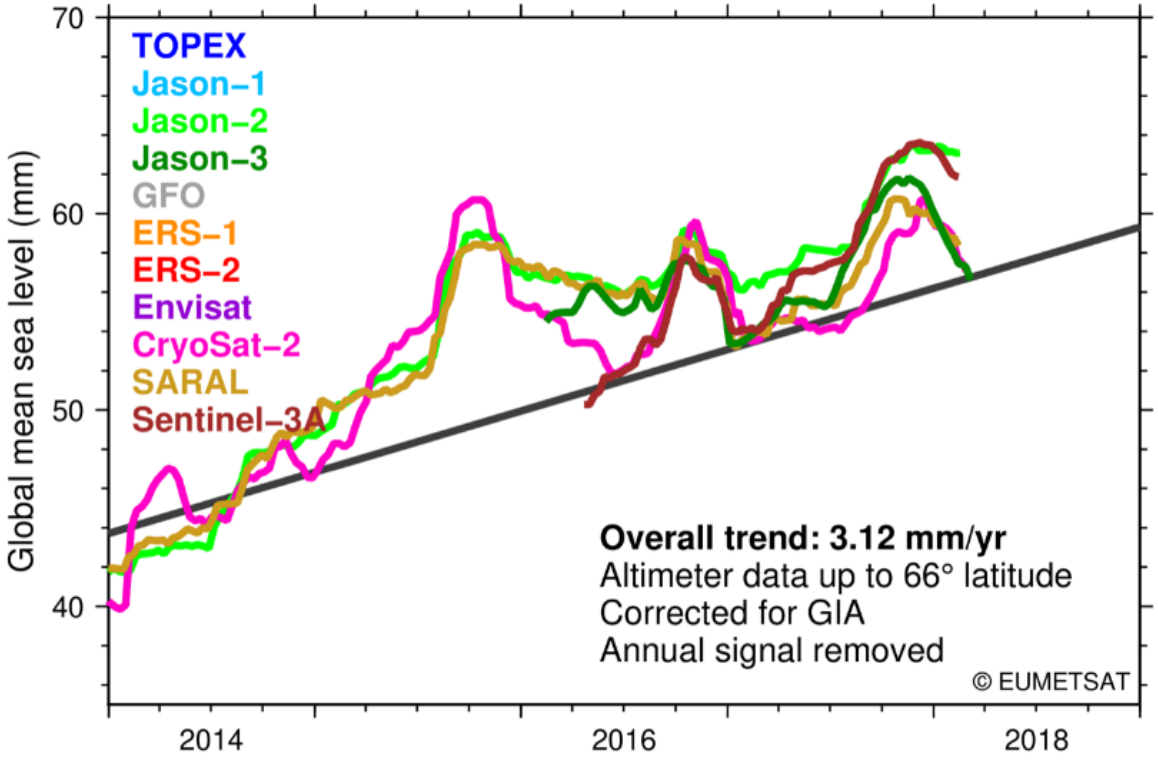

Figure 124 – Global mean sea level since 2014.